EMISSIONS FROM AND WITHIN AN ALLISON J-33 COMBUSTOR

Environmental Protection Agency Contract No. 68-04-0001 - Final Report

by

A. M. Mellor, R. D. Anderson,

R. A. Altenkirch, and J. H. Tuttle

Report No. CL - 72 - 1

THE COMBUSTION LABORATORY
SCHOOL OF MECHANICAL ENGINEERING
PURDUE UNIVERSITY
LAFAYETTE, INDIANA

June 1972

EPA-R2-72-097

Emissions from and within an Allison J-33 Combustor

Environmental Protection Agency Contract
No. 68-04-0001 - Final Report

by

A. M. Mellor, R. D. Anderson, R. A. Altenkirch, and J. H. Tuttle

Report No. CL-72-1

The Combustion Laboratory
School of Mechanical Engineering
Purdue University
Lafayette, Indiana

June 1972

ACKNOWLEDGEMENTS

Special thanks are extended to Mr. Thomas Miller for his assistance in the construction and maintenance of the experimental facility and also for his assistance in obtaining the data contained in this report.

Messrs. P. Leonard, M. Franzen, S. Jochem, R. Shisler, S. Jones, G. McFarron, and K. Gross greatly aided in both the construction and maintenance of the experimental facility and data gathering and analysis.

The initial phase of the facility development was conducted under Contract DAAE07-69-C-0756 with the Army Tank and Automotive Command; subsequent facility development and the research described herein were supported by the Environmental Protection Agency under Contract 68-04-0001. G. Kittredge, B. McNutt, and K. Hellman of the Office of Air Programs provided valuable assistance.

TABLE OF CONTENTS

		Page
LIST OF TABLES		v
LIST OF FIGURES		vi
ABSTRACT		ix
SECTION I.	INTRODUCTION AND SUMMARY	1
SECTION II.	DESIGN AND OPERATION OF THE EXPERIMENTAL GAS TURBINE COMBUSTION FACILITY	4
A.	Test Cell Hardware	5
	1. Air System Description	5
	2. Fuel System Description	7
	3. Combustor Description	7
	4. Probe Addition Section Description	9
	5. Probe Description	9
	6. Probe Positioner Description	20
	7. Back-Pressure System Description	23
	8. Water System Description	28
B.	Control Room Instrumentation	28
	1. Temperature Monitoring Instrumentation	30
	2. Emission Monitoring Instrumentation	31
	2.1 The Carbon Monoxide Analyzer System	31
	2.2 The Nitric Oxide Analyzer System	33
	2.3 Total Hydrocarbon Analyzer System	40
C.	Summary	40
SECTION III.	RESULTS AND DISCUSSION	42
A.	Combustor Operating Points	47
B.	Internal Measurements	50
	1. Gas Temperatures	50
	2. Nitric Oxide	54
	3. Carbon Monoxide	59
	4. Summary	64
C.	Combustor Exhaust Plane Measurements	64
	1. Gas Temperatures	66
	2. Exhaust Plane Emissions of Nitric Oxide and Carbon Monoxide	66
	2.1 The Influence of Air Flow Rate	69
	2.2 The Influence of Overall Equivalence Ratio	74
	2.3 The Influence of Combustor Pressure	75
D.	Other Parameters	84
E.	Summary	84

Page

SECTION IV. FUTURE EFFORTS 86

LIST OF REFERENCES 93

APPENDIX A: EFFECT OF NO_2 CONVERTER ON NO 95

LIST OF TABLES

Table		Page
2-1.	J-33 Design Resume	11
2-2.	NO Interference Data (after Fontijn et al., 1969, 1970)	39
3-1.	Selected Combustor Operating Points	49
4-1.	Operating Point and Emissions Obtained from Two J-33 Combustors in Series	89

LIST OF FIGURES

Figure		Page
2-1.	Combustion facility air system	6
2-2.	Combustion facility fuel system	8
2-3.	Combustor arrangement	10
2-4.	Combustor and probe addition section	12
2-5.	Combustion facility schematic	13
2-6.	Gas sampling probe body	16
2-7.	Gas sampling probe block	17
2-8.	Gas sampling probe tip	18
2-9.	Gas sampling probe	21
2-10.	Gas sampling probe and positioning systems	22
2-11.	Axial and radial (black box) probe positioners	24
2-12.	Back pressure valve schematic	26
2-13.	Back pressure valve guidance system and engine	27
2-14.	Combustion facility water system	29
2-15.	Gas handling system	32
2-16.	CO analyzer system	34
2-17.	Nitric oxide detector schematic	36
2-18.	Hydrocarbon sample handling and analyzer system	41
3-1.	Typical gas turbine combustor flow schematic	43
3-2.	J-33 combustor configuration, gas sampling planes (4 of 6), and probe trace position	45

Figure		Page
3-3.	Relationship of probe trace and gas sampling points to J-33 combustor configuration	46
3-4.	Combustor operating point matrix	48
3-5.	Temperature versus axial position ($\dot{m}_a$ = 6.0 lbs/sec, ϕ = .217, p = 5 atm)	51
3-6.	NO concentration versus axial position for 0° ($\dot{m}_a$ = 6.0 lbs/sec, ϕ = .217, p = 5 atm)	55
3-7.	NO concentration versus axial position for 90° ccw ($\dot{m}_a$ = 6.0 lbs/sec, ϕ = .217, p = 5 atm)	56
3-8.	NO concentration versus axial position for 90° cw ($\dot{m}_a$ = 6.0 lbs/sec, ϕ = .217, p = 5 atm)	57
3-9.	NO concentration versus axial position for 180° ($\dot{m}_a$ = 6.0 lbs/sec, ϕ = .217, p = 5 atm)	58
3-10.	CO concentration versus axial position for 0° ($\dot{m}_a$ = 6.0 lbs/sec, ϕ = .217, p = 5 atm)	60
3-11.	CO concentration versus axial position for 90° ccw ($\dot{m}_a$ = 6.0 lbs/sec, ϕ = .217, p = 5 atm)	61
3-12.	CO concentration versus axial position for 90° cw ($\dot{m}_a$ = 6.0 lbs/sec, ϕ = .217, p = 5 atm)	62
3-13.	CO concentration versus axial position for 180° cw ($\dot{m}_a$ = 6.0 lbs/sec, ϕ = .217, p = 5 atm)	63
3-14.	Schematic of postulated primary and secondary zone flow pattern for the J-33 combustor	65
3-15.	Combustor exit plane temperature traverse (probes in locations numbered one in Fig. 3-3)	67

Figure		Page
3-16.	Combustor exit plane temperature traverse (probes in locations numbered two in Fig. 3-3)	68
3-17.	Radial NO concentrations at combustor exit plane versus air flow rate (average)	70
3-18.	Radial NO concentrations at combustor exit plane versus air flow rate	71
3-19.	Radial CO concentrations at combustor exit plane versus air flow rate (average)	72
3-20.	Radial CO concentrations at combustor exit plane versus air flow rate	73
3-21.	Radial NO concentrations at the combustor exit plane versus overall equivalence ratio (average)	76
3-22.	Radial NO concentrations at the combustor exit plane versus overall equivalence ratio	77
3-23.	Radial CO concentrations at the combustor exit plane versus overall equivalence ratio (average)	78
3-24.	Radial CO concentrations at the combustor exit plane versus overall equivalence ratio	79
3-25.	Radial NO concentrations at combustor exit plane versus pressure (average)	80
3-26.	Radial NO concentrations at combustor exit plane versus pressure	81
3-27.	Radial CO concentrations at combustor exit plane versus pressure (average)	82
3-28.	Radial CO concentrations at combustor exit plane versus pressure	83
4-1.	Complete combustion facility schematic	87
A-1.	Normalized concentration versus inverse temperature	97

ABSTRACT

Because of the possible future widespread use of the gas turbine engine in automobiles, and the imminence of federal emission standards for aircraft, gas turbine combustion and emission characteristics are currently being investigated in earnest. Much information concerning specific pollutant concentrations as measured at the engine exhaust is presently available. Several analytical combustor modeling programs have also been developed (Mellor, 1971). The basic processes of pollutant formation and destruction occurring within the combustor have, however, received little attention to date. In an effort, therefore, to obtain this fundamental type of experimental information, a gas turbine combustion facility has been designed and constructed.

After a review and description of the combustion facility, results are presented which include gas temperature, carbon monoxide, and nitric oxide concentration profiles as a function of axial and radial position inside an Allison J-33 combustor. In addition some combustor exit plane measurements are reported. Specifically, the isolated effects of combustor pressure, overall equivalence ratio, and air flow rate on CO and NO concentration at various radial positions are investigated. These results are qualitatively explained in terms of basic combustor processes.

Unheated combustor inlet air was used for the above studies; a few preliminary experiments using heated air are also described.

I. INTRODUCTION AND SUMMARY

Emissions from various types of combustion systems have been investigated in some detail in recent years. Government legislation has attempted to force the advancement of emission control technology through the establishment of federal emission standards for many mobile and stationary pollution sources. As effort has been expended to meet the federal emission standards, continuous flow combustion systems have received increasing attention. A continuous flow combustion device of wide application is the gas turbine.

Because reasonably precise control of the combustion process is possible in a gas turbine combustor, it is felt to possess inherent emission control advantages over other types of combustion systems. In a gas turbine combustor, for example, it is theoretically possible and practically realistic to tailor the combustion zones to those conditions of local equivalence ratio best suited to total emission reduction. In general, this tailoring of the combustion zones is made possible because of the relative freedom of the combustor designer to specify the combustion chamber configuration. This configuration, of course, controls such things as fuel and air flow distributions, recirculation patterns, residence times, and other parameters of importance in emission control.

In contrast, the combustion event in the spark or compression ignition engine combustion chamber is difficult to control. Those techniques which have been utilized to reduce spark ignition engine emissions, such as the alteration of ignition timing and exhaust gas recirculation, have in general resulted in the deterioration of that engine's performance.

Therefore to couple good vehicle performance with a minimum of pollutant emission is one reason that the gas turbine engine is being considered as a possible replacement for spark and compression ignition engines in many vehicular applications.

Because of the possible future widespread use of the gas turbine engine in automobiles, and the imminence of federal emission standards for aircraft (which are in large part powered by gas turbine engines), a definite need exists for fundamental information concerning gas turbine emissions. It is most logical to begin a basic study of gas turbine pollution by investigating the effect of combustor operating parameters on pollutant emissions. It is, however, imperative that the operating parameters be varied individually and that the effect of each single operating parameter change upon pollutant emission levels be noted. To this end, an experimental program, to be discussed in detail in the following pages, has been started.

Briefly, the experimental setup consists of a J-33 combustor burning liquid propane. Variable engine parameters are combustor pressure, equivalence ratio, and air flow rate. Later experiments will also include combustor inlet air temperature. The condition of the engine is monitored remotely during any experimental investigation. A continuous gas-sampling system for the determination of CO, NO and HC concentrations is employed. Samples can be extracted at the exit plane of the combustor as well as at various internal locations. Temperatures are monitored both at the exit plane and internally, using a probe-mounted Pt/PtRh thermocouple.

Exit plane and internal combustor CO and NO concentrations and gas temperatures have been collected. Temperature measurements indicate that strong radial gradients exist, a result of the influence of penetration

jets. CO and NO concentration measurements at various axial positions in the combustor yield the same trends reported in the literature. These internal measurements were for a single operating point.

Exit plane CO and NO concentrations at various radial positions were studied as functions of combustor pressure, equivalence ratio, and air flow rate. Combustor centerline CO concentrations increased with pressure; other radial positions exhibited more erratic behavior. NO concentrations generally increased with pressure. CO and NO exit plane concentrations increased with increasing equivalence ratio for almost all radial positions; this trend is consistent with the observations of other investigators. Increasing air flow rate caused the NO concentrations to decrease only slightly and CO to increase.

II. DESIGN AND OPERATION OF THE EXPERIMENTAL GAS TURBINE COMBUSTION FACILITY

Once the determination was made to pursue in earnest gas turbine pollutant emissions research, the design and construction of an experimental facility capable of realistically simulating gas turbine combustion was necessary. The design, construction, and testing of such a facility occupied the major portion of the preceding year's experimental program. The facility was to be capable of simulating both automotive and aircraft type gas turbine combustion realistically so that combustor operating parameters (pressure, air flow, and overall equivalence ratio) could be varied to determine fundamental trends concerning gas turbine emissions. With the exception only of inlet air temperature (which was not varied for most of the experiments conducted to date), it is felt that the facility to be described is in fact such a realistic simulation and that the data obtained and reported in the following section verify the facility's ability to provide the desired fundamental gas turbine emission information.

This chapter essentially is divided into two sections. The first section provides a description of the test cell hardware and those auxiliary systems necessary for combustor parameter control or component survivability. The second section of this chapter entails a description of control room instrumentation. Included are descriptions of those systems required for monitoring the combustor condition, various temperatures associated with the combustion process, and most significantly, the combustor emissions.

A. TEST CELL HARDWARE

1. Air System Description

Because of the large mass flow rates and high compressor pressure ratios used in many modern aircraft gas turbine engines, a large air compressor network is essential to any research laboratory attempting to study realistic gas turbine combustion. The air compressor system which supplied the test facility had a capacity of approximately 3000 cu ft and could provide air system pressures of up to 2400 psig. Sustained air flow rates of 6 lbs/sec were possible for run durations of approximately 40 minutes under normal combustor operating conditions. In addition, the basic combustion system could pass air flow rates of up to 10 lbs/sec for short periods. Although the main air system compressors were in service throughout any run situation, the system was basically of the blowdown type. To date the air system has proven satisfactory for the needs of the program.

The basic test cell air system is shown schematically in Fig. 2-1. The three inch main air supply ducting was of heavy wall carbon steel, and all high pressure control lines were stainless steel. The main air supply system included two 3000 psig inlet capacity remotely controlled air regulators mounted in parallel, a safety burst disc, a 2 1/8 inch orifice type flow meter, a pneumatically operated air throttle valve, and finally a diffuser section mounted immediately upstream of the combustor. Orifice plate differential pressure was monitored continuously on a differential pressure gage in the control room and recorded permanently and continuously through a differential pressure transducer/Ellis bridge amplifier/Honeywell Model 1508 Visicorder system.

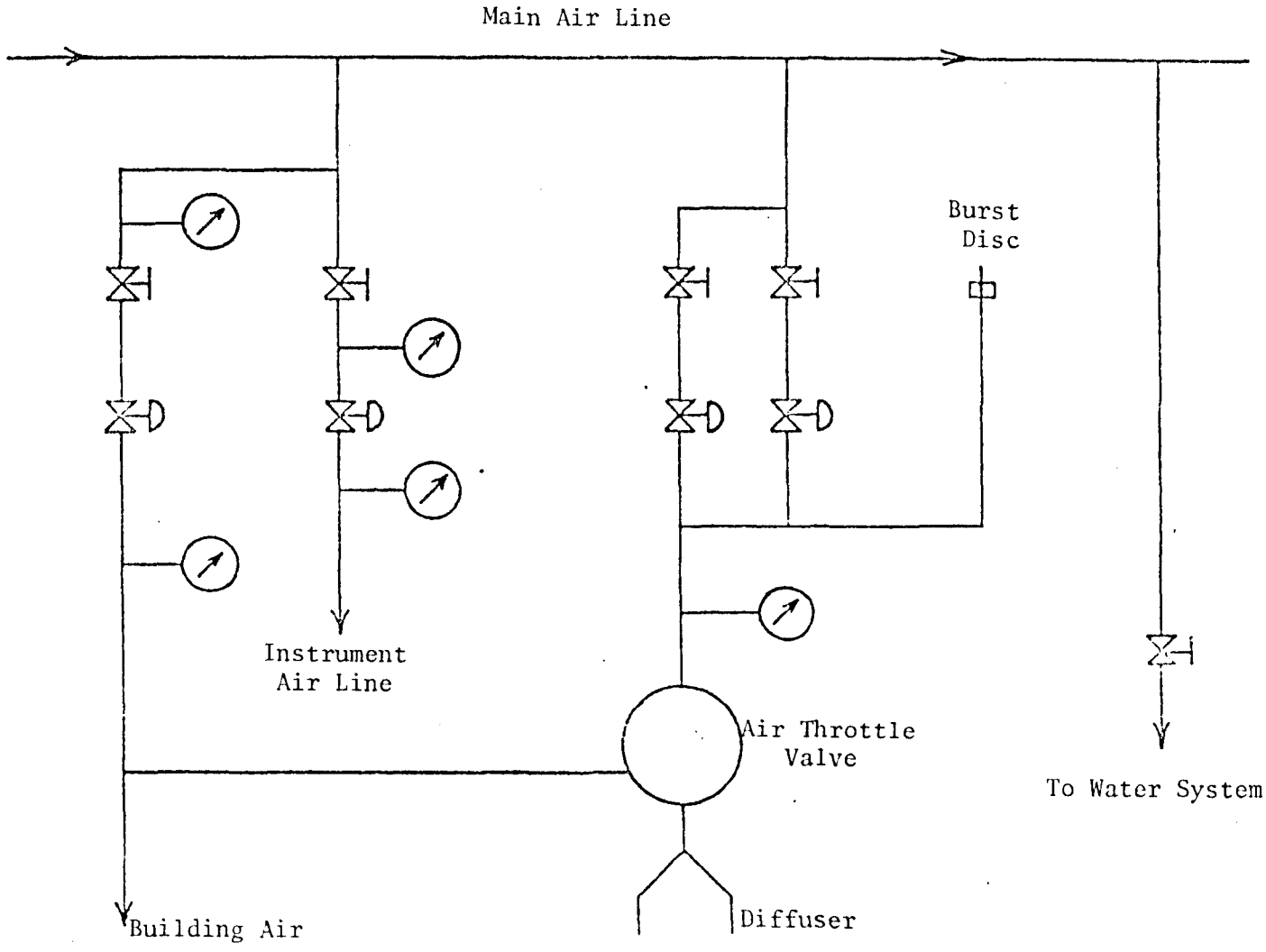

Figure 2-1. Combustion facility air system

2. Fuel System Description

The fuel used in the combustion study was commercial purity liquid propane since it is inexpensive and readily available. The fuel system is shown schematically in Fig. 2-2. When the 500 gallon storage tank was pressurized with nitrogen, the five 10 in x 10 ft cylindrical steel fuel delivery tanks were filled from the storage tank. This tank was then isolated, and the fuel delivery tanks were pressurized to the desired supply pressure using a ten bottle nitrogen supply manifold. All fuel flow was passed through a suitable fuel filter and then underground to the test cell area. Fuel flow rate was controlled through a pneumatically operated fuel throttle valve and measured using a Potter turbine flow meter. Frequency converters were used to convert the flow meter output to a calibrated milliamp output signal. Like the air flow, fuel flow was also permanently and continuously recorded using a six channel Honeywell Visicorder.

In the interests of safety the main fuel system tanks were positioned away from the test cell area, stainless steel lines and fittings were extensively used, both manual and solenoid type vent valves and automatic pressure relief valves were judiciously placed at various system locations, and all fuel system pressures were continuously monitored. The fuel system as shown in Fig. 2-2 has performed satisfactorily to date.

3. Combustor Description

In the initial facility configuration all combustion occurred in an Allison J-33 turbojet combustor mounted in a stainless steel converging housing. The combustor housing, in turn, was secured to a thrust table. The standard J-33 fuel nozzle and conventional magneto-energized igniter

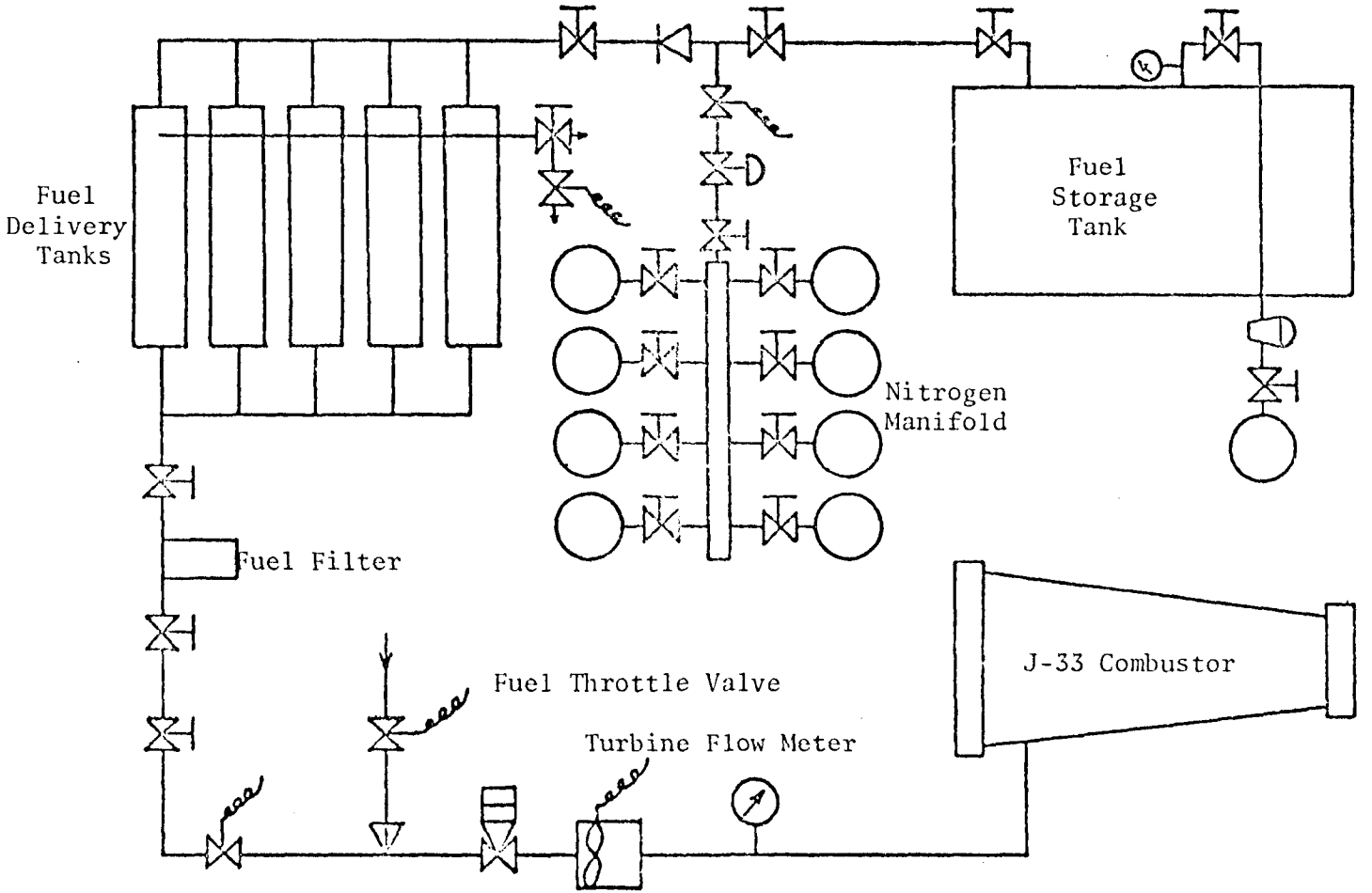

Figure 2-2. Combustion facility fuel system

were employed. The basic combustor arrangement is shown in Fig. 2-3. In order to provide the necessary experimental data for a simultaneous analytical heat transfer study, the J-33 flame tube was outfitted with several chromel-alumel thermocouples; the results of this study have been reported by Owens (1972). Through the courtesy of the Detroit Diesel Allison Division of General Motors, the J-33 design resume shown in Table 2-1 was obtained.

4. Probe Addition Section Description

The J-33 combustor casing exit was flanged to accept the probe addition section as shown in Fig. 2-4. The purpose of this stainless steel section was to change the direction of the exhaust gas flow such that a probe could be directly inserted into the combustor. The surface of this section was wrapped with copper water cooling lines, and the probe window was cooled with injected nitrogen. Fig. 2-5 schematically shows the overall facility configuration.

5. Probe Description

The combustion chamber of a gas turbine engine is a most severe environment. It is characterized by relatively high mass flows, excessive turbulence, large temperature gradients, high pressure in many cases, recirculating flow patterns, and extremely high local temperatures which in some locations approach the adiabatic flame temperature. The task of designing a probe capable of surviving this type of environment for long periods of time is very challenging. Some probe failures have in fact been mentioned in the open literature for probes attempting to sample gas turbine engine exhaust at the engine exit station (Hare et al.,

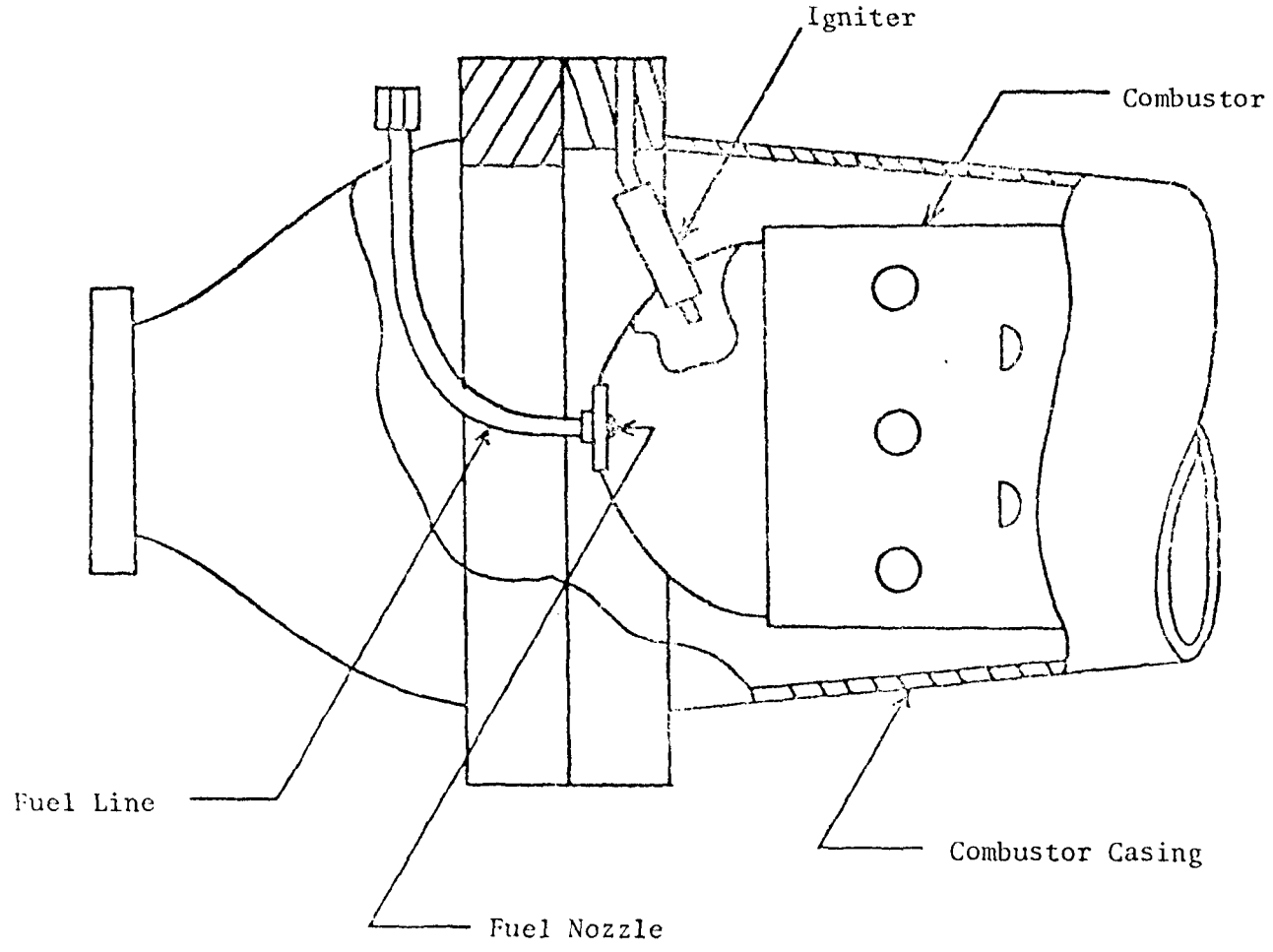

Figure 2-3. Combustor arrangement

Table 2-1. J-33 Design Resume

Military Air Flow	7.64 lbs/sec
Normal Air Flow	7.17 lbs/sec
Military Inlet Temperature	435° F
Normal Inlet Temperature	390° F
Military Inlet Pressure	141 in Hg abs
Normal Inlet Pressure	126 in Hg abs
Military Volume Flow	40.7 cu ft/sec
Normal Volume Flow	40.9 cu ft/sec
Average Pressure Loss	4.5%
Liner Cooling Air Flow	8.0%
Primary Combustion Air Flow	23.4%
Secondary Combustion Air Flow	68.3%

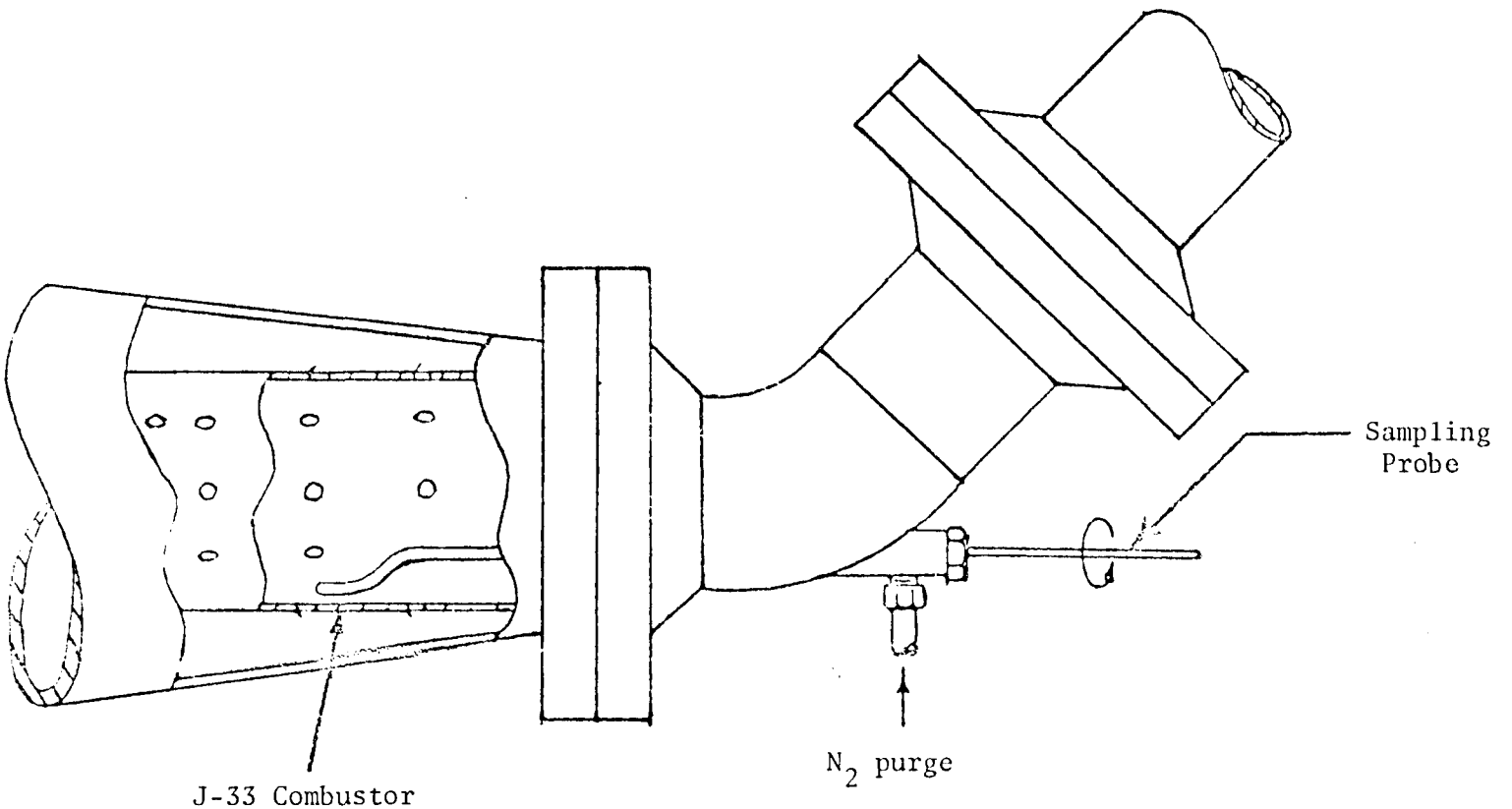

Figure 2-4. Combustor and probe addition section

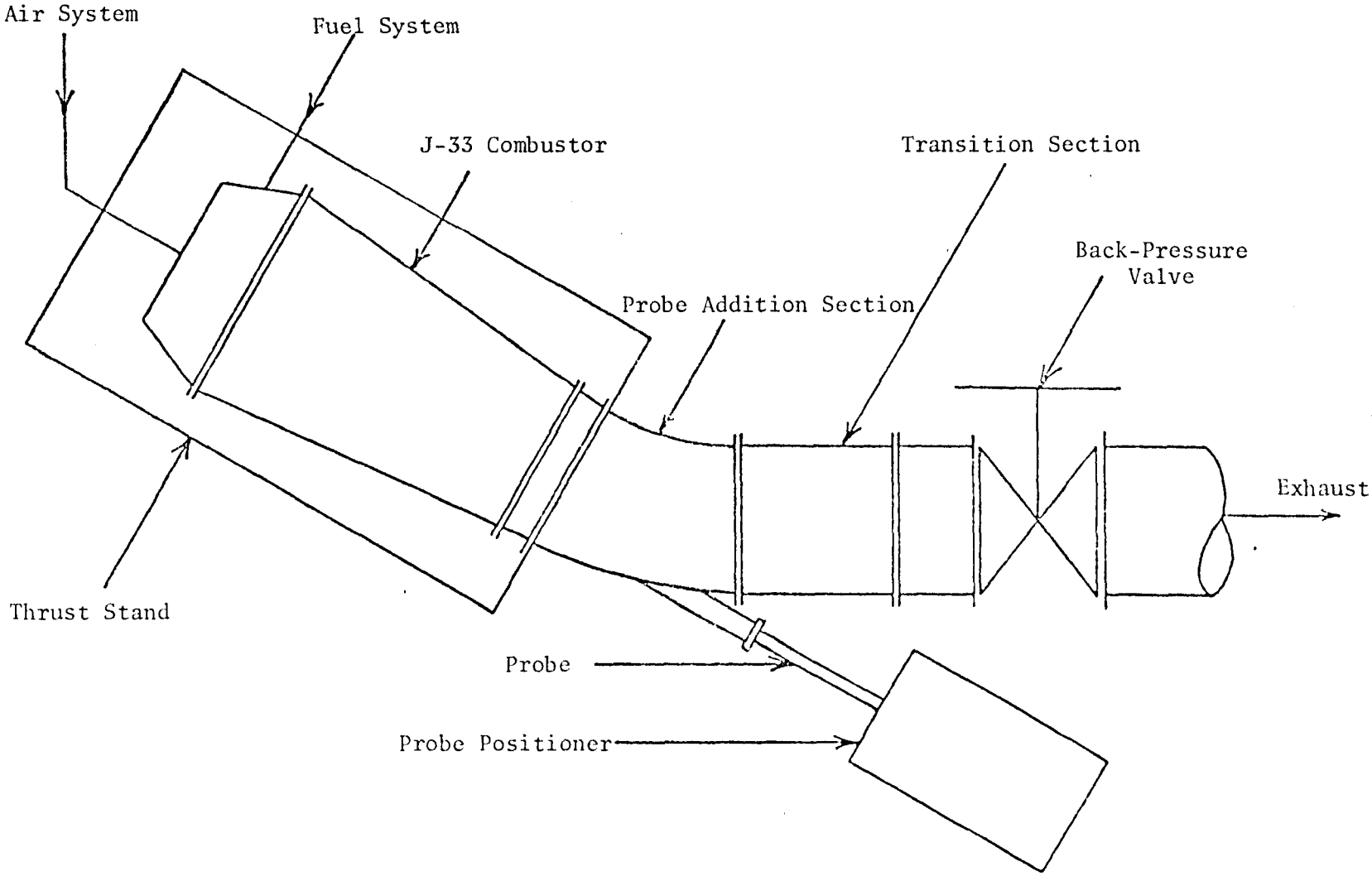

Figure 2-5. Combustion facility schematic

1971). It is apparent that the engine exit station, although itself a severe environment, is orders of magnitude less severe than the combustion chamber. The probe design which is to be reported below was found able to withstand the combustor environment. One probe has sampled combustor exit plane gases for approximately eleven hours with only the development of a relatively minor probe tip leak during the eleventh hour and has also sampled within the combustor for approximately 85 minutes (including a large fraction of that time sampling from the primary zone). A second probe of similar design has withstood over two hours inside the combustor.

The development of the final successful probe design reflected the difficulties mentioned above. Two early probe designs failed quickly but did provide through their failure the information needed to design an acceptable probe.

The intent of the probe was to sample gases and monitor gas temperature at various axial and radial positions within the combustor or at the combustor exit. For purposes of gas temperature measurement a platinum/10% platinum rhodium thermocouple (MgO insulation, sheathed in inconel) was mounted through small "half-moon" shaped sections directly to the side of a gas sampling probe; the resulting bead position was about 1/16 in ahead of the gas sampling tip. The thermocouple was of the exposed junction type and was intended to provide only gross estimates of the local combustor temperatures. A 1/16 in diameter thermocouple with .01 in wires failed, however, to provide the desired temperature estimates. Typical behavior was as follows: upon insertion of the probe into the combustor the thermocouple provided reasonable temperature estimates. After the probe was rotated through approximately 90°, however,

the thermocouple signal became very erratic possibly indicating an intermittent breaking and making or short-circuiting of the thermocouple lead. The same behavior was noted with two other Pt/10%PtRh thermocouples of similar dimensions. Consideration of the very brittle nature of the platinum leg of this thermocouple indicated that the failure of the two thermocouples was caused, most probably, by stresses in the platinum leg induced through the mechanical rotation of the probe. New 1/8 in diameter thermocouples with .025 in wire diameter and with the platinum leg replaced by "Fibro Platinum" (which is better able to withstand turbulent high temperature conditions) have been mounted to the probe for subsequent temperature measurements and proved satisfactory for the experiments conducted to date.

The probe was inserted into the J-33 combustor through the probe addition section (see Fig. 2-4) and supported both at the probe window and at the cradle of the probe positioner (to be described later). The gas sampling portion of the probe body consisted of three concentric 316 stainless steel tubes as shown in Fig. 2-6. The relative position of the three concentric tubes was maintained through the use of several small welded beads at various locations along the length of the probe, and three distinct passages inside the probe body were thus assured. Pressurized cooling water entered the probe at the probe block (Fig. 2-7) and flowed to the probe tip in the outer annulus. At the probe tip the cooling water flow was reversed (see Fig. 2-8) and proceeded through the center annulus back to the probe block where it exited. The center probe body tube carried sample gases to the gas sampling system delivery lines. Cooling water flow pressure was variable to approximately 250 psig.

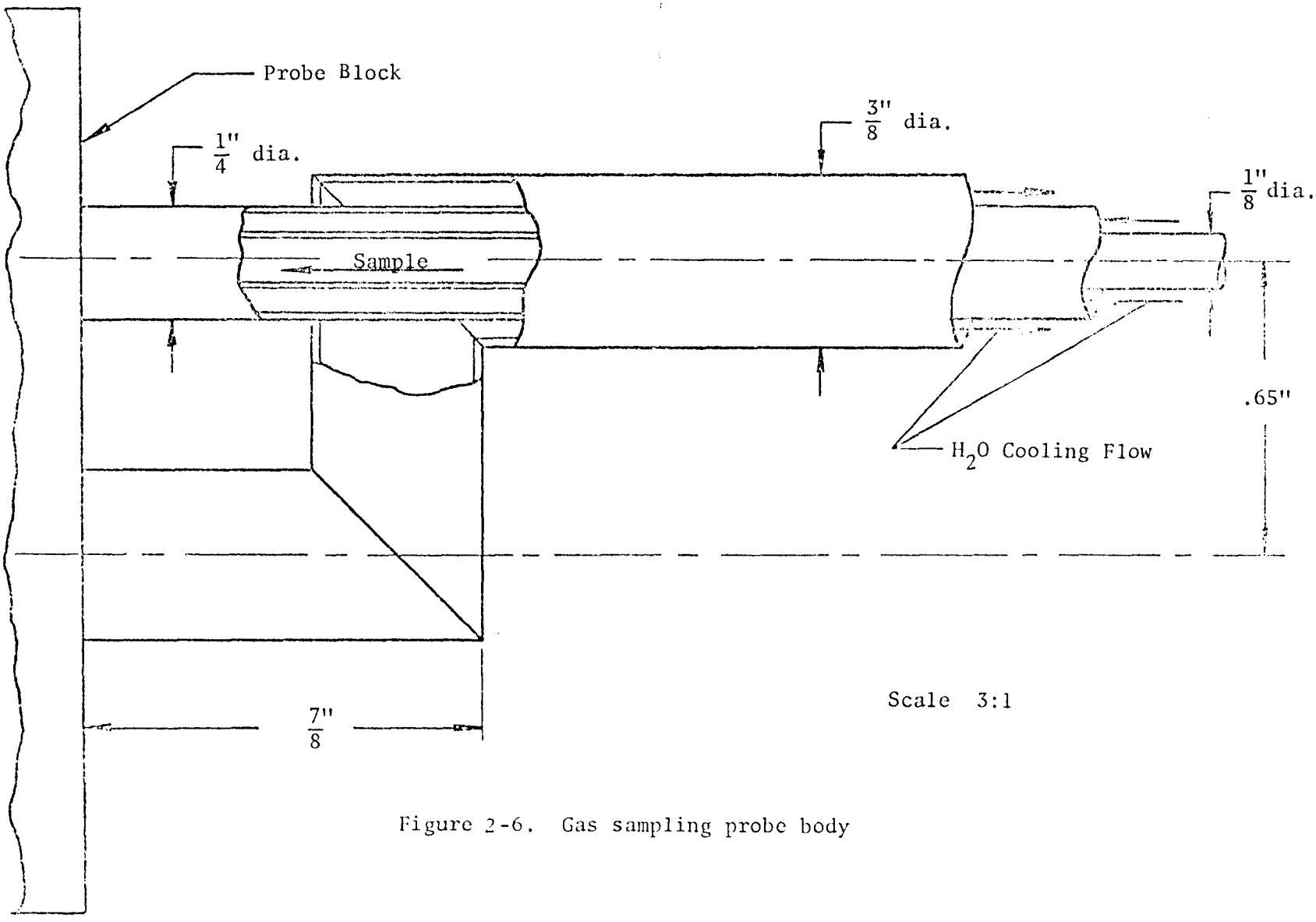

Figure 2-6. Gas sampling probe body

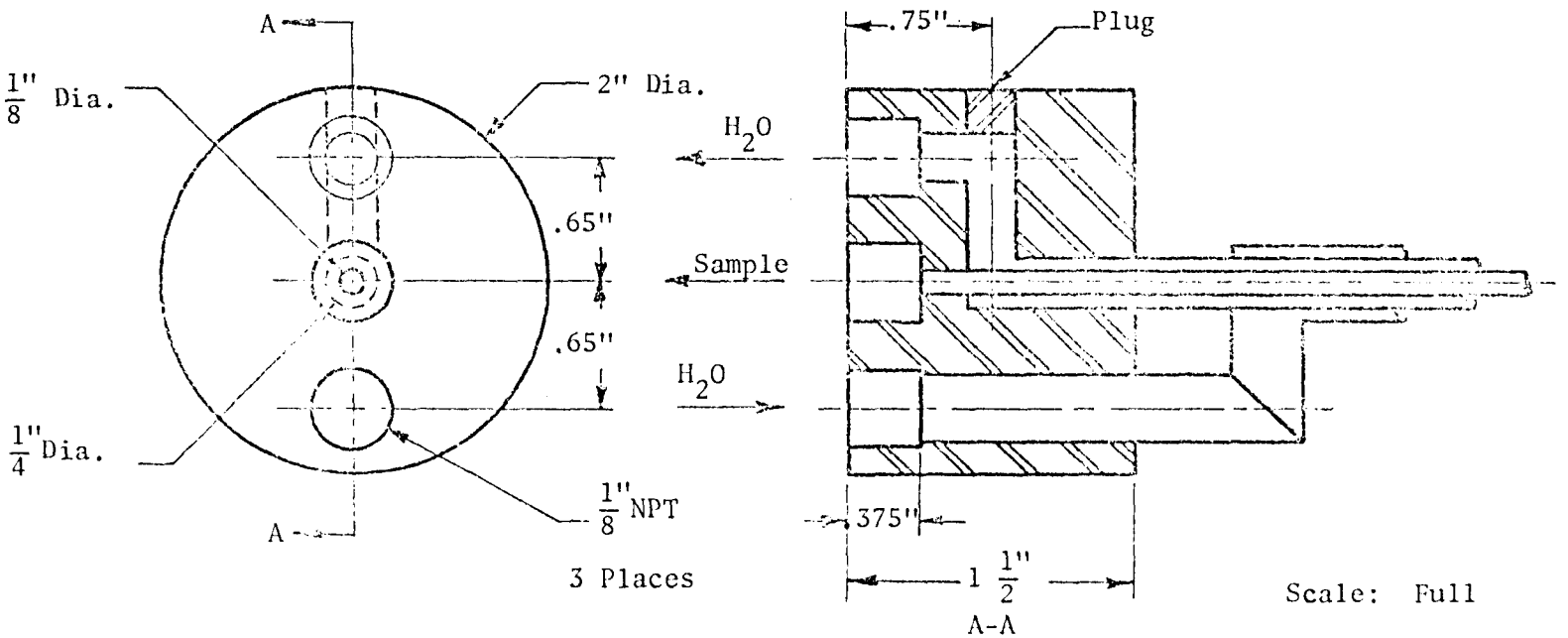

Figure 2-7. Gas sampling probe block

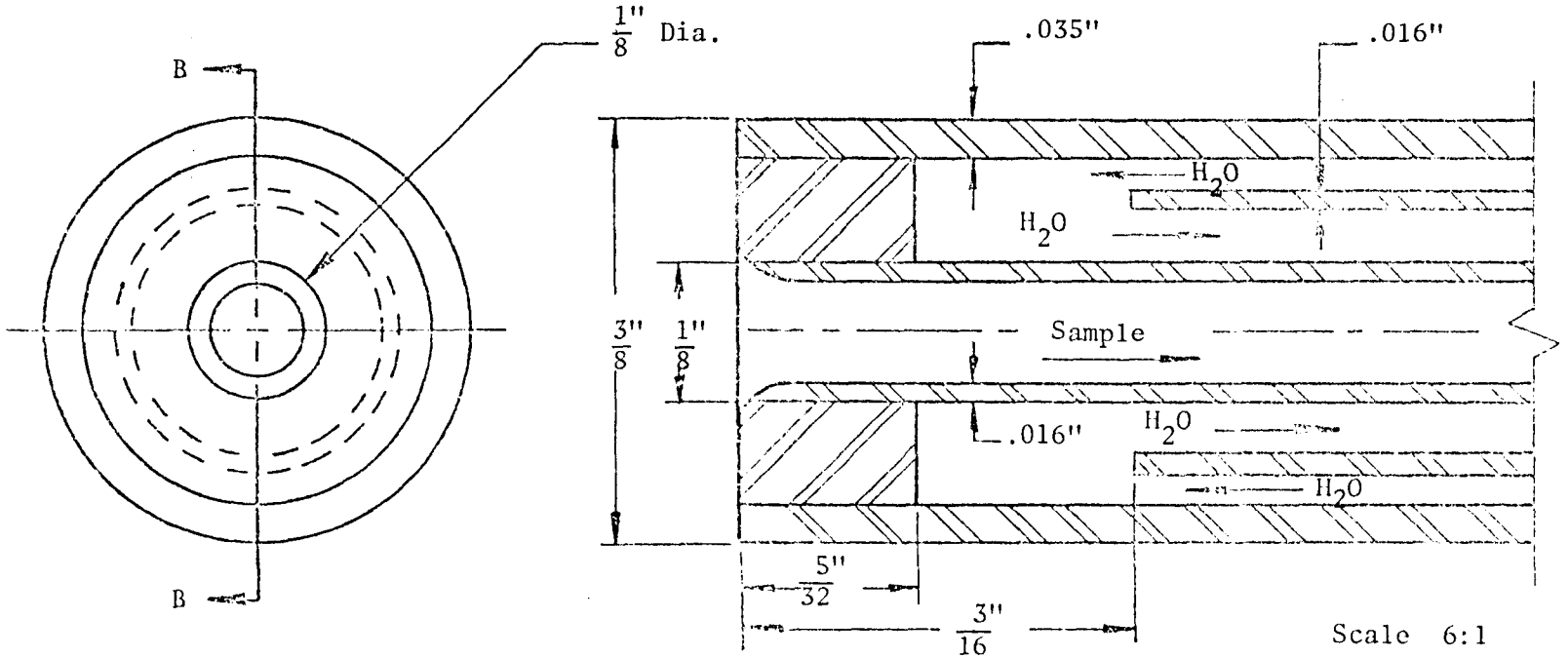

Figure 2-8. Gas sampling probe tip

The design of the gas sampling tip reflects consideration of the requirements inherent in any suitable sampling probe design as well as consideration of those factors peculiar to the particular combustor environment encountered. In order to obtain accurate information concerning combustor gas composition, the composition of the gases at the entrance of the gas sampling probe must be essentially identical to the gas composition at the entrance of the emission monitoring instrumentation. In other words, all gas reactions must be quenched in the shortest possible distance in the sampling probe. One ideal way in which to accomplish this immediate quenching entails the use of a converging-diverging probe tip nozzle for rapid sample flow acceleration and expansion. As the sampled gases then flow through the probe body, additional reduction in gas static temperature may be realized through the added quenching effect provided by the probe cooling water flow. These two combined quenching methods have been used frequently in the past in elementary flame studies and other assorted combustion experiments.

However, one of the operating characteristics of the J-33 combustor-fuel nozzle combination used in the subject research was the rapid increase in carbon formation associated with operation at superatmospheric pressures. Consequently, the final probe tip design shown in Fig. 2-8 represents a compromise between the ideal sampling probe and a probe able to withstand the combustor environment. For example, the ideal sampling probe would be of infinitesimal diameter to prevent flow disturbance whereas a working probe must be of sufficient diameter to allow a suitable cooling water flow, as well as provide sufficient structural rigidity to withstand the combustor environment. Similarly, an ideal sampling probe tip would

consist of a converging-diverging nozzle; however, such a tip could not be constructed so that mechanical integrity could be maintained and blockage by soot prevented. Thus the final tip design and dimensions shown in Fig. 2-8 were finalized. As an added safeguard against the possibility of carbon blockage, the probe gas sampling tube was purged with nitrogen during all combustor starts, all purposely induced combustor transients, all probe rotations, and all combustor shutdowns. Whereas probe blockage had consistently occurred with the earlier probe designs, this major inconvenience was successfully avoided through the use of the above mentioned operating procedures and probe design.

In order to obtain a circular probe trace upon probe rotation, the tip section of the probe was offset from the probe centerline by a distance of 1 9/32 in following Sawyer et al. (1969). This offset, as well as probe body, block, mounting plate, and drive gear are shown in Fig. 2-9.

6. Probe Positioner Description

As previously mentioned, gas sampling and temperature measurements were made inside the J-33 combustor as a function of axial and radial position. For the purpose of providing accurate, reproducible, and remotely controllable positioning of the probe tip within the combustor, the probe positioning system as shown pictorially in Fig. 2-10 was constructed. The circular probe block was positioned inside a roller bearing pressed into the probe mounting plate. The probe mounting plate in turn was attached adjustably to the positioner carriage. Remotely controllable longitudinal movement of the positioner carriage was accomplished through a worm gear/electric motor combination. A series of micro-switches

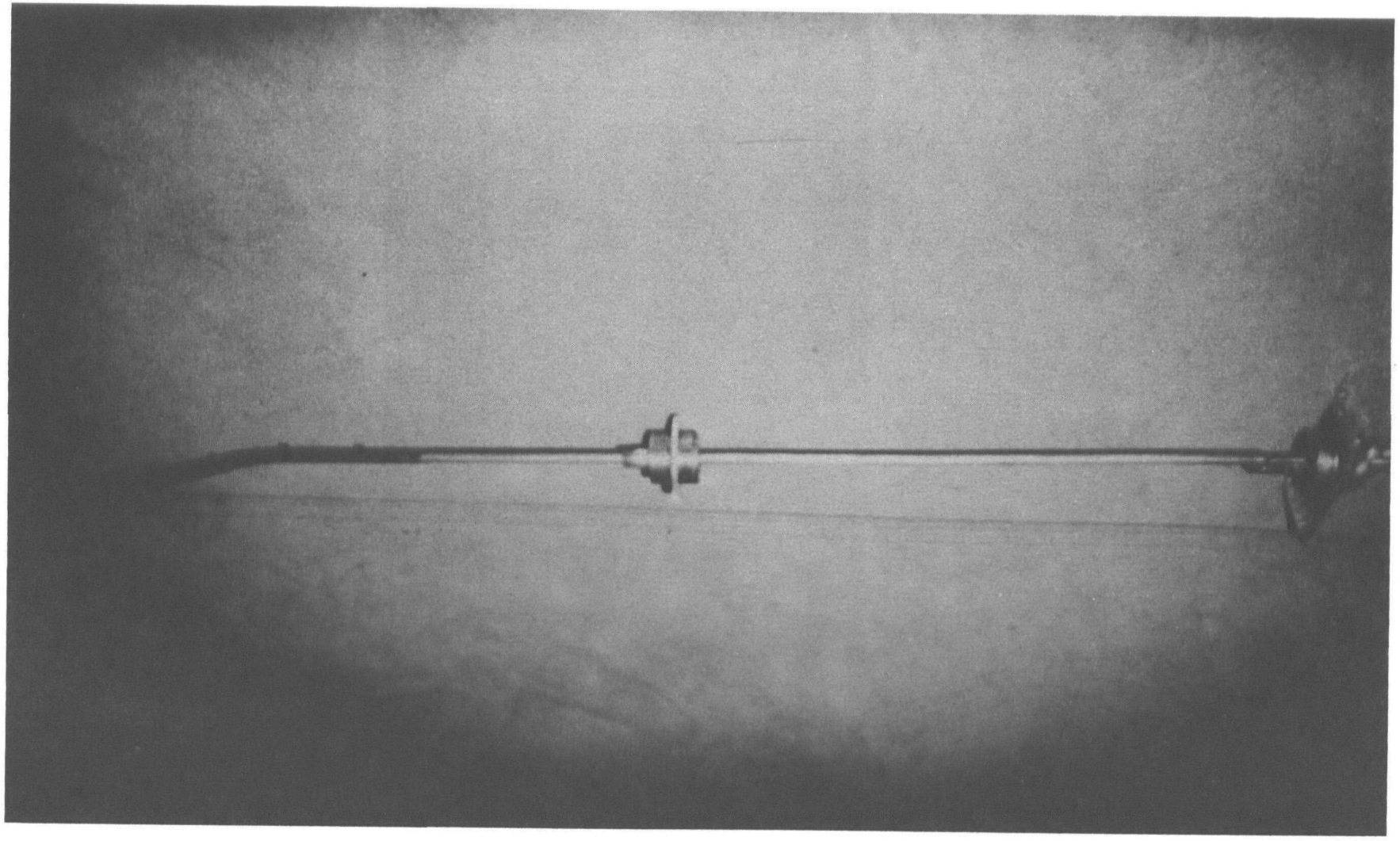

Figure 2-9. Gas sampling probe

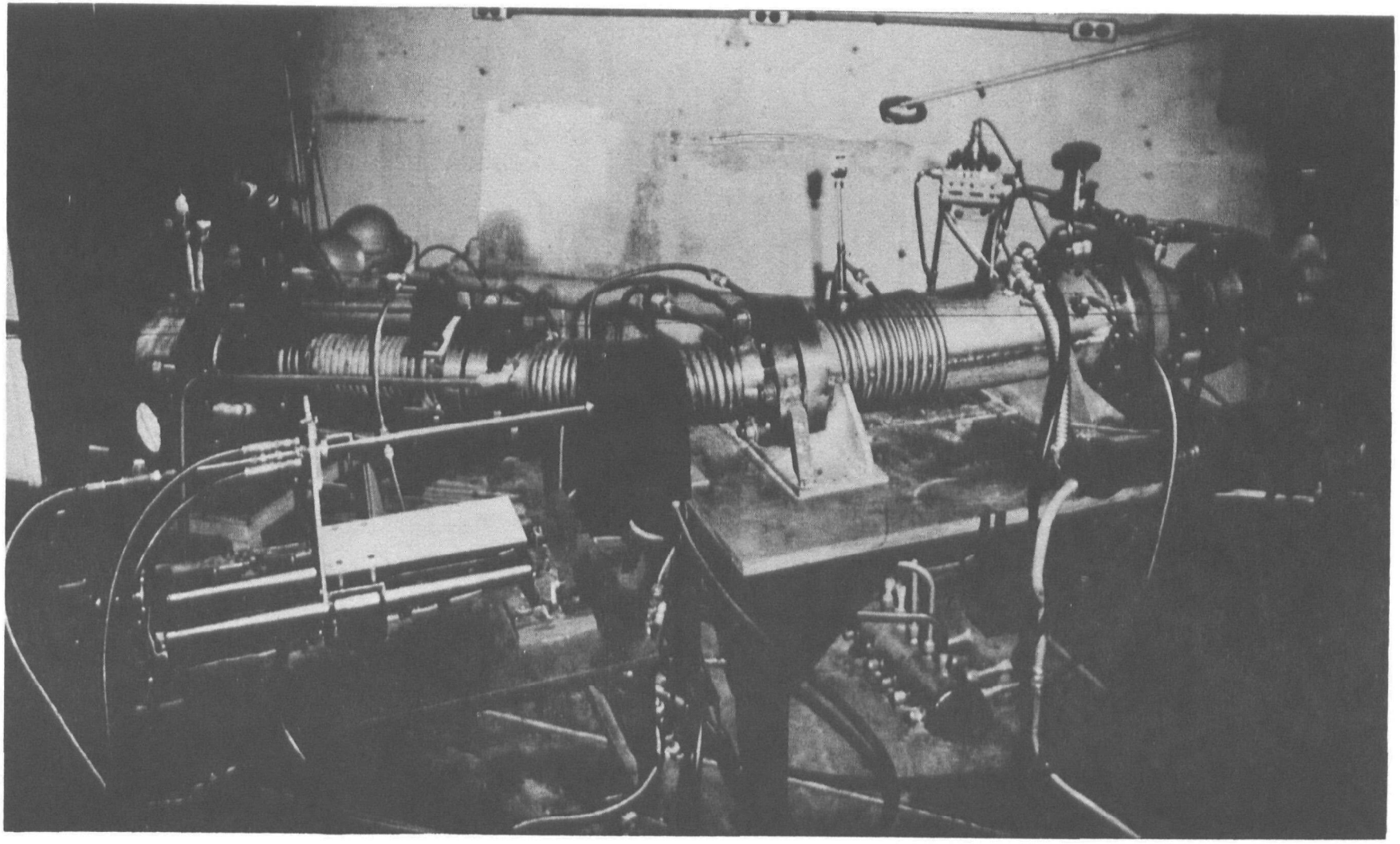

Figure 2-10. Gas sampling probe and positioning systems

(see Fig. 2-11) aligned parallel to the carriage travel and actuated by a cam extending from the positioner carriage provided accurate control room information concerning the probe tip axial position by lighting appropriate control panel lamps. To achieve remotely controllable probe rotation an electric motor/drive gear combination was mounted on the thrust stand near the probe addition section window. This drive gear then meshed with the probe gear (seen in Fig. 2-9) which was welded to a collar mounted on the probe body. A small, rounded pin extended through the collar and traveled in a smooth longitudinal slot which had been machined in the probe body. In this way the probe body was allowed to slide axially through the collar but was prevented from rotating relative to the collar. A helipot driven by the probe gear and constituting part of a battery powered electrical circuit impressed a variable voltage on the Honeywell Visicorder. After calibration of this assembly, the probe radial position was continuously and permanently recorded via the oscillograph trace. Both axial and radial remote probe positioning schemes performed satisfactorily through the extent of the research effort.

7. Back-Pressure System Description

In order to simulate modern gas turbine combustion, certain requirements are imposed upon combustor pressure. In general aircraft gas turbine applications, combustor pressures on the order of 15 atmospheres are common. However, in automotive gas turbine applications combustor pressures rarely exceed six atmospheres. Therefore, in an attempt to construct a facility acceptable for general gas turbine combustion research, it was necessary to provide the capability for continuous combustor

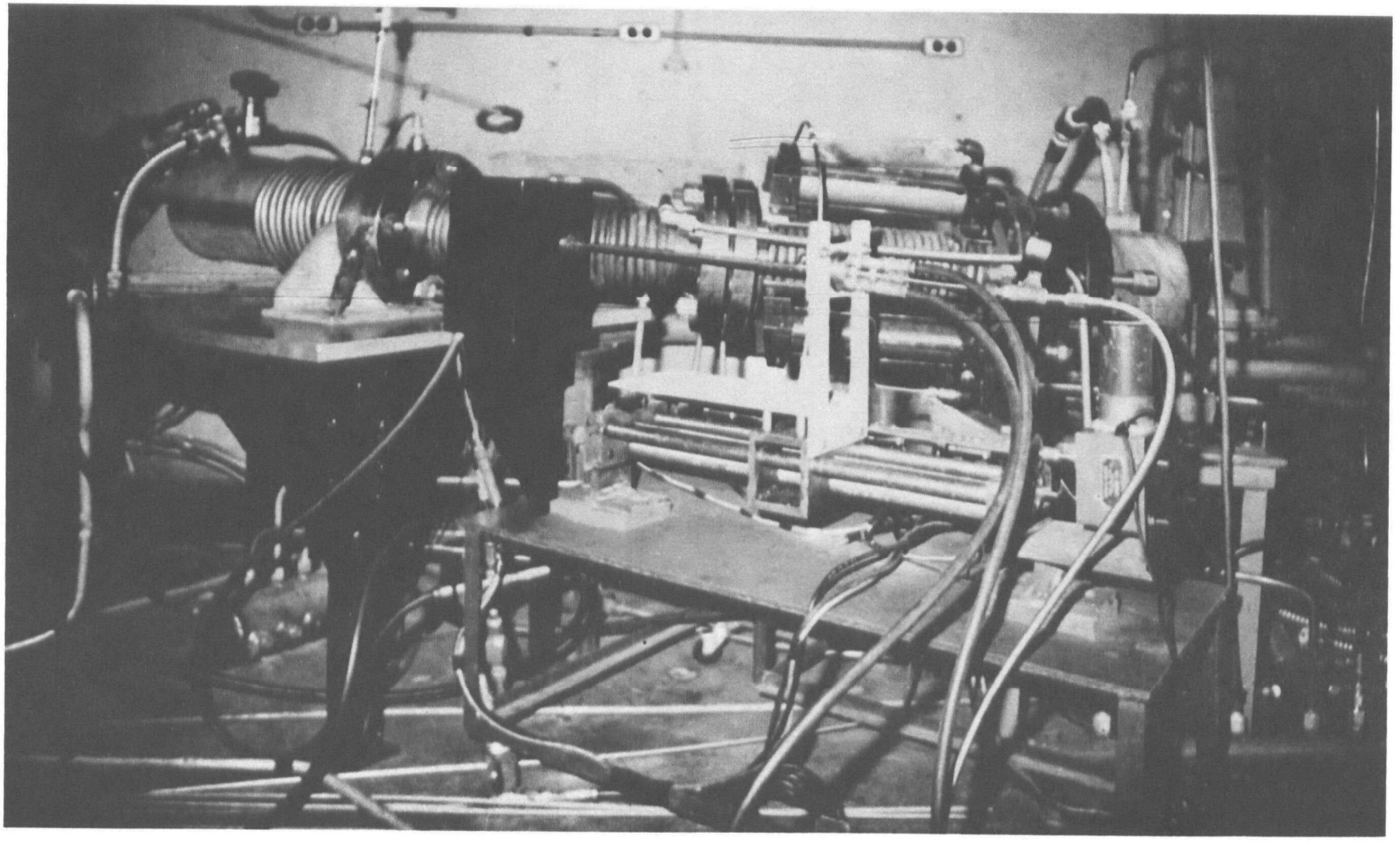

Figure 2-11. Axial and radial (black box) probe positioners

pressure regulation from 1-15 atmospheres. The device designed for this purpose and shown in Fig. 2-12 and 2-13 consists of a translating, conical center-body, a beveled engine exit plane surface, and two concentric cylinders.

To insure the survival of the center-body in the hot exhaust gas stream, pressurized cooling water was forced through a large number of small holes drilled through the front center-body cone. This method of cone cooling essentially placed a protective sheet of water over the leading cone surface and to date has successfully prevented any noticeable erosion of the center body cone.

As can be seen in Fig. 2-13 the translating section of the back-pressure valve assembly was mounted on a dolly and accurately guided in movement through the use of linear bearings and precisely positioned hardened and ground steel guide shafts. Adjusting mechanisms were provided on the dolly to insure the accurate positioning of the center-body cone and concentric cylinders.

Control of combustor pressure was effected through the action of three air cylinders mounted on the engine transition section (Fig. 2-13) and connected to the translating section of the back-pressure valve. By increasing air cylinder pressure the back pressure valve cone was forced forward effectively reducing the engine exit area and thereby increasing combustor pressure. The positioning of heavy springs against the piston head on the unpressurized side of each air cylinder eliminated the jerking effects of starting friction on the translating section motion and also insured that atmospheric combustor pressure would be realized in the event of an air system failure. To date relatively precise and remote control

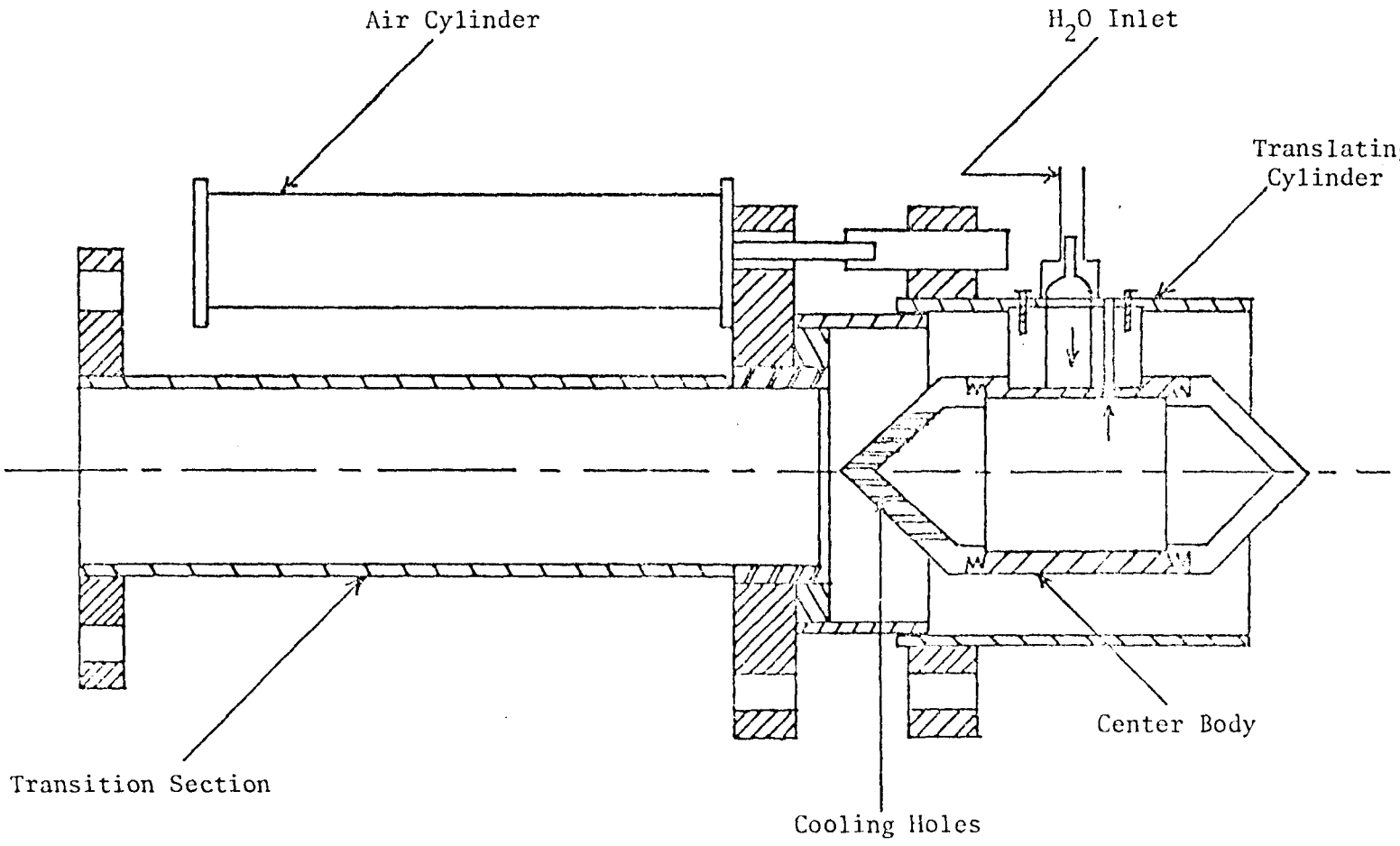

Figure 2-12. Back pressure valve schematic

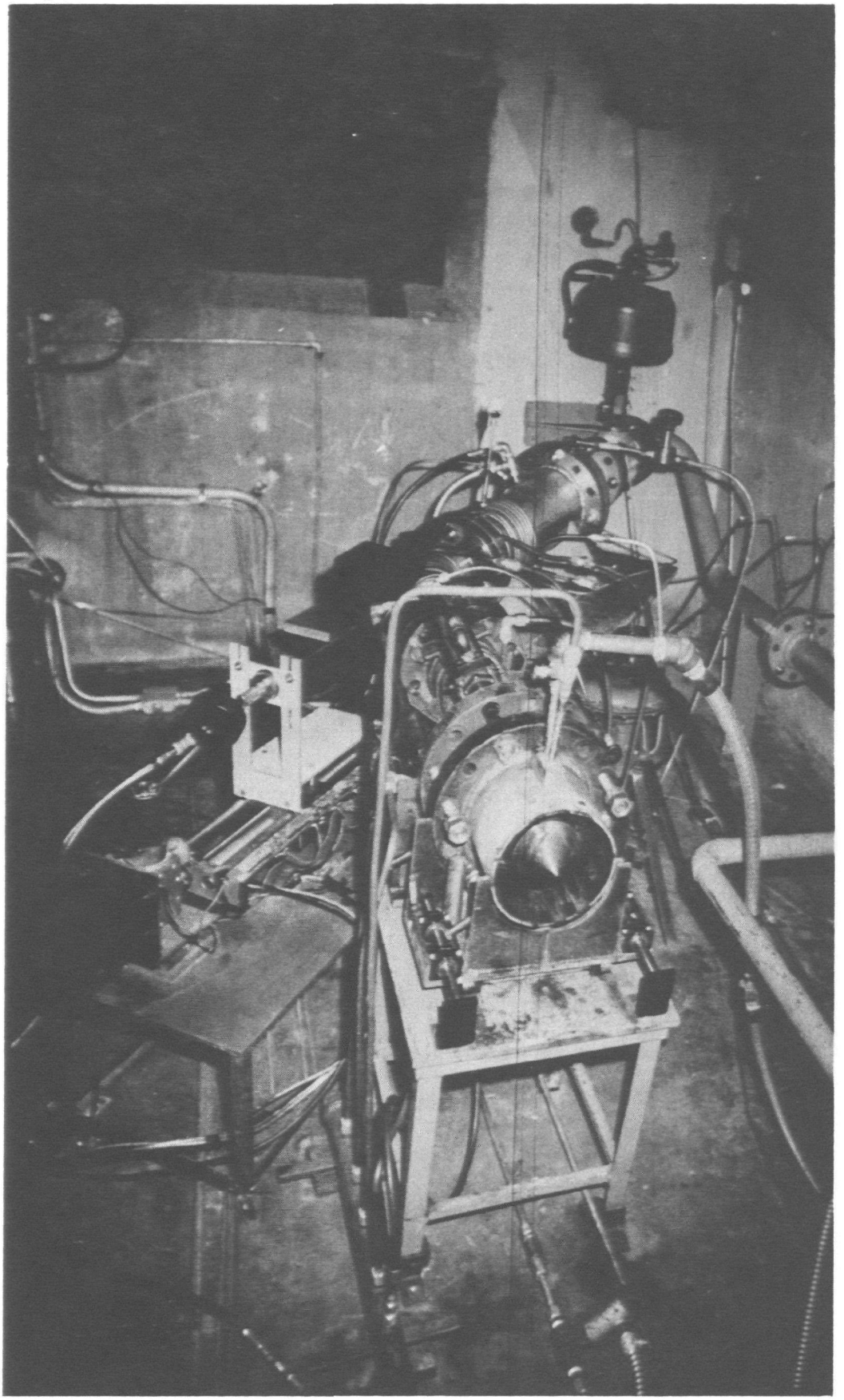

Figure 2-13. Back pressure valve guidance system and engine

of combustor pressure to a value of 10 atmospheres has been routinely achieved.

8. Water System Description

In order to provide adequate cooling for the back-pressure valve cone and the gas sampling probe, a high pressure water supply system was designed and installed and is schematically shown in Fig. 2-14. The total system capacity was approximately 1000 gallons and could supply water as necessary at pressures up to 400 psig. For the purposes of insuring satisfactory water flow control, a remotely actuated main water throttle valve was installed and found to function well. All system pressures were monitored continuously from the control room.

B. CONTROL ROOM INSTRUMENTATION

Prompted by the magnitude and complexity of the experimental research effort and in the general interest of safety, all test cell activity was monitored from a separate control room. The instrumentation assembled within the control room can be conveniently divided into three broad categories. The first consists of that instrumentation necessary for the safe and accurate control of all systems relating to the actual operation of the main combustion system. These systems have been discussed previously and, therefore, need no further comment. The second class of instrumentation to be briefly discussed includes all temperature monitoring systems assembled for the research. The final instrumentation category, and one of utmost importance to the objectives of the research, includes all continuous flow emission monitoring

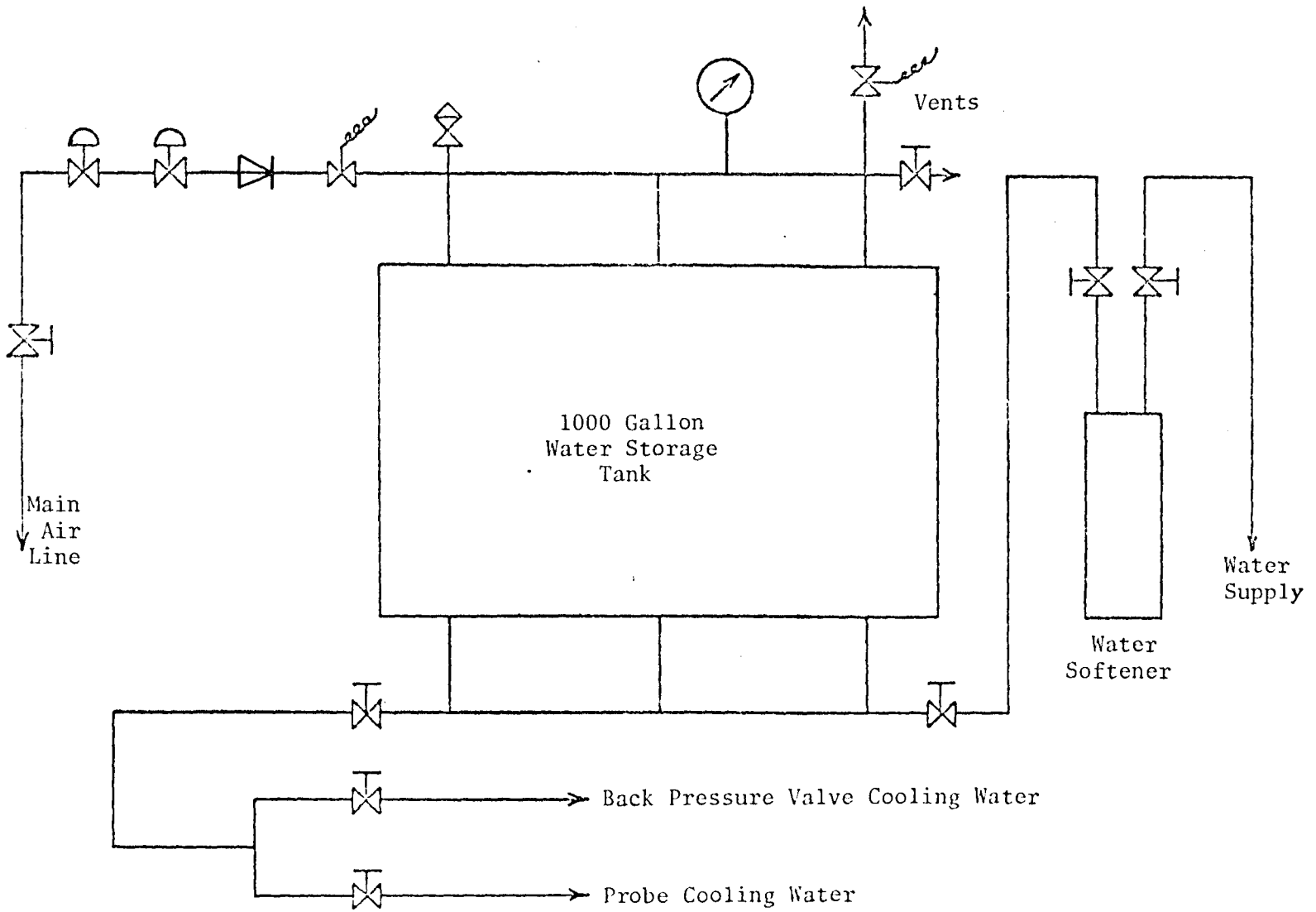

Figure 2-14. Combustion facility water system

equipment. These latter systems will be described fully in the following section. A six channel Honeywell Model 1508 Visicorder was used to record the output of the CO, NO, and HC detectors, as well as probe position and air and fuel flow rates, as mentioned previously.

1. Temperature Monitoring Instrumentation

In order to monitor the condition of the combustion facility continuously, it was necessary to measure certain important system temperatures. Included in this list were local combustor temperature as measured through the use of a probe-mounted platinum/10% platinum rhodium exposed junction thermocouple. At the combustor exit sampling plane, combustor exit temperatures were measured with two United Sensor Corporation aspirated and radiation shielded chromel-alumel thermocouples. These thermocouple probes were positioned with compression fittings through the combustor casing and could be moved manually to various, accurately known radial depths into the combustor exhaust plane. Specially designed thermocouple positioners were used for this purpose. All thermocouple outputs were recorded continuously on Honeywell class 15 self-balancing potentiometers. The data to be reported were all referenced to a temperature of 0° C.

In addition, the back-pressure valve front cone temperature was monitored during the initial testing of the back-pressure system. Once it was determined that the cone water cooling provisions were more than adequate to insure the cone's survival, this thermocouple was taken out of service.

The final thermocouple employment was in the collection of flame tube wall temperature data to be used in conjunction with an analytical

gas turbine heat transfer study (Owens and Mellor, 1971, Owens, 1972). For this purpose the J-33 flame tube was outfitted with a series of ten chromel-alumel thermocouples. The results of this investigation as well as information concerning the relative positions of the thermocouples and flame tube cooling slots and penetration air holes are presented in Owens (1972).

2. Emission Monitoring Instrumentation

The gas concentrations measured during the present study were predominantly CO and NO, as discussed in Section I; the overall gas sampling system as well as the specific CO, NO, and hydrocarbon detection systems are fully described below.

The sample gas handling system is shown schematically in Fig. 2-15. Unless otherwise noted, all lines, fittings, and other components were stainless steel and/or teflon coated to minimize surface reactions or adsorption causing distortion of the true gas composition as the sample gas was transported to the various analyzers; essentially the techniques recommended by Chase and Hurn (1970) were used.

All instrumentation received span and zero checks before and after each run, as well as frequent zero checks during each run. In addition, the entire sampling system was inspected weekly and cleaned as required.

2.1 The Carbon Monoxide Analyzer System

A Beckman Model 315A (short path) NDIR (non-dispersive infrared) analyzer was used for the continuous monitoring of sample gas CO concentration. The analyzer section of this instrument employed a stacked sample cell configuration with both a 13 1/2 inch cell for a useful range of 0-250 ppm (without back pressure), and a 1/8 inch cell for a

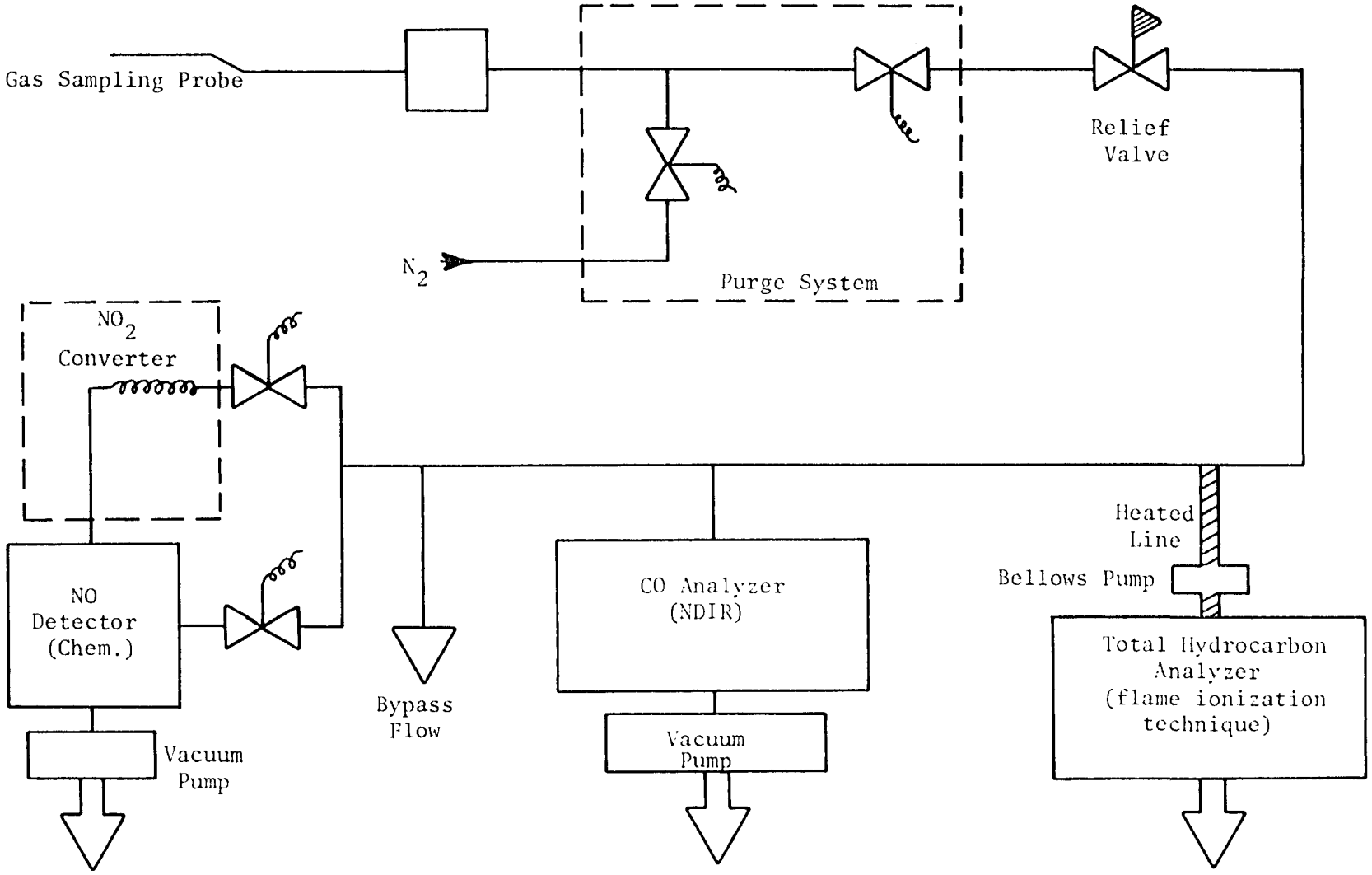

Figure 2-15. Gas handling system

range of 0-20%. In addition, the CO detector flow system incorporated a back-pressure regulator in the 0-250 ppm flow line, which allowed the cell pressure to be increased to 75 psig (limited by the thickness of the sapphire windows in the cell). This modification allowed the lower range sensitivity to be increased to 0-100 ppm full scale. Repeatability for the NDIR measurements was guaranteed to be 1% of full scale reading for both ranges. The specific CO analyzer flow system is shown schematically in Fig. 2-16. Normal CO concentrations encountered in the J-33 combustor dictated the constant use of the 0-20% range.

Condensate traps positioned in the sample line and capable of withstanding 10 atmospheres pressure were reported by Beckman to eliminate the problem of water vapor interference on sampling measurement accuracy. However, it should be mentioned that the presence of CO_2 in concentrations on the order of 300 ppm can cause approximately a 10 ppm CO measurement error.

The normal CO detector sample flow rate was 1600 cc/min. Since for future run conditions low or atmospheric combustor pressure (not conducive to natural sample flow) might be desired, a vacuum pump was installed to insure adequate sample flow to the CO analyzer. For the experiments described in Section III (with combustor pressures of three atm and above), the CO analyzer response time was on the order of one second, indicating rapid passage of the gas sample from the combustor to the instrumentation.

2.2 The Nitric Oxide Analyzer System

The second gas constituent monitored was nitric oxide, and was measured continuously using a chemiluminescent technique similar to that recently developed by Fontijn et al. (1969, 1970). This method involves

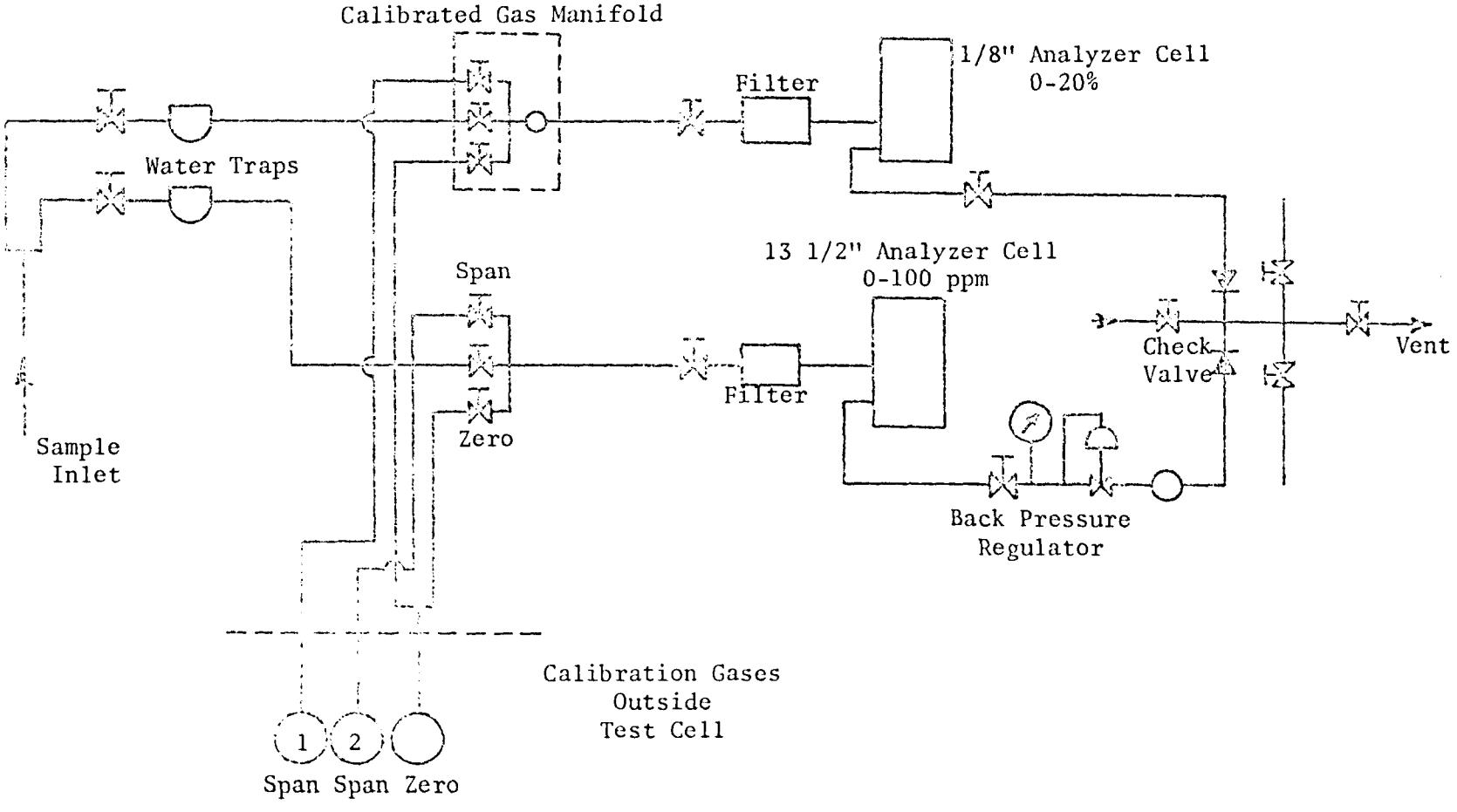

Figure 2-16. CO analyzer system

the measurement of the intensity emitted by the chemiluminescent reaction between nitric oxide and ozone. The NO detector designed and constructed for the present research is shown schematically in Fig. 2-17.

After the completion of the initial construction of the NO detector, the linearity of the instrument and its dark current behavior were thoroughly investigated. For the linearity study a gas mixture of known NO concentration was prepared by a partial pressure technique. A known volume of this prepared NO/N_2 mixture was then injected into the system's exponential dilution flask while N_2 pressure upstream of the dilution flask was maintained at a constant pressure of 100 torr. Total reaction flask pressure was maintained at 3 torr through a microvalve throttling control. The dilution flask nitric oxide concentration will vary according to the equation (Fontijn et al., 1969, 1970):

$$C = C_o \exp(-Qt/V)$$

where

C_o = initial NO concentration in the injected sample

Q = volume flow rate

V = dilution flask volume

t = time

Therefore, if the electrometrometer net signal (i.e., total signal less dark current), when plotted on a semi-log scale versus time, is a straight line, the linearity of the instrument has been shown. After every NO detector system modification, a linearity check was accomplished. The system linearity was always realized.

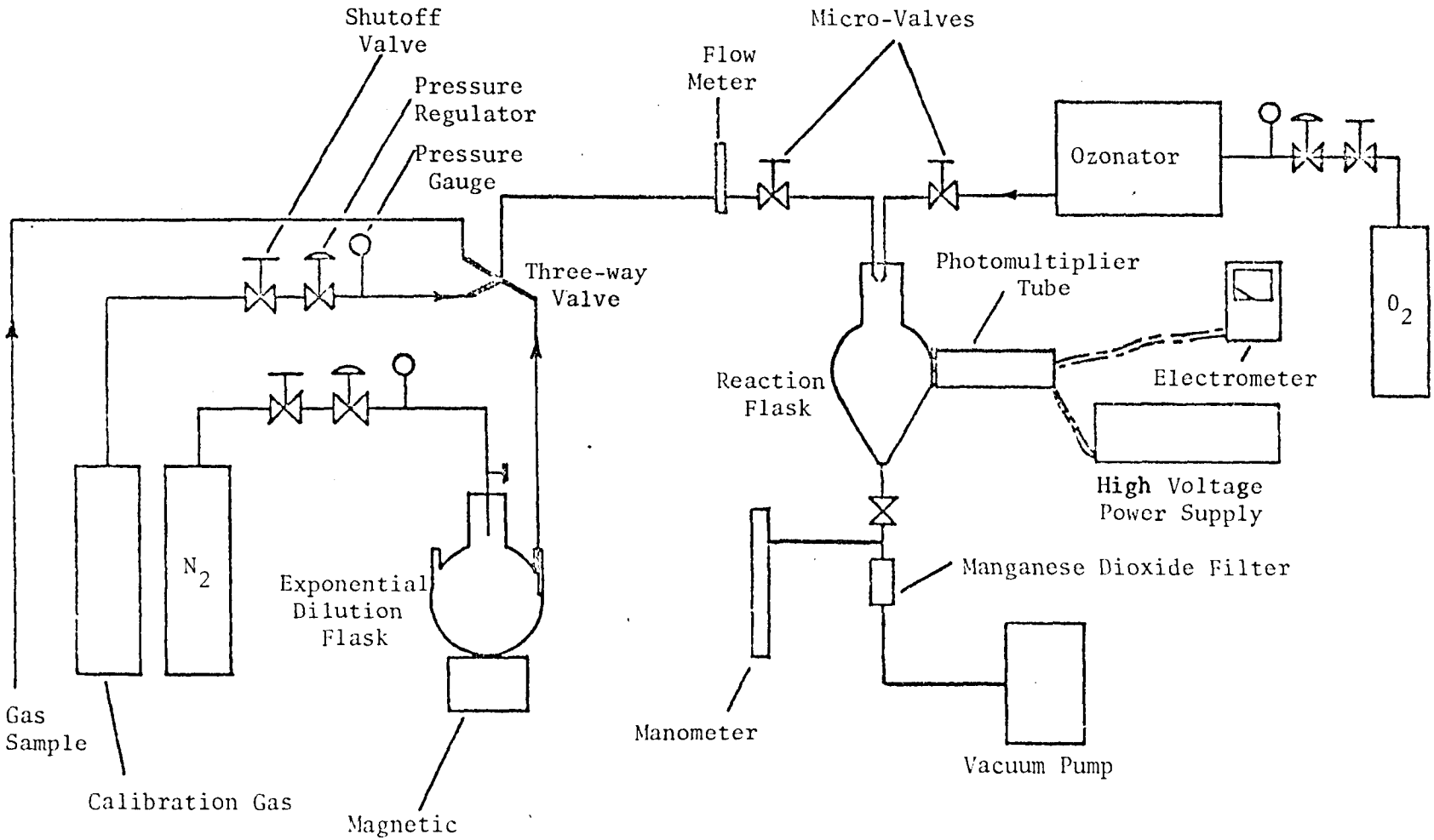

Figure 2-17. Nitric oxide detector schematic

With the assurance of linearity, meaningful calibration of the NO detector was then accomplished with the use of only one span gas of known NO concentration (usually 202 ppm in N_2). This gas was passed through the NO detector and the electrometer signal noted. The dark current electrometer signal was also recorded. From the linearity check the calibration curve was known to be a straight line. The two points then determining the calibration graph of NO concentration versus net electrometer signal were the known concentration and net signal of the single span gas and the zero concentration point characterized by a net signal of zero. The NO detector was calibrated using the above single span gas technique before and after every experimental run.

The method of operation of the nitric oxide detector is determined by the chemiluminescent reaction between NO and O_3. It has been well verified that the chemiluminescence is due to the following reaction scheme (Fontijn et al., 1969, 1970):

$$NO + O_3 \rightarrow NO_2^* + O_2$$

$$NO_2^* \rightarrow NO_2 + h\nu$$

To prevent collisional deactivation of the excited NO_2^* molecule and thus to insure that a chemiluminescent type reaction does occur, total reaction flask pressure was maintained at a level of 3 torr. It was then necessary, of course, to establish a vacuum tight flow system through the NO detector. A Welsh duo seal vacuum pump having a capacity of 500 ℓ/min at STP was used to draw sample gas through the instrument. Sample and ozone flows were monitored through observation of reaction flask pressure and reactant partial pressures.

Normal operation of the NO detector commenced with the establishment of a "relatively absolute" vacuum throughout the nitric oxide detector flow system and reaction flask. An ozone flow sufficient to maintain a steady 2 torr reaction flask pressure was then established. This ozone flow magnitude assured that O_3 would be present in sufficient excess to insure that the overall reaction be first order in NO. The ozone flow rate was then held constant through the duration of the run. A micro-metering valve on the sample line was subsequently adjusted to allow sufficient sample flow to establish a 3 torr total pressure in the reaction flask. The electrometer net signal was noted and the NO concentration of the sample gas could then be deduced from the previously discussed calibration curve.

One difficulty was encountered initially with the NO detector total response time, here defined as that time necessary for the complete removable of an unwanted, "old" sample gas from the flow system and the establishment of the correct reaction flask pressure and electrometer output signal for the new sample. This total response time was on the order of 5 minutes and considerably reduced the amount of NO data which could be compiled during any one run. Testing of the total system showed that the MnO_2 filter shown in Fig. 2-17 was responsible, as the filter was packed too tightly. Modification of the filter design has reduced the response time to about one minute.

In large part responsible for the great accuracy inherent in the chemiluminescent technique of NO concentration measurement is the relatively complete lack of interference of other sample gas constituents upon the accuracy of the NO measurement. Table 2-2 presents data

Table 2-2. NO Interference Data

(after Fontijn et al., 1969,1970)

Constituent	Max Concentration Generally Encountered in Air Quality Monitoring, PPM	Concentration Used at which NO Interference Was Detected at NO $\leq$ 10 PPB, PPM
NO_2	3	9
CO_2	500	650
CO	100	300
C_2H_4	1	5
NH_3	3	9
SO_2	3	25
H_2O	100% Saturation	75% Saturation

taken by Fontijn et al. (1969, 1970) which illustrate this most desirable quality.

The nitric oxide detector system also included a NO_2 converter as shown in Fig. 2-15. A detailed discussion of the converter and limited experimental results obtained from it are contained in Appendix A.

2.3 Total Hydrocarbon Analyzer System

Although a Beckman Model 402 Total Hydrocarbon Analyzer utilizing flame ionization detection was purchased for use in the subject research effort, instrument malfunctions delayed its use until late in the contract period. For this reason only a few unburned hydrocarbon measurements are reported. In Fig. 2-18 is shown the flow schematic for the hydrocarbon analyzer. Note that a portion (5 1/2 feet) of the sample line between the probe block and the relief valve was unheated; the use of a flexible teflon-coated high pressure line between the block and the purge system prohibited the use of heating tapes.

C. SUMMARY

Data have been obtained in the above-described facility and will be described and discussed in the following section. To repeat, the only aspect of this work which limits its application to practical engines is that unheated air was used at the combustor inlet for most of the studies. However, as will be shown below, much insight into the combustion process in a J-33 combustor has been gained.

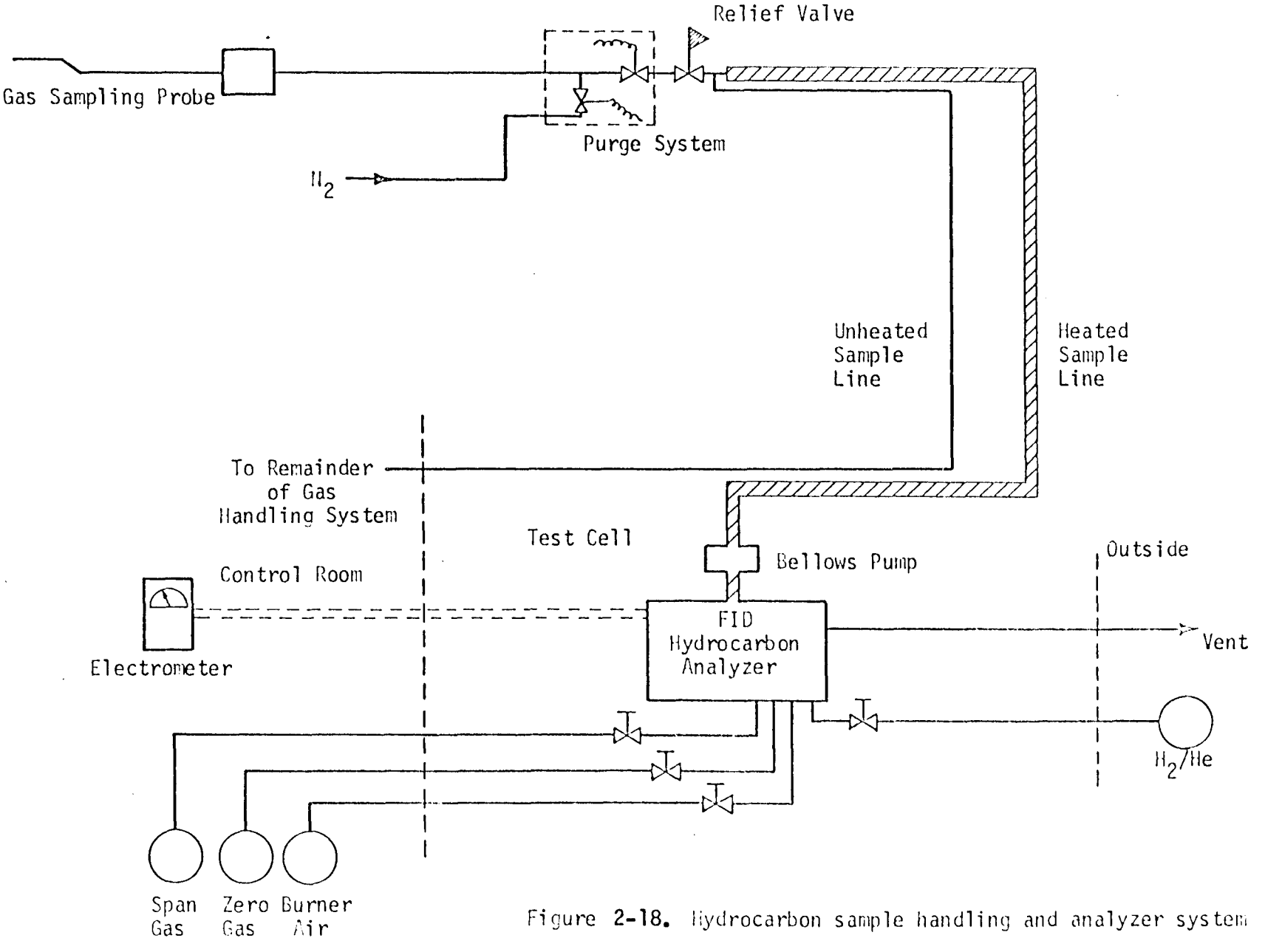

Figure 2-18. Hydrocarbon sample handling and analyzer system

III. RESULTS AND DISCUSSION

In order to intelligently present the data contained in this section, it is first necessary to understand generally the basic gas turbine combustion scheme. Typical gas turbine combustors may be divided into three characteristic regions as shown in Fig. 3-1: the primary zone, the secondary zone, and the dilution zone. The primary zone extends normally from the fuel nozzle face to the first row of air addition holes and is the region of most intense combustion. Typical primary zone equivalence ratios vary to either side of unity. The secondary zone serves primarily to complete the combustion initiated in the primary zone and for this purpose receives additional air from penetration air jets. The final downstream combustor volume is termed the dilution zone. Its purpose is to reduce the combustor exit plane bulk temperature through air addition to an acceptable turbine inlet temperature.

For the Allison J-33 combustor used in the present investigation, a NASA air flow program (Tacina and Grobman, 1969) has been used to estimate that approximately eight percent of the total combustor air flow enters the primary zone through the air swirler located around the fuel nozzle in the combustor dome. The swirled inlet primary air is characterized by a low pressure region in the center of the swirl necessary to induce the primary zone flow recirculation (see Fig. 3-1) required for flameholding. That remaining air not entering through the combustor dome is directed into the combustor either through film cooling slots or through secondary and dilution air holes.

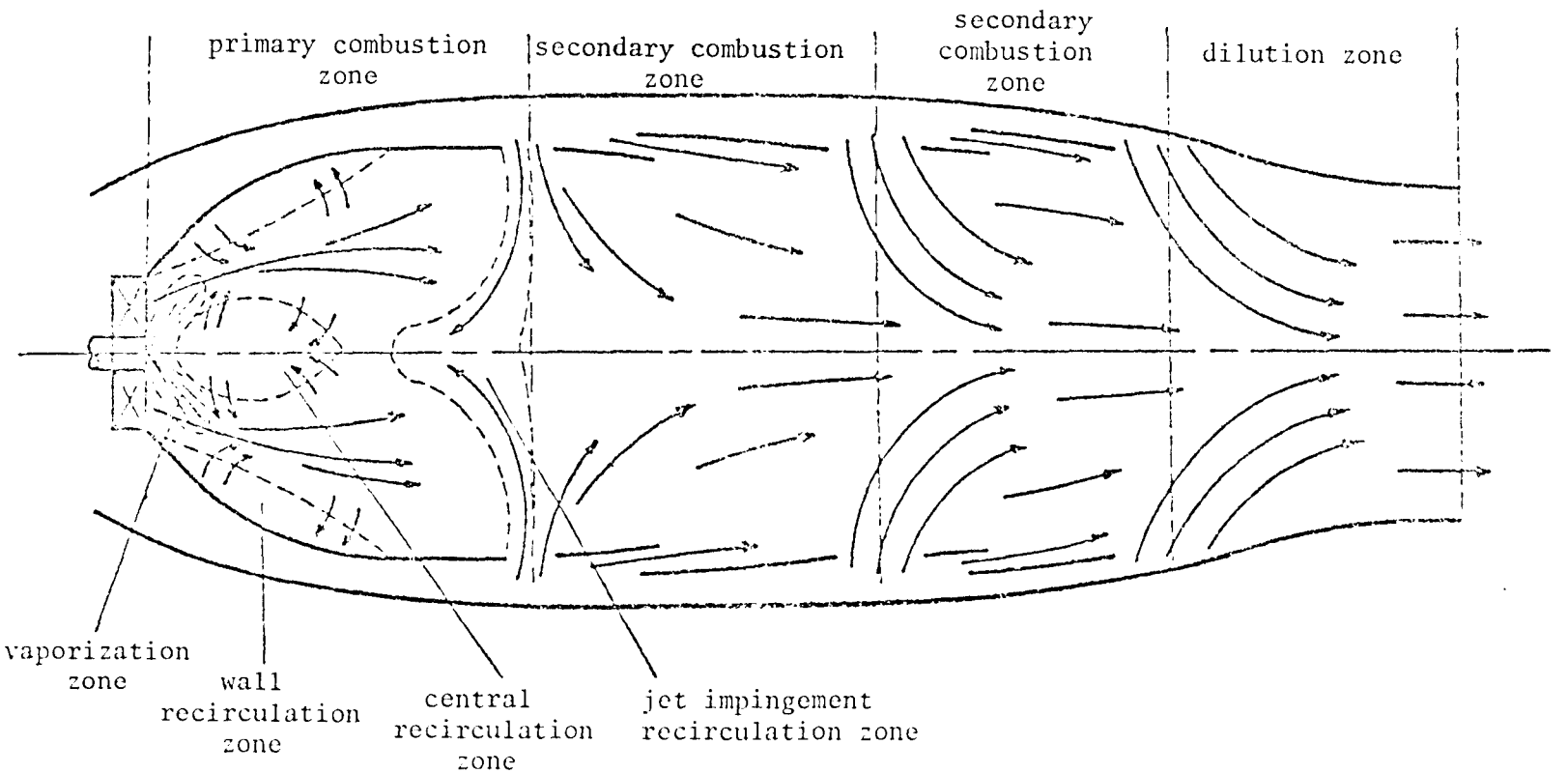

Figure 3-1. Typical gas turbine combustor flow schematic

The Allison J-33 combustor is shown in Fig. 3-2. Plane "c" in the figure cuts through the first row of secondary air holes and corresponds approximately to the end of the primary combustion zone. The volume contained between planes "c" and "e" can be considered the secondary combution zone, while that combustor volume downstream of plane "e", the dilution zone. The three small holes aligned upstream of plane "c" are primary zone air addition holes and the intermittently spaced wedges are the film cooling slots. Finally, the dome cutaway shows the combustor fuel nozzle and air swirler assembly.

The four planes shown in Fig. 3-2 constitute four of the axial locations from which internal gas composition samples were taken. Planes "a" and "f", both not shown in Fig. 3-2, are located respectively 3 inches downstream of the fuel nozzle face (i.e. 2 1/2 inches upstream of plane "b") and 1 3/8 inches downstream of the actual combustor exit plane. Henceforth plane "f" will be designated the combustor exit plane. Total combustor length (from fuel nozzle face to actual combustor exit) is approximately 18 5/8 inches.

As previously mentioned, the gas sampling probe tip was offset to provide a circular trace upon probe rotation. Fig. 3-3 shows the location of the probe trace in the combustor exit plane sampling station as viewed from the combustor dome. The relative positions of the combustor cooling slots, penetration air holes, and gas sampling probe positions should be noted. (It should be mentioned again that the designated combustor exit plane is in reality a plane 1 3/8 inches downstream of the actual combustor exit.) The 0°, 90° cw (clockwise), 180°, and 90° ccw (counter-clockwise)

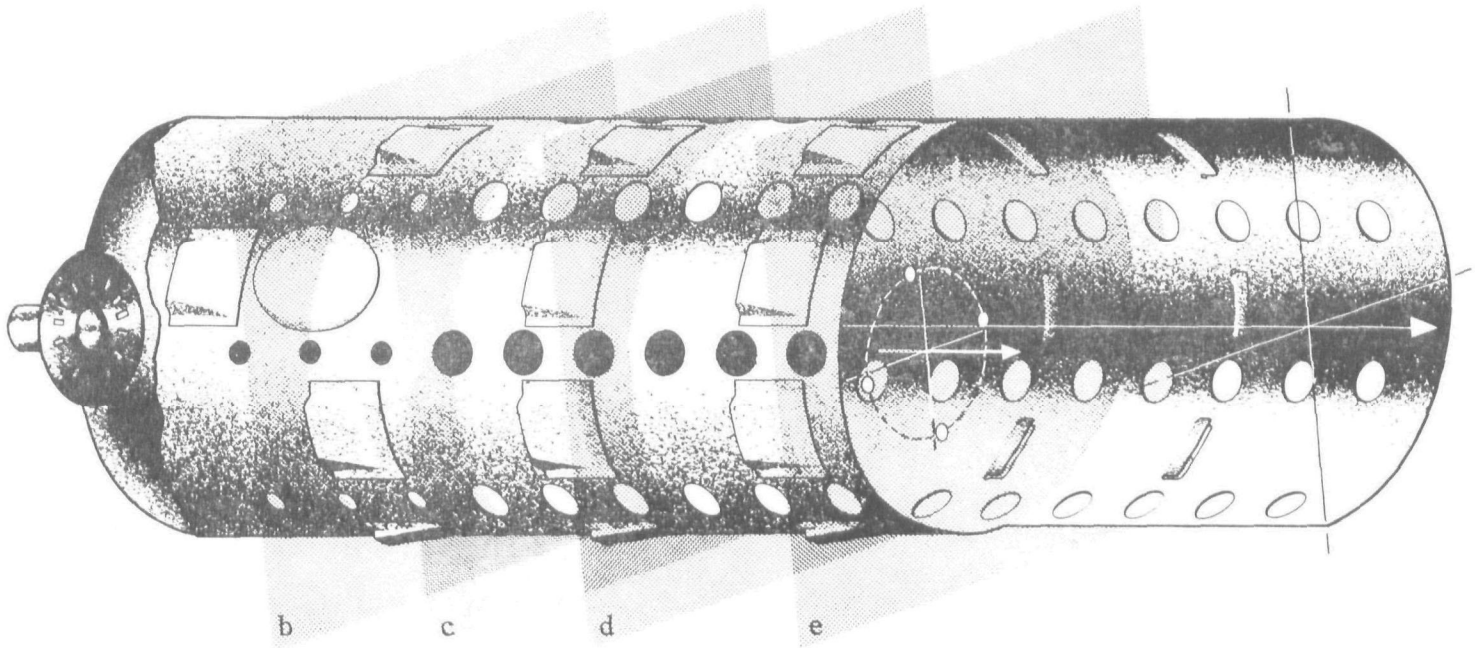

Figure 3- 2 . J-33 combustor configuration, gas sampling planes (4 of 6), and probe trace position

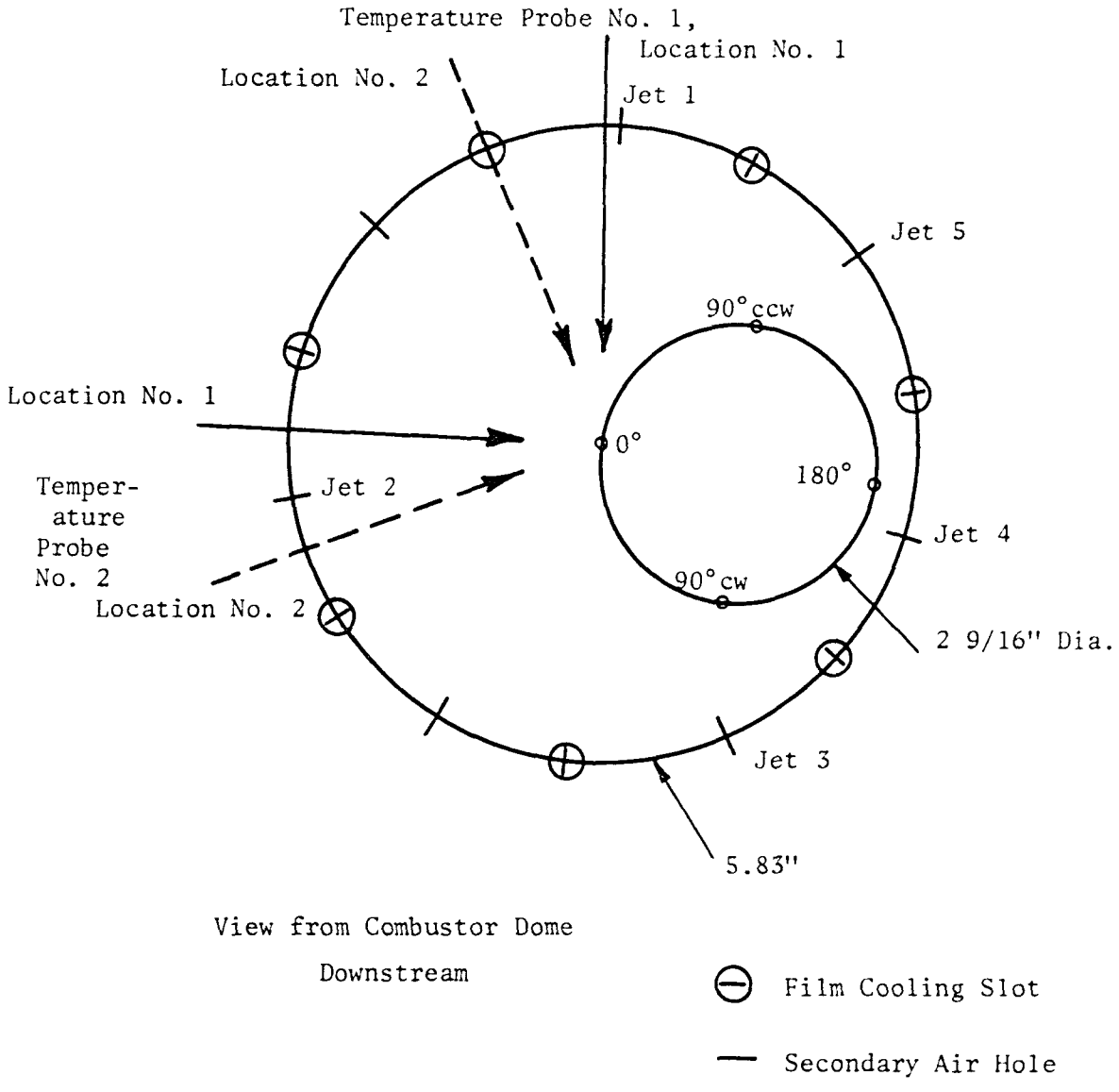

Figure 3-3. Relationship of probe trace and gas sampling points to J-33 combustor configuration

designations will be used consistently to refer to the different radial probe positions as shown in the figure.

A. COMBUSTOR OPERATING POINTS

Having now established the particular J-33 combustor configuration, it is appropriate to detail the selected J-33 combustor operating points. For the subject research combustor air flows of 3.75, 4.57, and 6.0 lbs/sec, combustor absolute pressures of 3, 5, and 10 atmospheres, and combustor overall equivalence ratios of 0.217, 0.283, and 0.345 were used, with liquid propane as fuel. Unheated inlet air was used for the experiments described in this section. Those combinations of the above parameters that were investigated are shown graphically in Fig. 3-4 and in tabular form in Table 3-1. The base combustor operating point corresponded to an airflow of 6.0 lbs/sec, an overall equivalence ratio of 0.217, and a combustor pressure of 5 atmospheres. It is of importance to emphasize that during any run only one parameter was varied from the base condition. As can be inferred from Fig. 3-4, and unlike the technique of Sawyer et al. (1969), equivalence ratio variation was accomplished through fuel flow rate alteration at a constant air flow rate, thus eliminating major concomitant primary zone and overall residence time changes.

Because of time limitations and the unrealistic use of unheated combustor inlet air for these experiments, combustor traverses were made only at the base operating point, B in Table 3-1. Measurements at the other six operating points were limited to the exit plane. Due to the unavailablity of functioning hydrocarbon analyzing instrumentation during

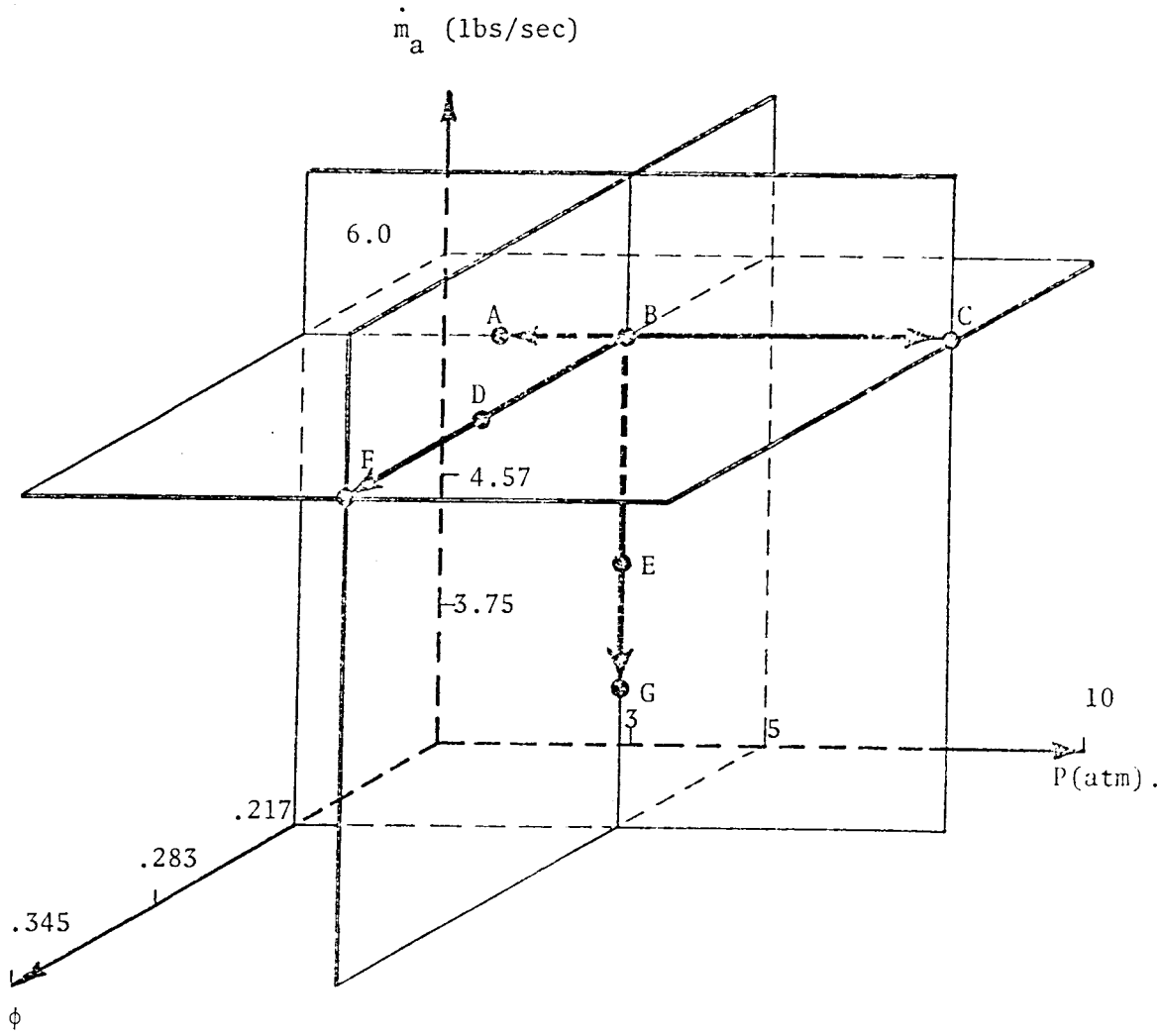

Figure 3-4. Combustor operating point matrix

Table 3-1. Selected Combustor Operating Points[±,Δ]

Fig. 3-4 Point Designation	Overall Equivalence Ratio	Air flow Rate, lbs/sec	Combustor Pressure, atm abs
A	0.217	6.0	3
B[*,θ]	0.217	6.0	5
C	0.217	6.0	10
D	0.283	6.0	5
E	0.217	4.57	5
F	0.345	6.0	5
G	0.217	3.75	5
Normal Design Operation:			
-	0.232[†]	7.17	4.2

± For each condition only a single parameter variation from the base point was allowed.

Δ The acquisition of a complete data set for each point required more than one run.

* Point B is designated the combustor base operating point.

θ Combustor traverses were made at this operating condition.

† Calculated for C_3H_8 as fuel, following Zucrow and Warner (1956).

this portion of the study, only gas temperatures and carbon monoxide and nitric oxide concentrations will be reported.

B. INTERNAL MEASUREMENTS

The long time required for accurate gas sampling measurements and the finite capacity of the air system prevented the completion of a combustor traverse during any one experiment; usually three to five runs were needed. Generally it was found that reproducibility within any given experiment was good, but somewhat poorer from run to run at a given operating point. Thus all of the data points obtained inside the combustor will be reported below. The difficulties with gas temperature measurement detailed in Section II prevented our obtaining as many local temperatures as concentrations.

For these internal measurements the probe was inserted into the combustor through the probe addition section window and stationed at one of the planes shown in Fig. 3-2. After steady combustion at the base operating point had been established, measurements were taken at the initial probe position. The probe could then be rotated to any of the three other radial positions shown in Fig. 3-2 and 3-3, or translated to another axial station.

1. Gas Temperatures

The internal temperature measurements shown in Fig. 3-5 provide much insight into the nature of the flow pattern and combustion process in the J-33 combustor. For convenience, the axial profiles at each radial position are connected by the heavy lines.

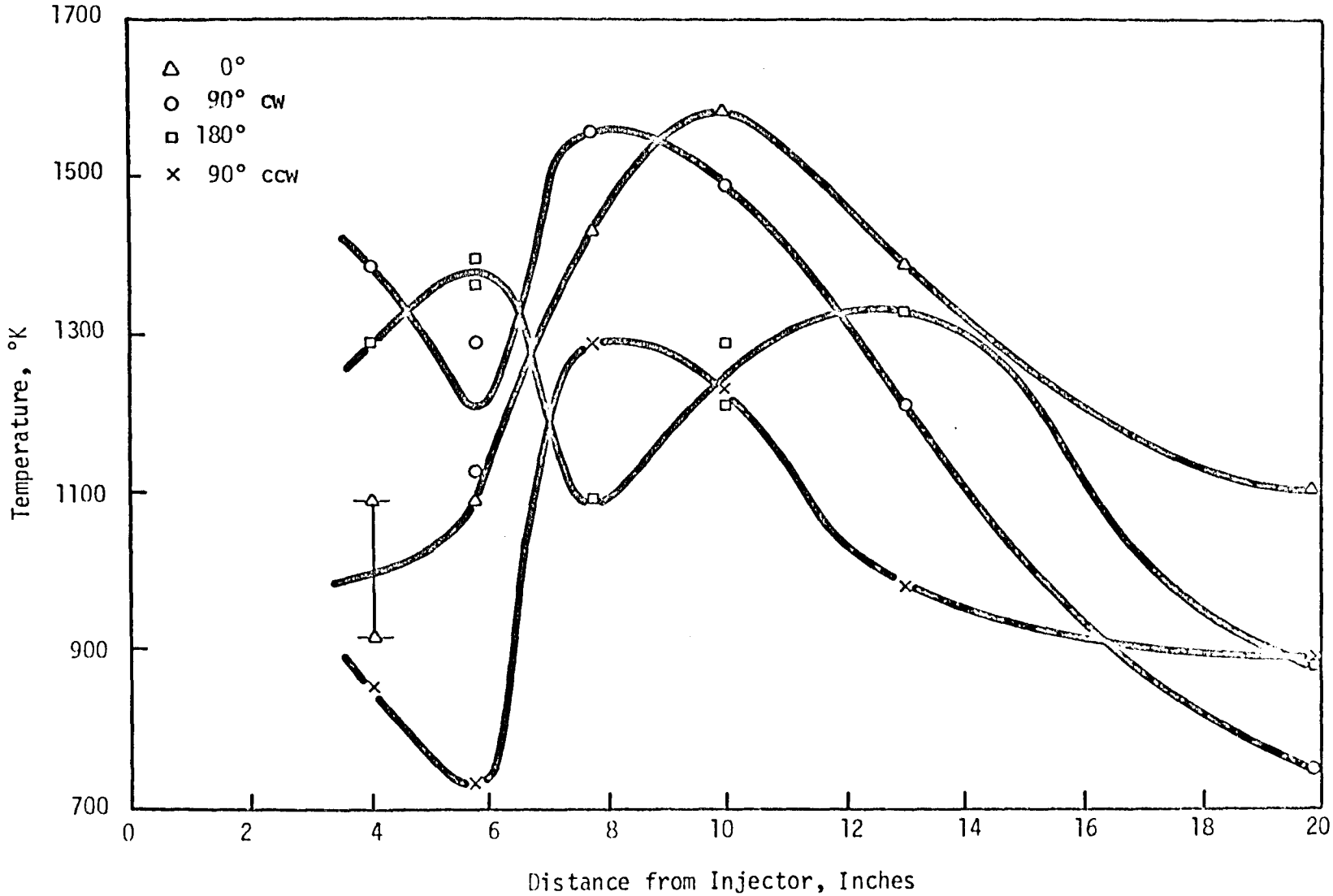

Figure 3-5. Temperature versus axial position
($\dot{m}_a$ = 6.0 lbs/sec, ϕ = .217, P = 5 atm)

In the first six inches of the combustor, the maximum gas temperatures are encountered near the wall of the combustor (180°) while the recirculation zone nearer to the centerline is relatively cold; this last observation suggests that a large portion of the air injected through the first row of large penetration holes at 8 inches recirculates back toward the injector. The presence of these holes is most clearly seen in the 180° profile at about 8 inches, in the 90° profiles at about 6 inches, and possibly in the centerline profile between 4 and 6 inches. Because of the asymmetry of the probe position at both 90° cw and ccw with respect to the penetration holes (as shown in Fig. 3-3) these two temperatures are never equal; the 90° ccw values are generally the lower, due to jet 5.

The flame closes to the centerline between 8 and 10 inches, where the maximum temperatures are observed. Downstream of this station the temperatures decay for the most part as the remainder of the air is added through the holes and slots. It thus appears that reaction continues well into the secondary zone of this combustor.

One surprising result of the temperature measurements is their low values in the first 10 inches of the combustor: the maximum value of about 1600° K (on the centerline at 10 inches) is at least 400° K lower than one would expect theoretically. However, since the thermocouple bead did not melt during the experiments, temperatures on this order could not have been experienced in any position through which the probe travelled.

There are several sources of error in temperature measurements with unshielded, uncoated junctions: one results from conduction along the thermocouple, but is negligible here due to the depth of immersion of the probe into the combustor. Catalyzed recombination reactions on the

uncoated Pt leg would increase the measured temperature over the gas temperature, which is the wrong trend. Radiation heat transfer losses from the bead to the relatively cold combustor walls must also be considered. However, assuming the bead to have an emissivity of one and to be surrounded by walls at 0° K results in a temperature measurement low by only 100° K for an indicated value of 1600° K (the Nusselt number for heat transfer to the bead is estimated as 43 in the primary zone). Thus radiative corrections have not been applied to the data of Fig. 3-5 and do not appear responsible for the unexpectedly low temperatures which were measured.

Most likely direct impingement and subsequent evaporation of liquid fuel on the thermocouple bead is the source of the error, particularly near the walls where the hollow fuel spray cone would be expected to persist (using H_2O injected into ambient air, the spray cone angle was measured to be about 80°). However, since even with this difficulty the highest temperatures at 4 inches were observed at 90° cw and 180°, the following qualitative picture of the combustion process can be assembled: the flame zone follows the fuel spray and is hollow in the primary, with a relatively cold embedded recirculation zone fed in part by the first large air holes at 8 inches. The zone ends at about the 8 inch position where the flame returns to the centerline.

Thus the schematic of Fig. 3-1 is a reasonable representation of the J-33 combustion process if the central and jet impingement recirculation zones are merged and substantial combustion is allowed in the secondary zone. It is also concluded that the particular 90° radial probe positions chosen for these experiments will not exhibit equal temperatures or

concentrations since the 90° ccw points are more directly aligned with penetration jets; as will be shown below, slightly lower NO and CO measurements were also obtained at 90° ccw.

2. Nitric Oxide

Axial NO profiles for the four radial positions are presented in Fig. 3-6 through 3-9; due to the large number of data points and considerable scatter four separate figures are shown. The general order of decreasing NO concentrations is 0°, 90° cw, 90° ccw, and 180°, respectively.

High NO concentrations are found on the centerline in the region thought to be within the recirculation zone (the first 6 or 8 inches in Fig. 3-6), but the scatter in the data is also the worst here. At 10 inches at 0°, where the maximum temperature was measured, NO also reaches its maximum value, falling off downstream probably as a result of dilution. The 90° ccw values (Fig. 3-7) are generally lower than those at 90° cw (Fig. 3-8) due to the closer proximity to penetration jets, and as in the temperature profiles, dilution from the first large jet (at 8 inches) can be seen at 8 and at 6 inches, respectively. In addition, the wall concentrations (Fig. 3-9) clearly show the influence of this jet at 8 inches. Only slight radial variations are seen at 3 inches from comparison of the four figures; more substantial variations are exhibited downstream of this point. The scatter in all of the data decreases in moving downstream.

All of the temperatures reported in Fig. 3-5 are too low for significant NO formation via homogeneous reactions. However, the general increase

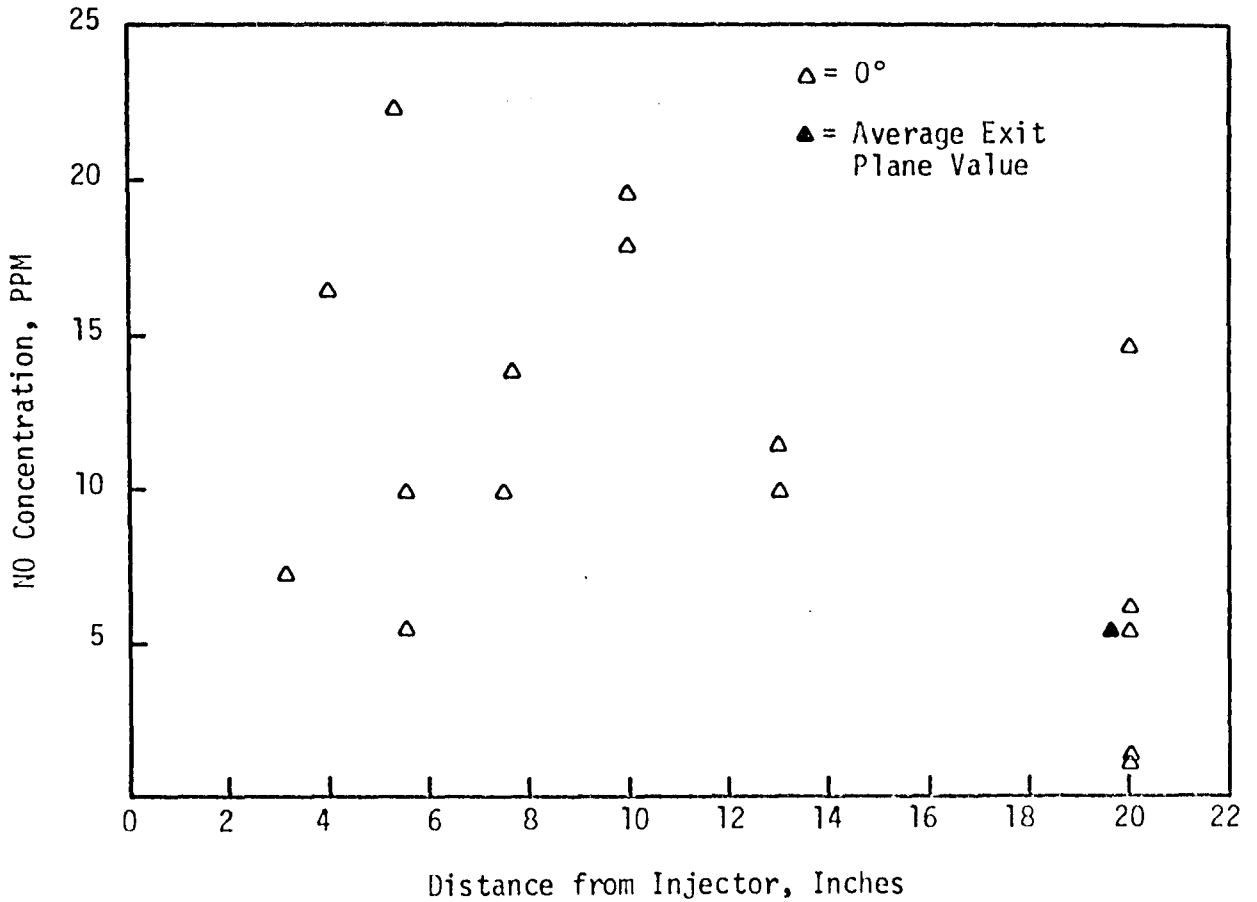

Figure 3-6. NO concentration versus axial position for 0° ($\dot{m}_a$ = 6.0 lbs/sec, ϕ = .217, P = 5 atm)

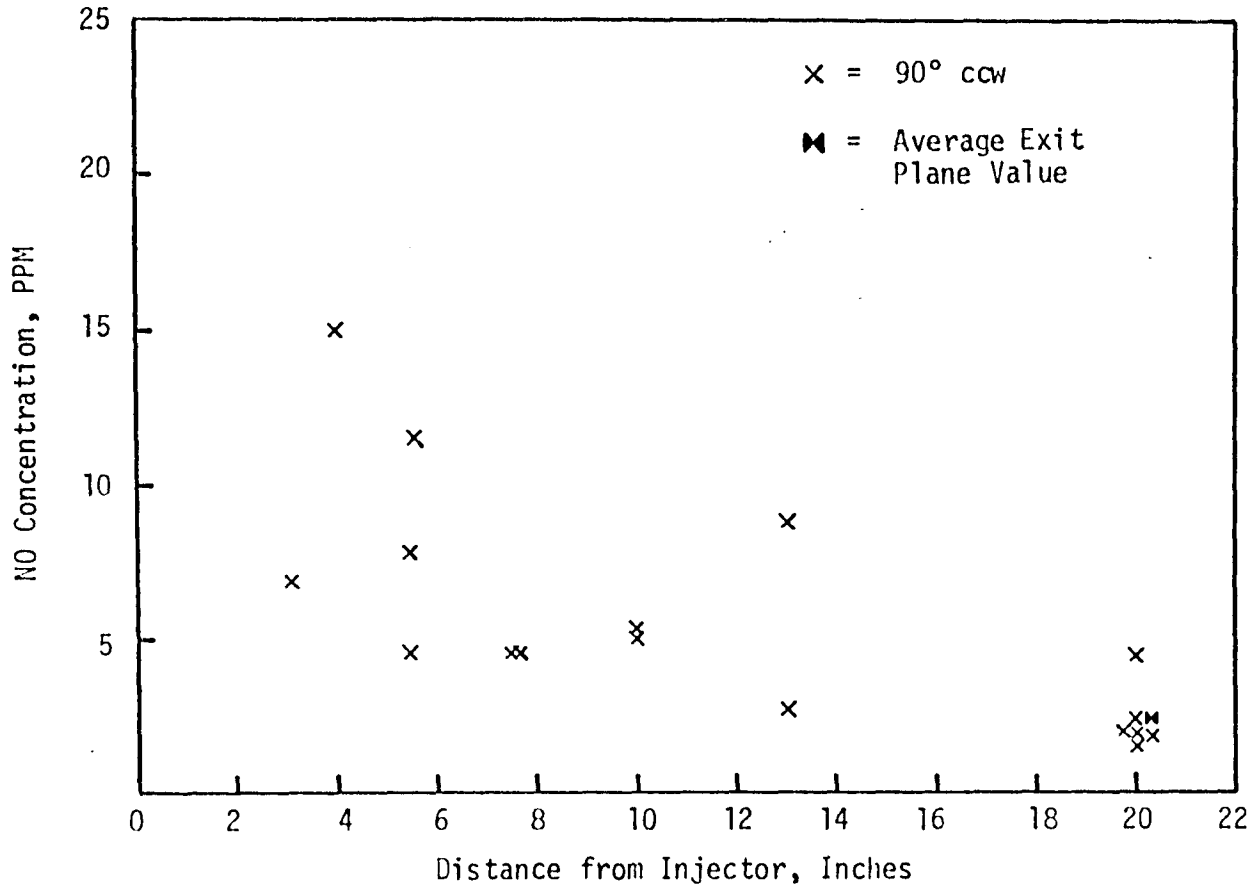

Figure 3-7. NO concentration versus axial position for 90° ccw ($\dot{m}_a$ = 6.0 lbs/sec, ϕ = .217, P = 5 atm)

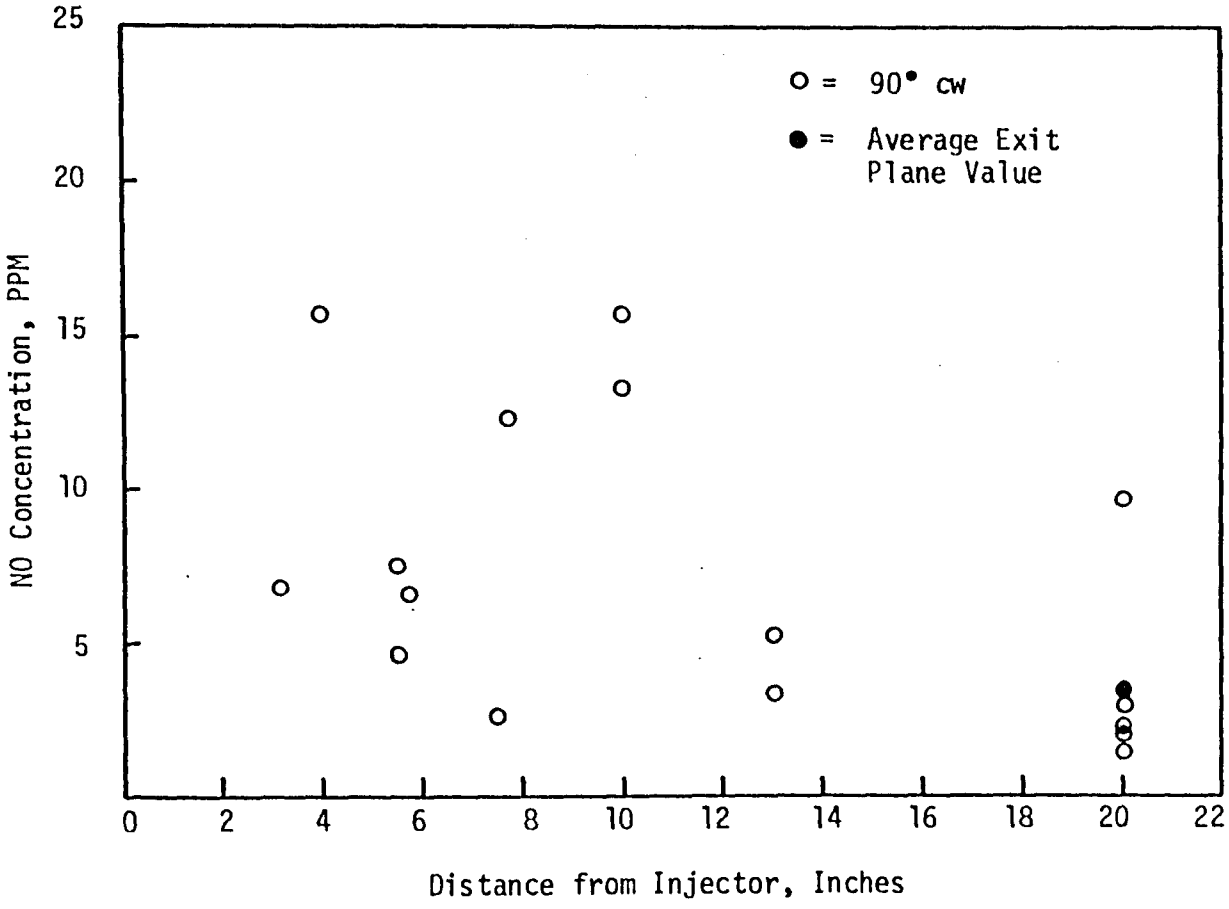

Figure 3-8. NO concentration versus axial position for 90° cw ($\dot{m}_a$ = 6.0 lbs/sec, ϕ = .217, P = 5 atm)

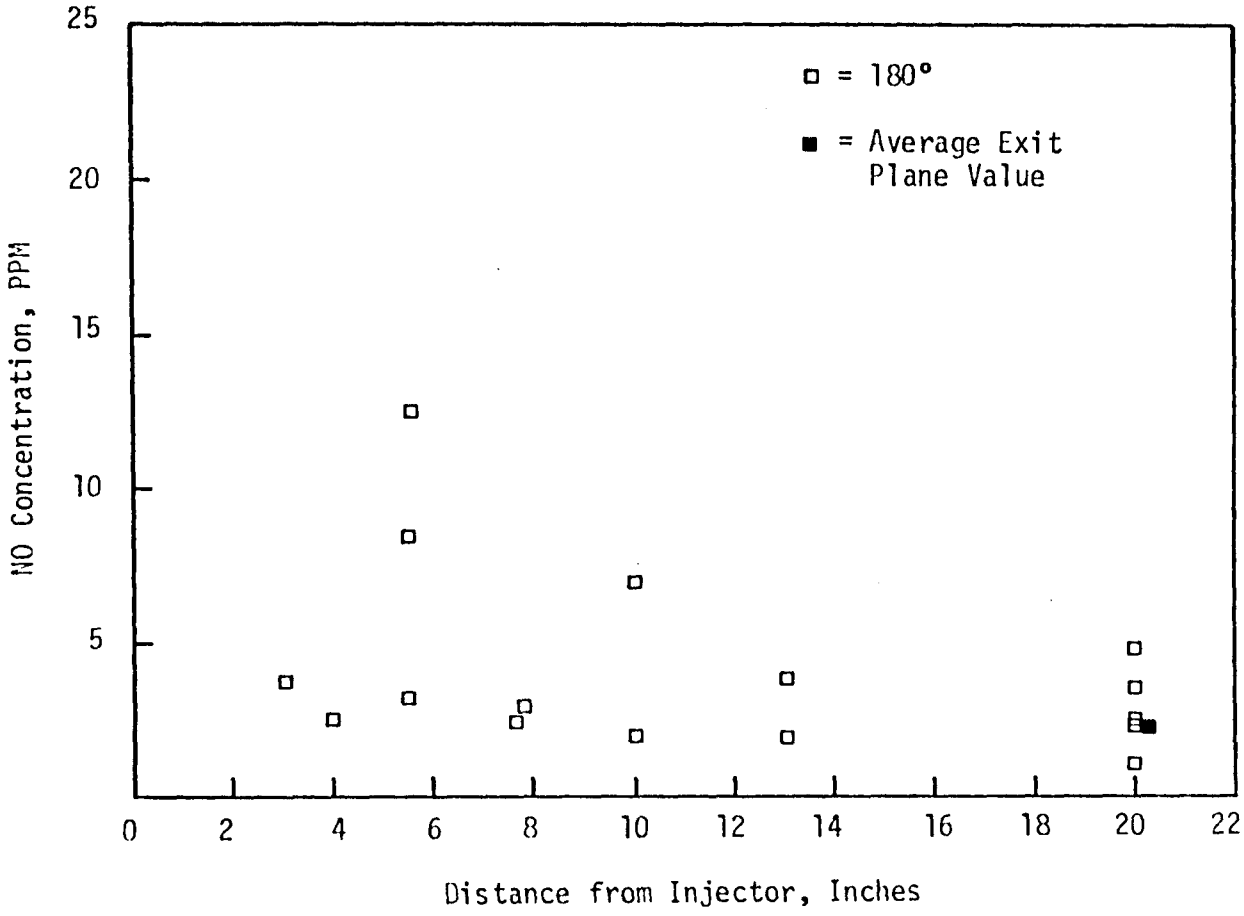

Figure 3-9. NO concentration versus axial position for 180° ($\dot{m}_a$ = 6.0 lbs/sec, ϕ = .217, P = 5 atm)

in NO concentration which follows the zone of maximum temperature (i.e., 3 to 6 inches at 180°, Fig. 3-9; about 7 inches at 90° cw, Fig. 3-8; and 8 to 10 inches at 0°, Fig. 3-6) suggests firstly that NO is still forming in this zone and secondly that the measured temperatures are low, as was concluded in the previous section. The high values of NO observed in the recirculation zone at the 4 through 7 inch positions are most likely a result of entrainment into this zone: although these values are suspect because of the large scatter in the data, it will be shown subsequently that NO is not formed in this region, when the results of varying the air flow rate are reported.

3. Carbon Monoxide

Semilogarithmic plots of axial CO concentrations are shown as Fig. 3-10 through 3-13, again grouped by radial probe position. The high concentrations observed at those stations closest to the injector suggest that the region in which CO is formed was not accessible to the probe, a finding which is consistent with the proposed fuel rich zone very near the injector face. In addition, the lower values at 180° suggest that CO oxidation is still occurring in the primary zone along the walls; the reaction has been quenched in the recirculation zone by the cold air flowing upstream from the large penetration jets at 8 inches. Because of the logarithmic concentration scale, the pattern of this jet is not as easily followed as in the temperature and NO concentration profiles.

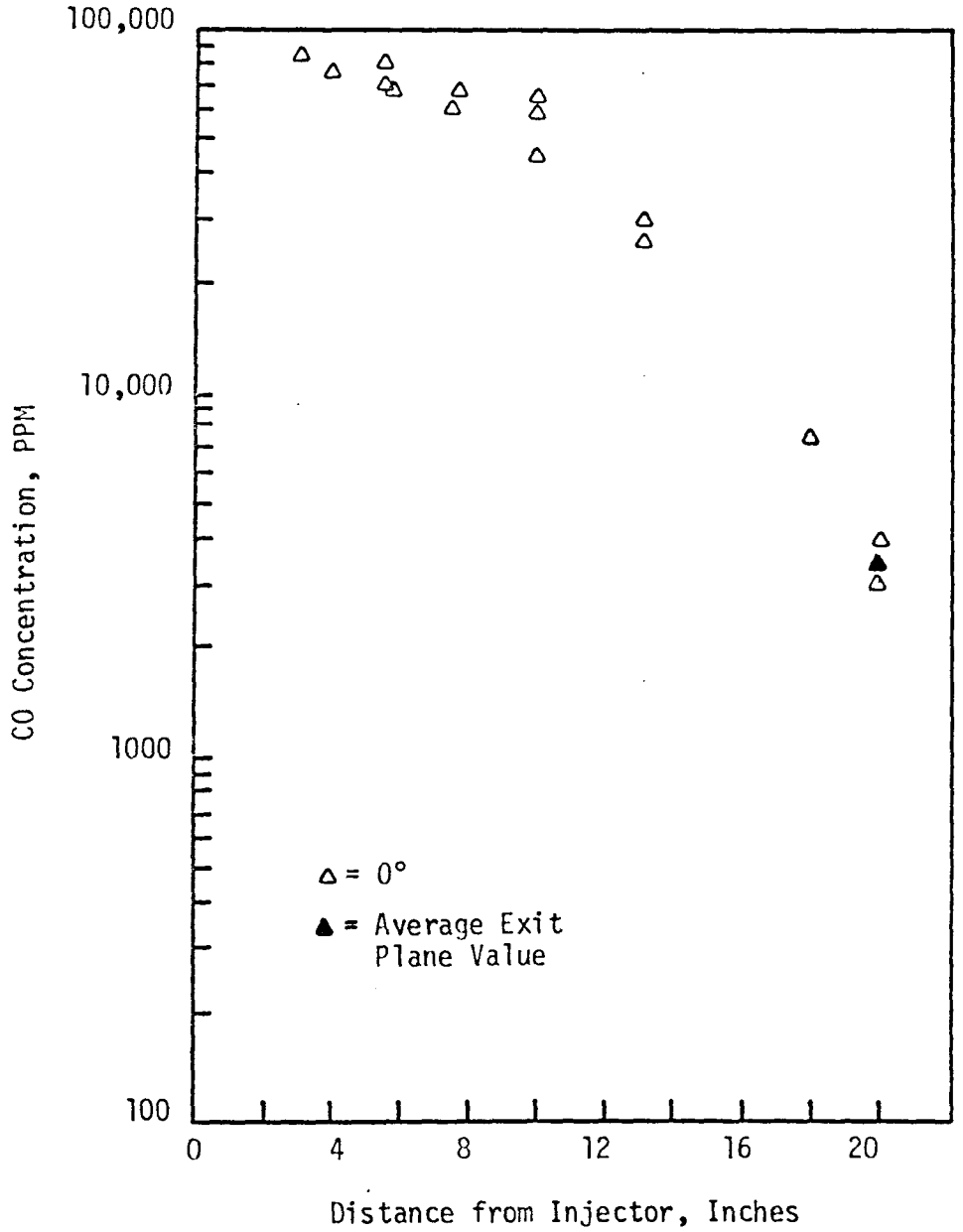

Figure 3-10. CO concentration versus axial position for 0° ($\dot{m}_a$ = 6.0 lbs/sec, ϕ = .217, P = 5 atm)

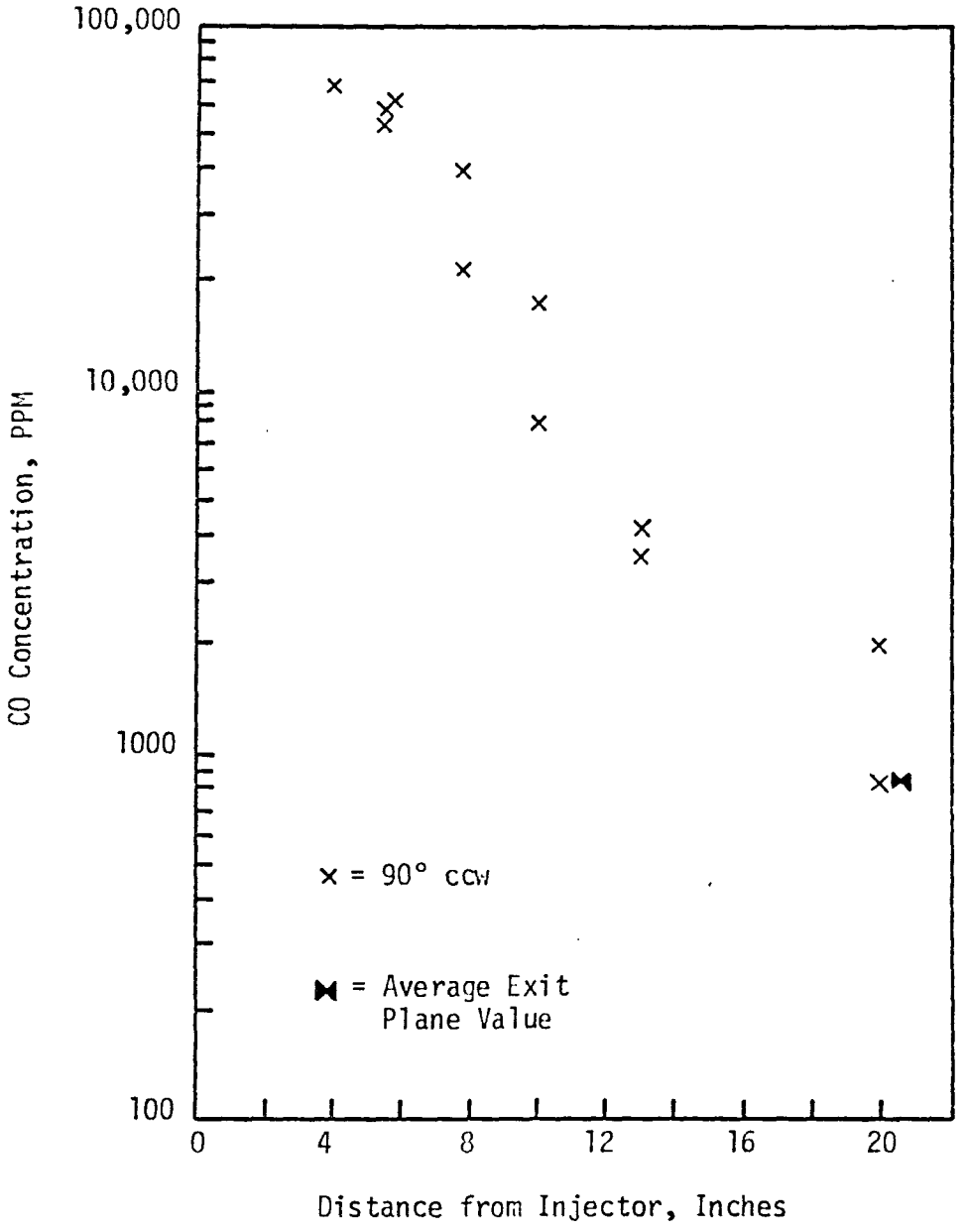

Figure 3-11. CO concentration versus axial position for 90° ccw ($\dot{m}_a$ = 6.0 lbs/sec, ϕ = .217, P = 5 atm)

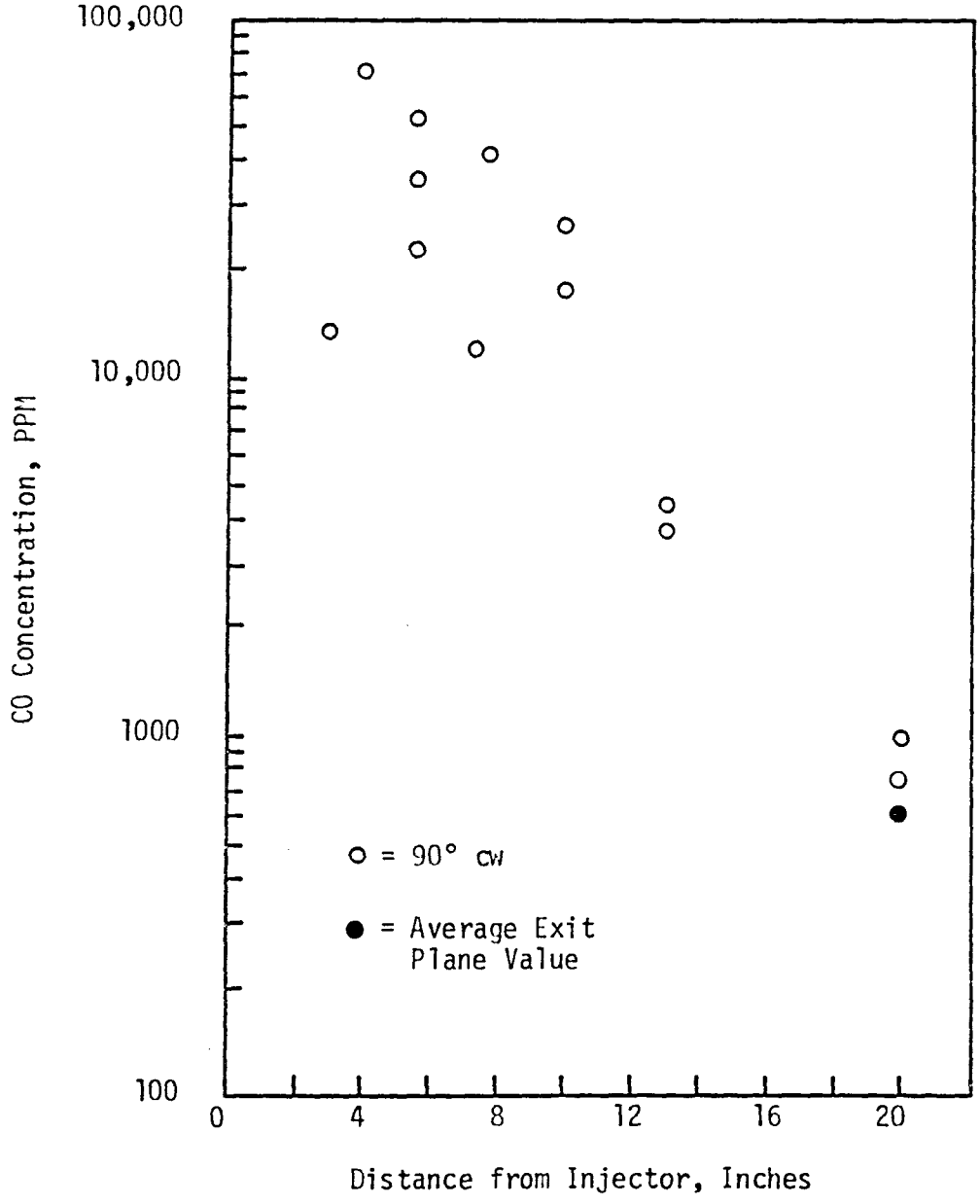

Figure 3-12. CO concentration versus axial position for 90° cw ($\dot{m}_a$ = 6.0 lbs/sec, ϕ = .217, P = 5 atm)

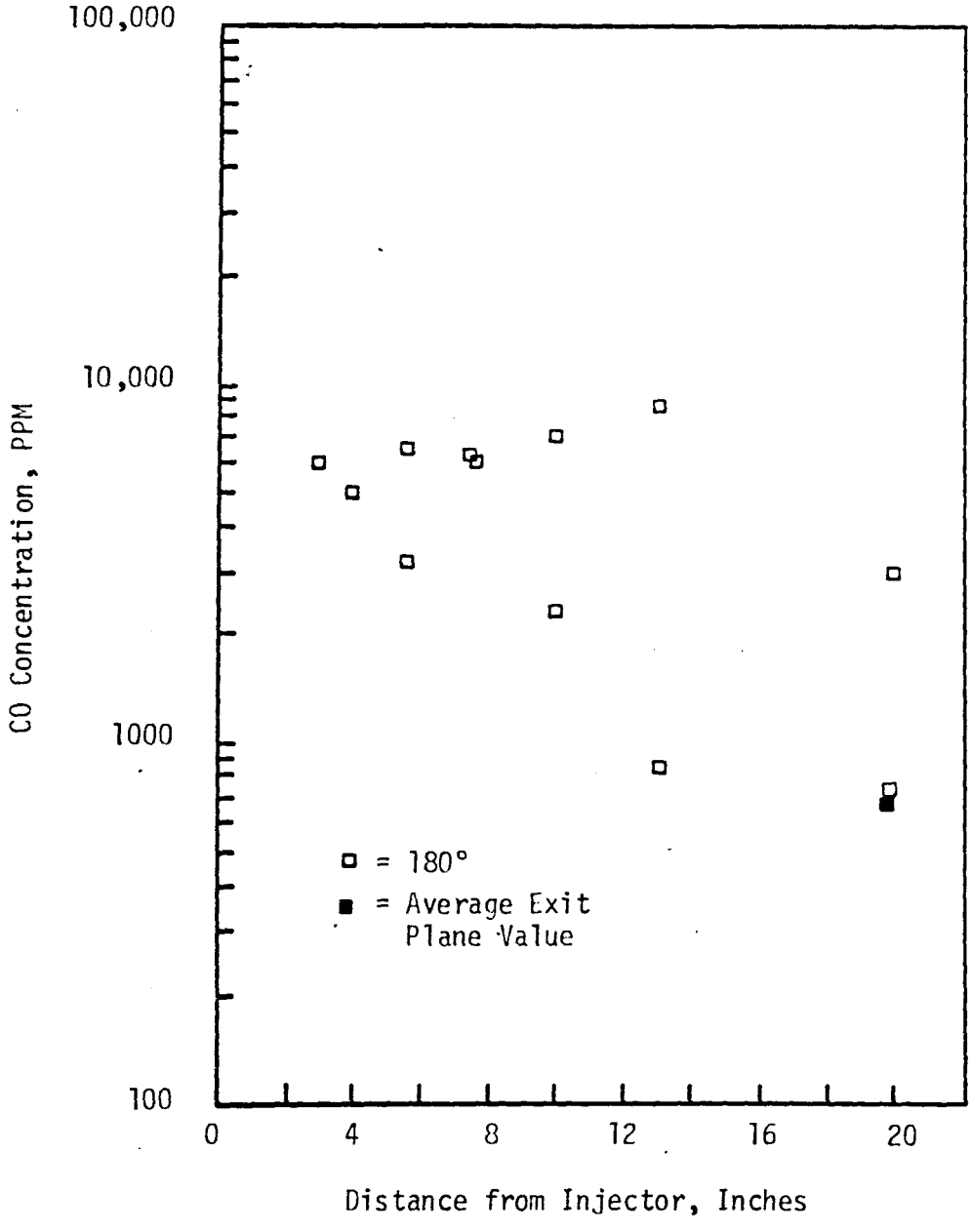

Figure 3-13. CO concentration versus axial position for 180° ($\dot{m}_a$ = 6.0 lbs/sec, ϕ = .217, P = 5 atm)

4. Summary

The flow pattern in the first 10 inches of the J-33 combustor postulated on the basis of the temperature and concentration measurements is shown schematically in Fig. 3-14. The most important features are the fuel rich zone along the dome and liner walls where CO (region 1) and NO (region 1-3-5) are formed and the strong backflow of air (region 4) which quenches CO oxidation in region 2. It is the lack of substantial air addition into the fuel rich region and too much air flow into the recirculation zone which is responsible for the high emissions of CO from this combustor. However, since the highest temperature zones are probably fuel rich, the NO emissions are low. For this particular liner, the results suggest that the placement of the first row of large penetration holes will largely determine the emissions.

C. COMBUSTOR EXHAUST PLANE MEASUREMENTS

Through internal measurements of temperature and composition the influence of liner design on CO and NO emissions has been discussed in the previous section; combustor exit plane measurements are not as useful for this purpose because they obscure the important chemical and physical phenomena occurring within the liner. However, studies of this latter type can help reveal the dependence of emissions on cycle design (as opposed to liner design) parameters. Most of the data to be reported in this section pertain to NO and CO emissions as functions of overall equivalence ratio, combustor pressure, and air flow rate, but the limited temperature measurements obtained with the exit plane chromel-alumel thermocouples will be presented first.

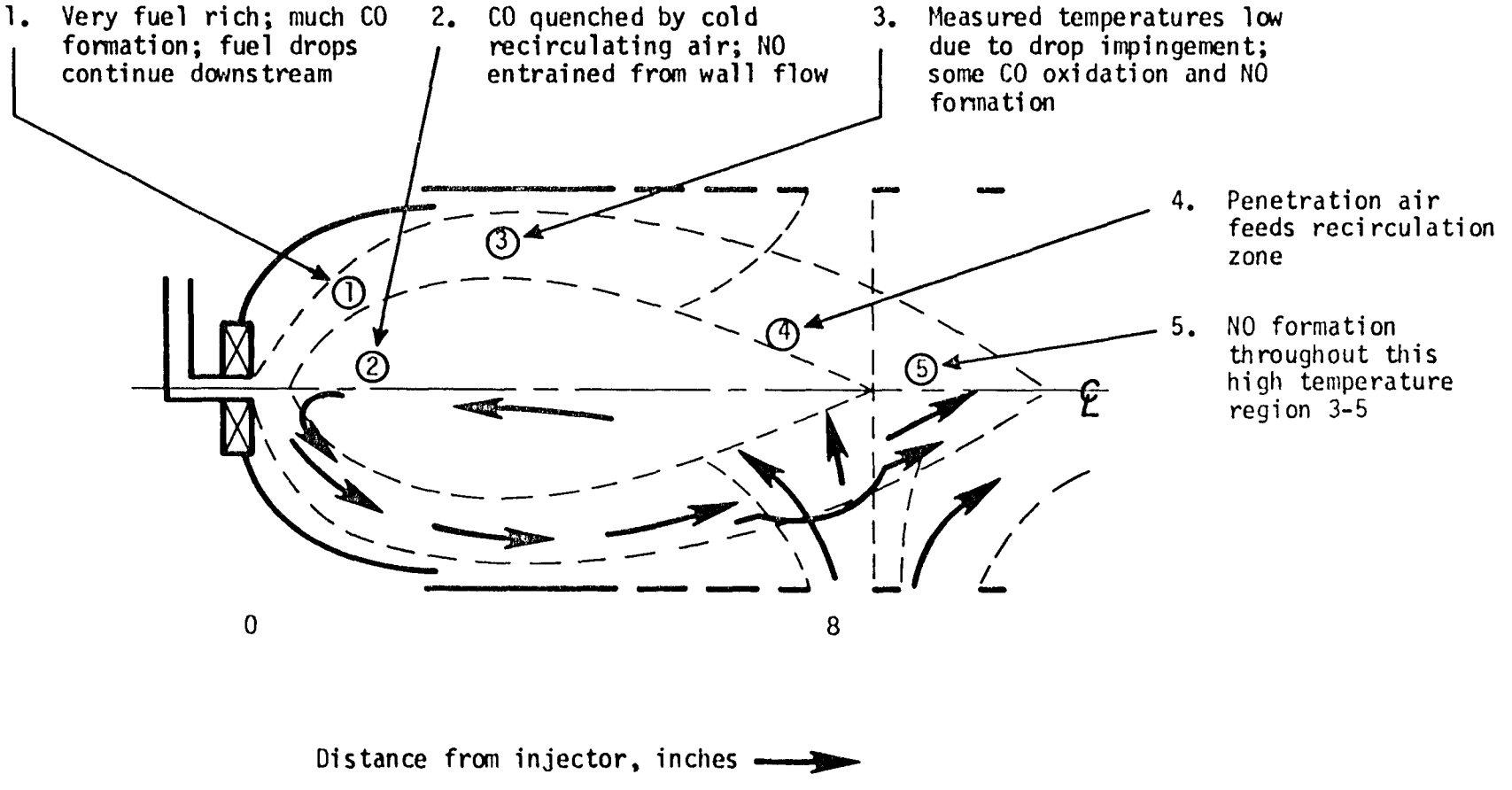

Figure 3-14. Schematic of postulated primary and secondary zone flow pattern for the J-33 combustor

1. Gas Temperatures

Only the influence of air flow rate on radial temperature profiles was determined, for the two sets of probe positions shown in Fig. 3-3. The data for location number one are shown in Fig. 3-15, and those for location number two in Fig. 3-16. Note that in the former position probe one is aligned with a penetration jet while probe two is midway between a jet and a film cooling slot; in location number two probe one was directly aligned with a slot.

As expected, the mean gas temperature is higher when measured above a film cooling slot than above a penetration jet: probe one exhibits higher values at both air flow rates in Fig. 3-16 than in Fig. 3-15. Probe two at location two reveals somewhat lower temperatures since in this position it is closer to a penetration jet (see Fig. 3-3). The minima in all of the curves represent the cores of the last row of penetration jets near the end of the liner.

These radial profiles clearly indicate the difficulty in calculating a meaningful mass averaged temperature at the combustor exit; in fact, Fig. 3-15 and 3-16 suggest that the exhaust temperature decreases with decreasing air flow rate, which is inconsistent with thermodynamics.

2. Exhaust Plane Emissions of Nitric Oxide and Carbon Monoxide

Exhaust plane concentration data as functions of the cycle design parameters air flow rate, overall equivalence ratio, and combustor pressure will be presented in two ways: firstly, numerical averages at each radial position will be shown, and secondly, in order to demonstrate the reproducibility of the measurements, all data will be shown. Recall

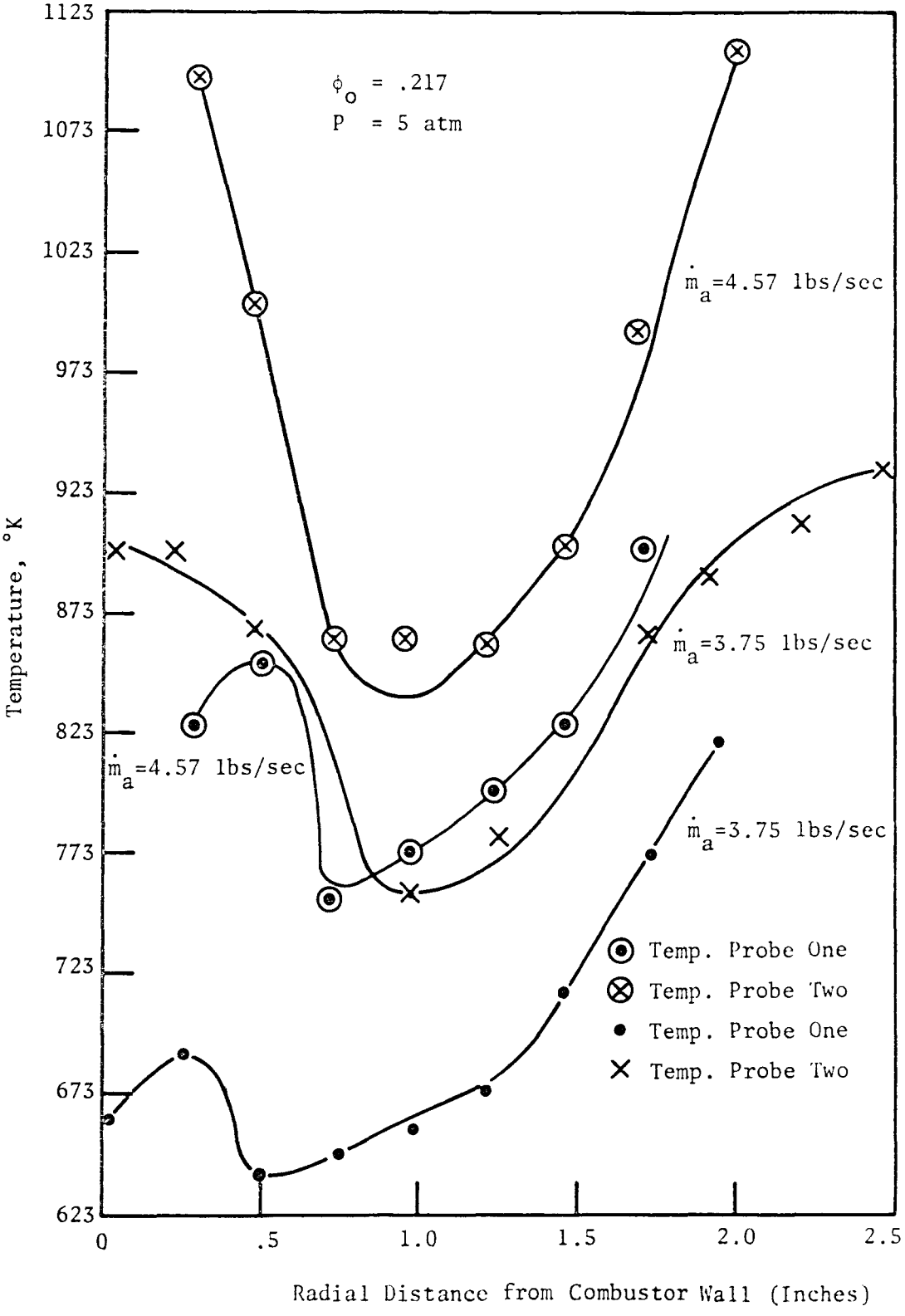

Figure 3-15. Combustor exit plane temperature traverse (probes in locations numbered one in Fig. 3-3)

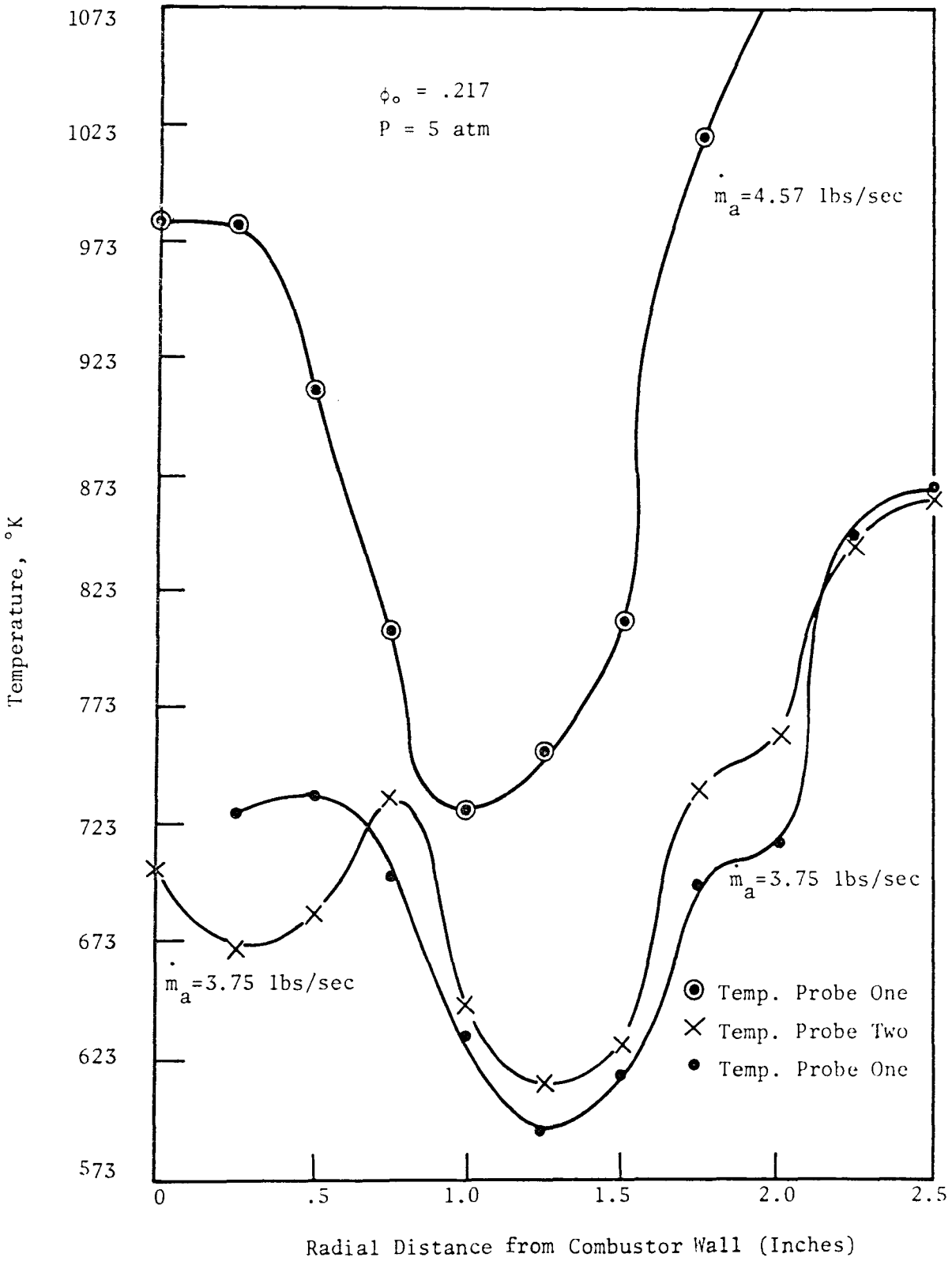

Figure 3-16. Combustor exit plane temperature traverse

(probes in locations numbered two in Fig. 3-3)

that only one cycle parameter was varied at a time, as shown in Fig. 3-4, in order to obtain these data.

2.1 The Influence of Air Flow Rate

Since the air flow rate was varied at constant overall equivalence ratio (and pressure), it was necessary to vary the fuel flow rate accordingly. This was accomplished by changing the fuel differential injection pressure. Thus in interpreting the effects of air flow rate on NO and CO emissions it may be necessary to consider changes in atomization and spray penetration as well as in primary zone and overall residence times.

As shown in Fig. 3-17 and 3-18, only a slight decrease in NO concentration occurs with a 60% decrease in air flow rate from the base condition; this result indicates that either the residence time in those zones responsible for NO formation does not change greatly, or liquid droplet combustion is the predominant source of NO and remains relatively unchanged throughout this set of experiments.

CO emissions demonstrate a more interesting behavior and are displayed in Fig. 3-19 and 3-20. A general decrease is observed in passing to the lowest air flow rate tested, particularly on the centerline and at 90° cw. At first these results seem inconsistent with the NO results, but both can be explained in terms of Fig. 3-14. It has been hypothesized that zone 1 is the predominant region of CO formation and zones 1 and 3 of NO formation. Since NO formation does not change appreciably with air flow rate, the flow pattern must remain essentially the same in zones 1 and 3. The decreased CO emissions at 3.75 lb/sec can then be attributed to poorer

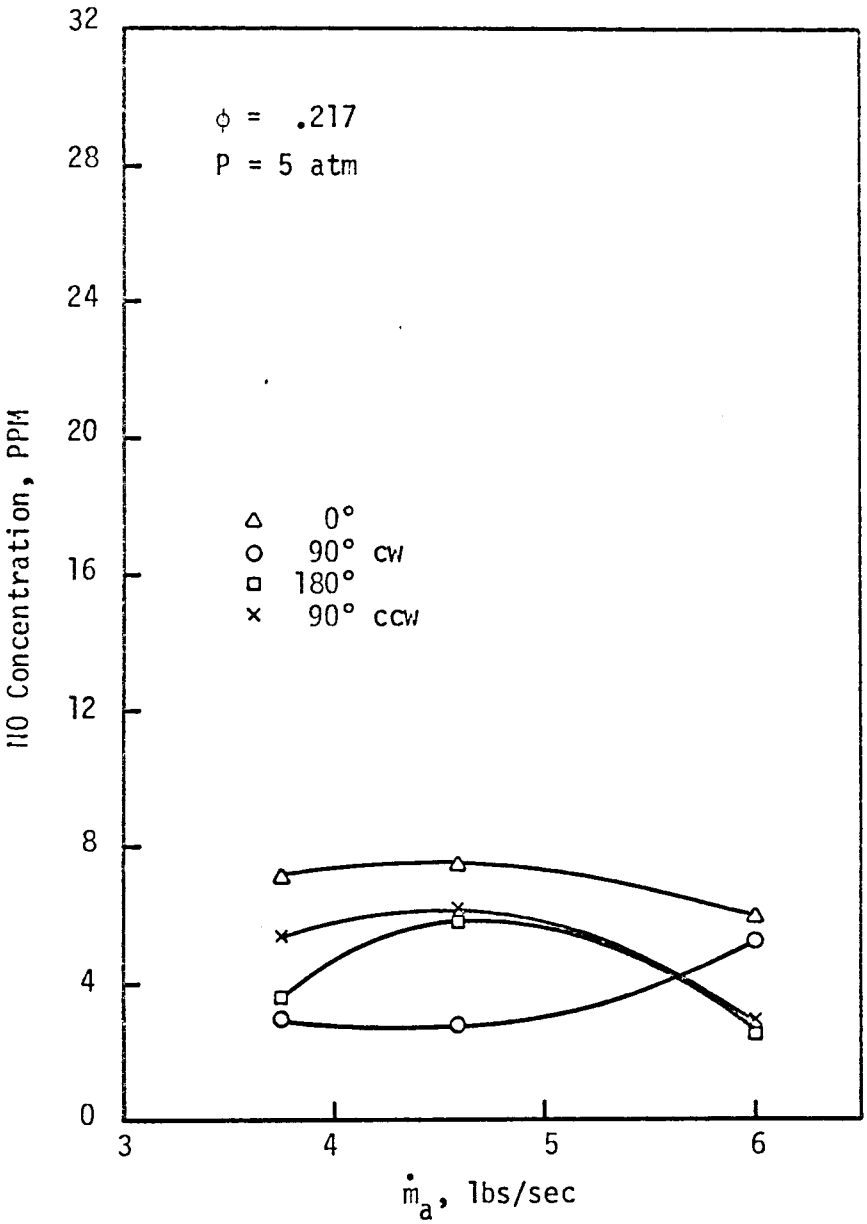

Figure 3-17. Radial NO concentrations at combustor exit plane versus air flow rate (average)

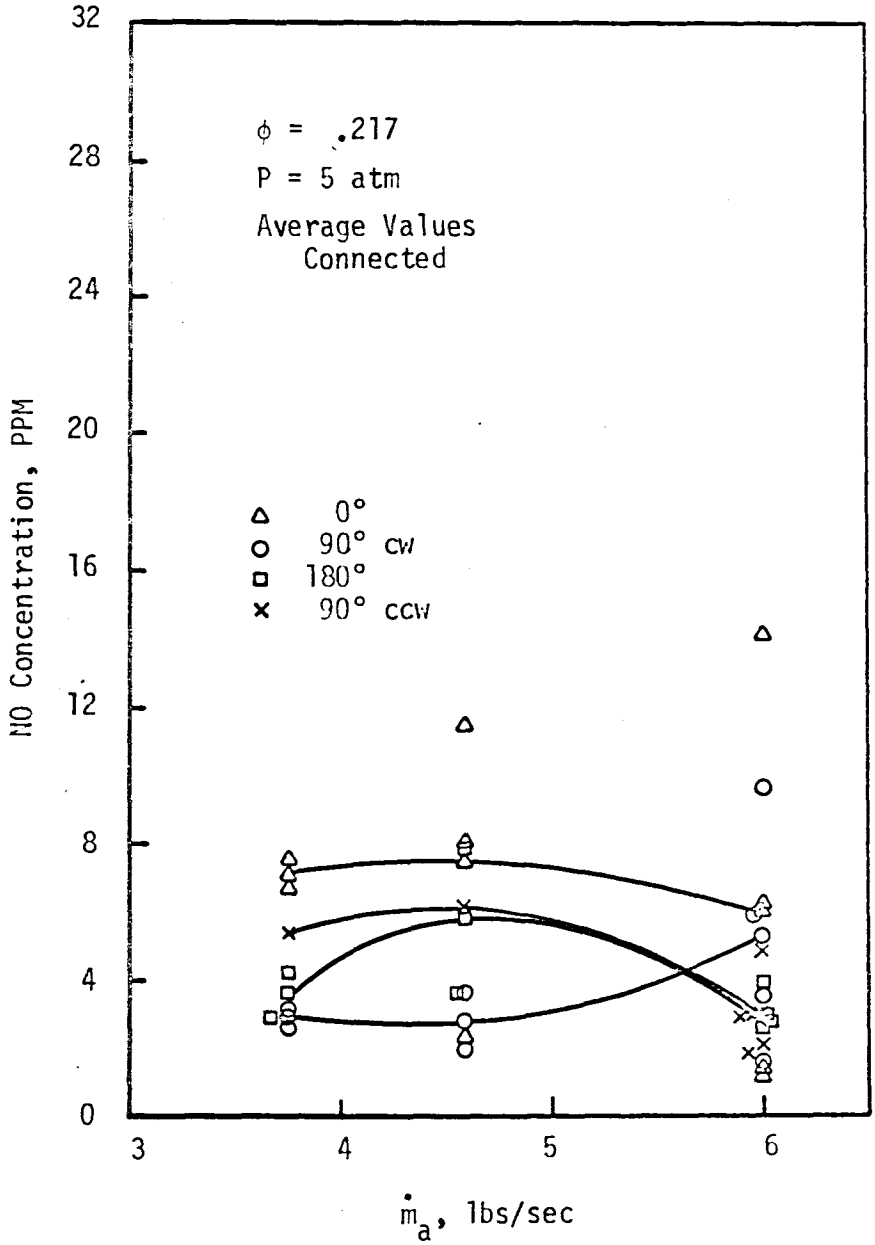

Figure 3-18. Radial NO concentrations at combustor exit plane versus air flow rate

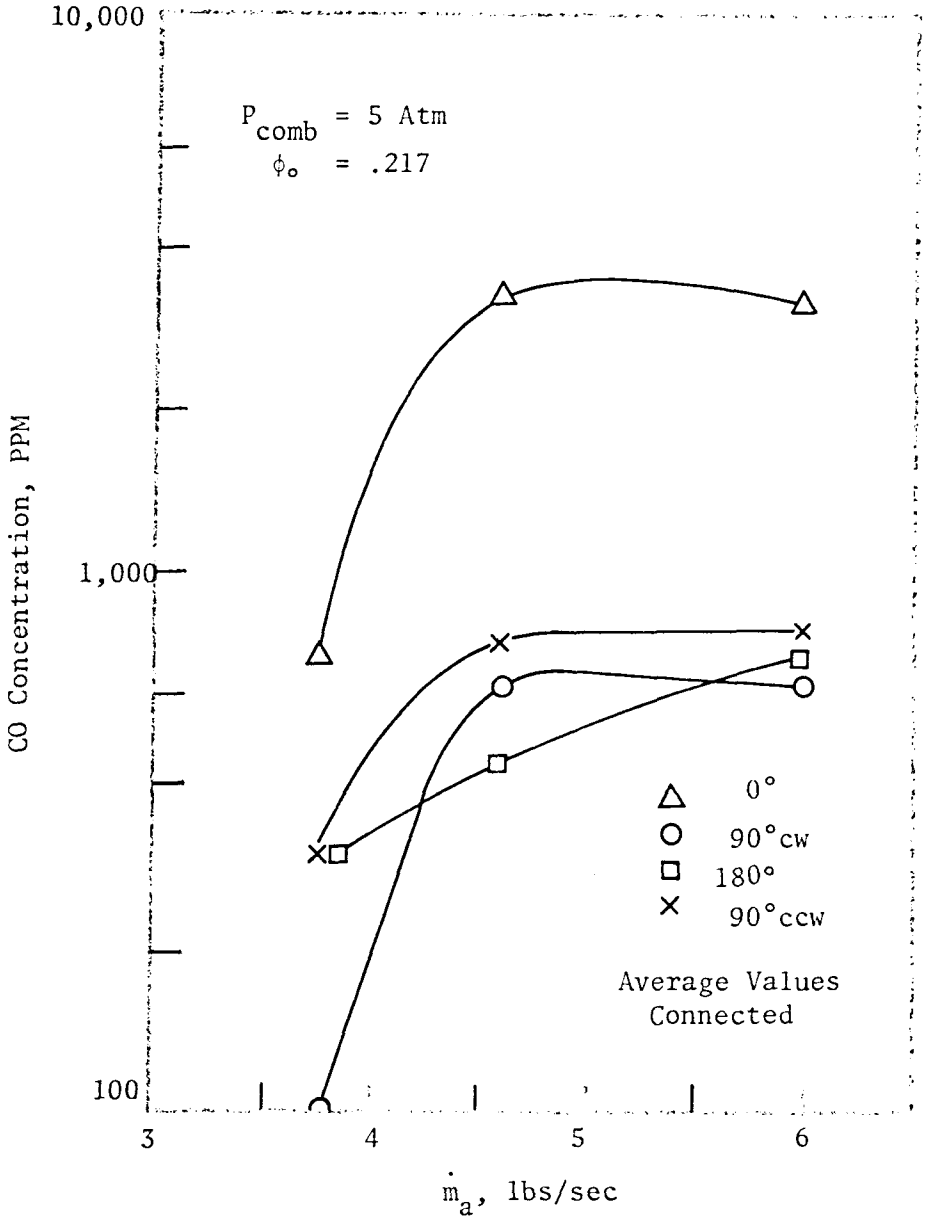

Figure 3-19. Radial CO concentrations at combustor exit plane versus air flow rate (average)

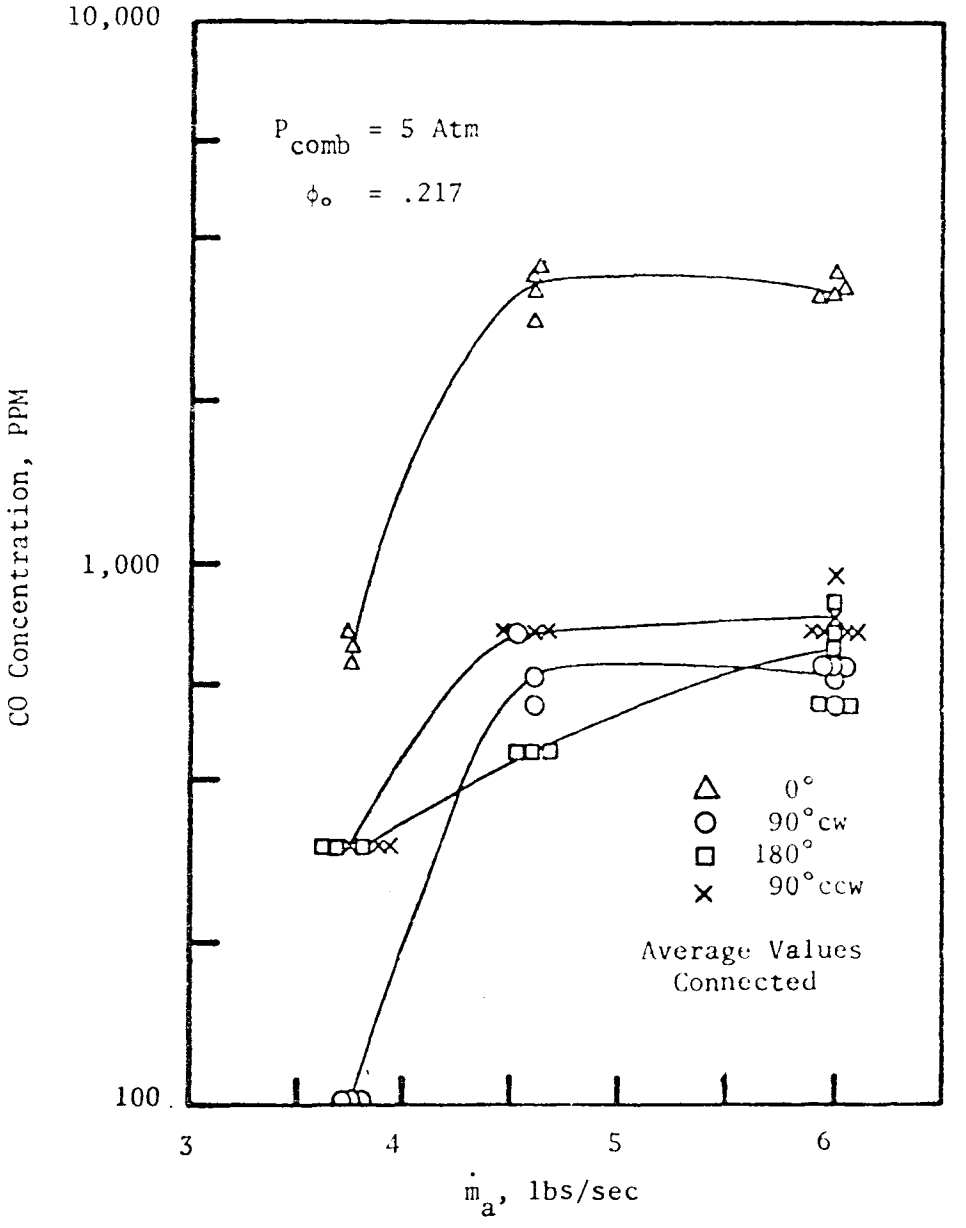

Figure 3-20. Radial CO concentrations at combustor exit plane versus air flow rate

quenching of the CO oxidation in zone 2 and results from less penetration air from zone 4 getting to zone 2 at the low air flow rate. At higher flow rates, approaching the design point of 7.17 lb/sec, the particular design of the J-33 can prevent substantial variations in primary zone residence time. These conclusions are also consistent with the postulate that the high NO concentrations in zone 2 (see Fig. 3-6) result from entrainment from zones 1 and 3 rather than NO formation in zone 2, since higher NO emissions were not observed at the lowest flow rate.

If this behavior were characteristic of combustors other than the J-33 liner, then it could be used to reduce CO (and probably HC) emissions at aircraft low speed ground idle and at automotive idle. While maintaining an overall equivalence ratio close to the design value, compressor bleed air flow could be increased to prevent quenching of the CO oxidation reaction in the combustor. The penalty for this method of emissions control would be an increased fuel consumption at idle.

2.2 The Influence of Overall Equivalence Ratio

The primary effect of an increase in overall equivalence ratio would be a change in the temperature in zones 1 and 3 of Fig. 3-14: if these zones were predominantly lean, then an increase in temperature and NO, and little change in CO would result; if rich, then temperature and NO would decrease while CO increased. On the other hand, if droplet combustion were important then NO (and possibly CO) should increase simply as a result of the presence of more droplets. Of minor significance would be a slight decrease in primary zone residence time due to the increased fuel flow rate.

The results of a change in equivalence ratio are shown in Fig. 3-21 through 3-24, and it is observed that both NO and CO increase strongly with overall equivalence ratio. Most likely this results from the droplet effect noted above; the CO increases as well because zones 1 and 3 are predominantly rich. Both the presence of droplets and the lack of sufficient air for complete combustion in these regions are entirely consistent with the other observations which led to the model depicted in Fig. 3-14.

2.3 The Influence of Combustor Pressure

The final cycle parameter which was varied was combustor pressure, at constant air flow rate and overall equivalence ratio; the results of this study are shown in Fig. 3-25 through 3-28. An increase in pressure will increase the homogeneous rate of NO formation and both CO formation and oxidation. In addition, small decreases in fuel spray cone angle and atomization may result.

In Fig. 3-25 and 3-26 it is seen that a substantial increase in NO occurs with increasing pressure at all radial probe positions: the mass-averaged NO concentration increases from 3 ppm at 5 atm to 11 ppm at 10 atm, a factor of 3.67. If one assumes that the Zeldovich mechanism, with O/O_2 equilibrium and N atoms in steady state, describes the gas-phase NO formation kinetics, then it can be shown that the rate of formation of NO increases with pressure to the 1.5 power; in other words, on the basis of homogeneous kinetics and under the assumption that the temperature and residence time in the NO forming region are relatively unaffected by total combustor pressure, the NO concentration at 10 atm

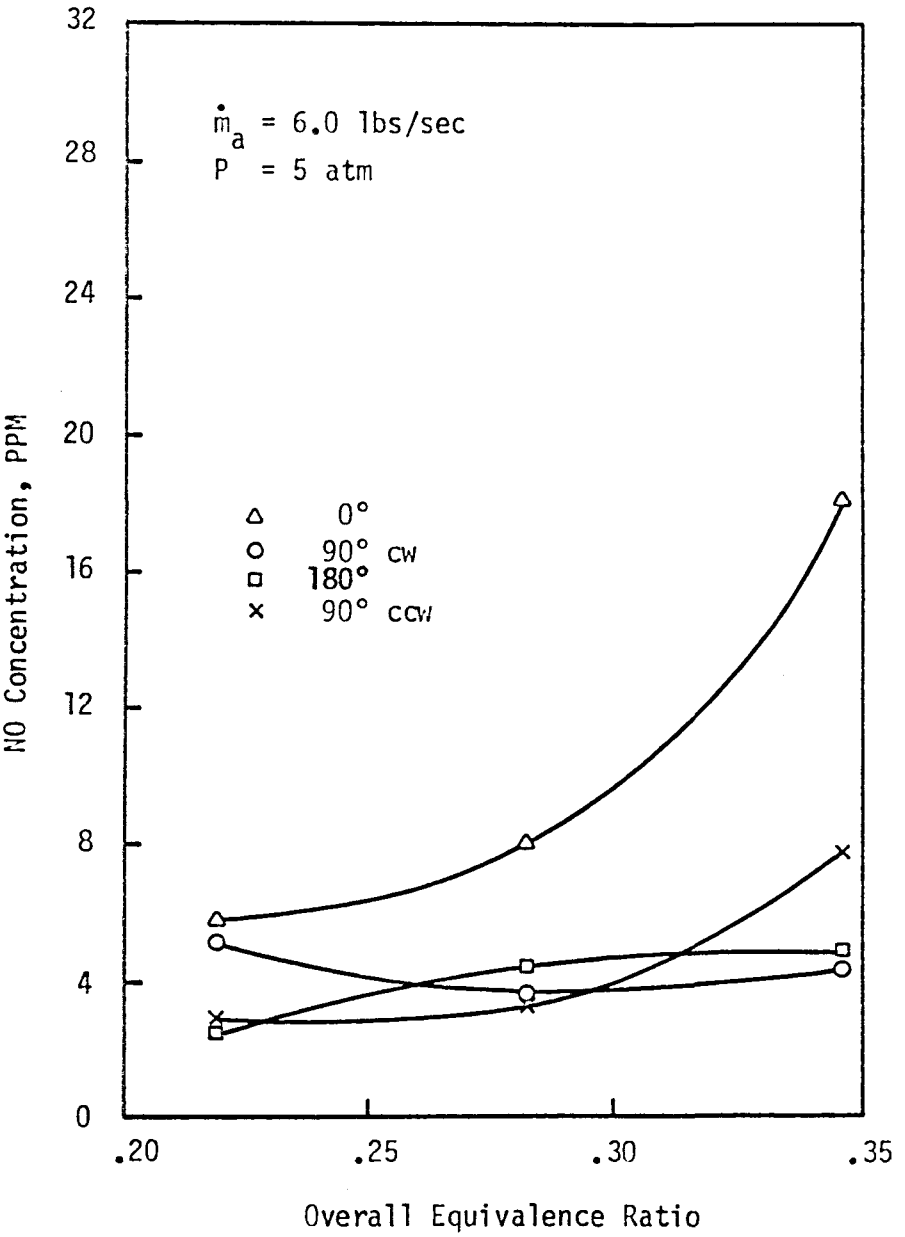

Figure 3-21. Radial NO concentrations at combustor exit plane versus overall equivalence ratio (average)

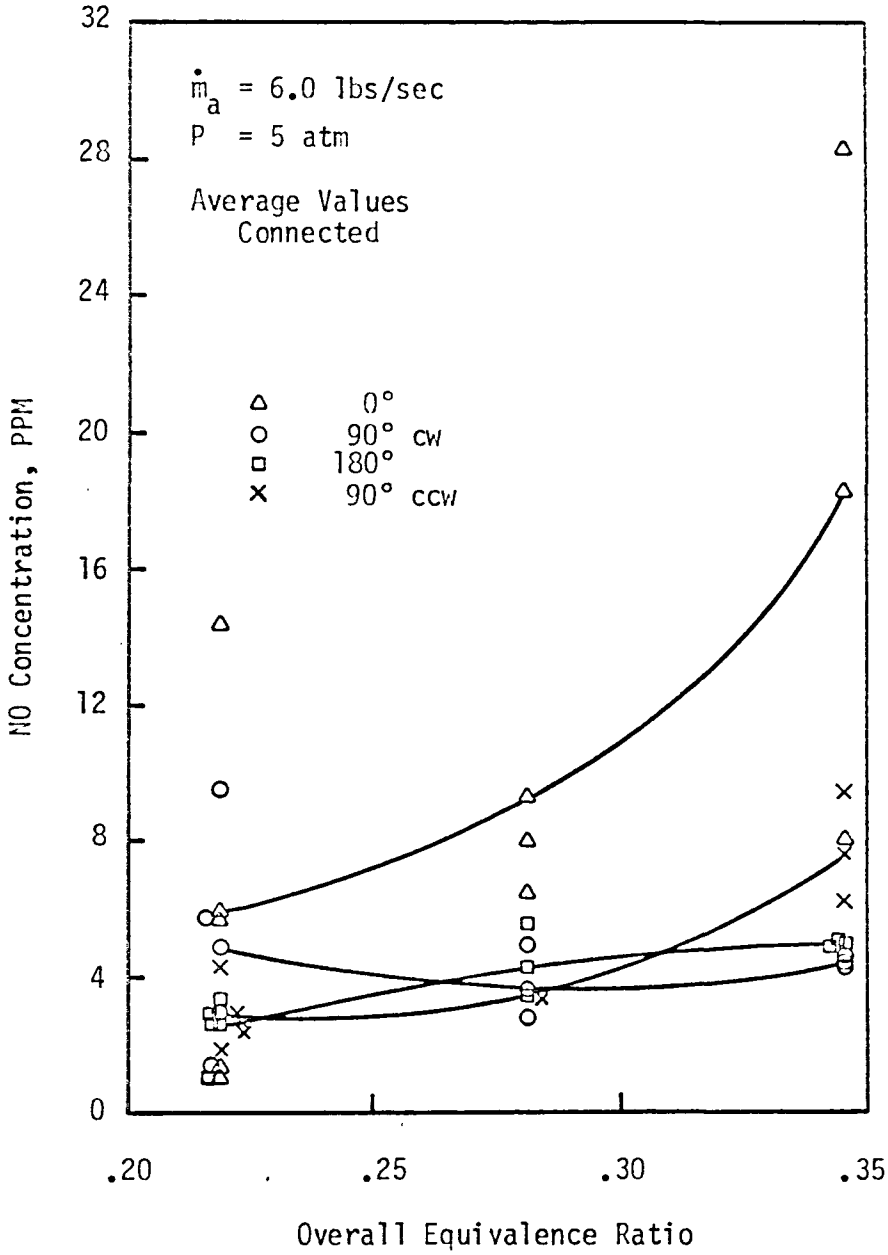

Figure 3-22. Radial NO concentrations at combustor exit plane versus overall equivalence ratio

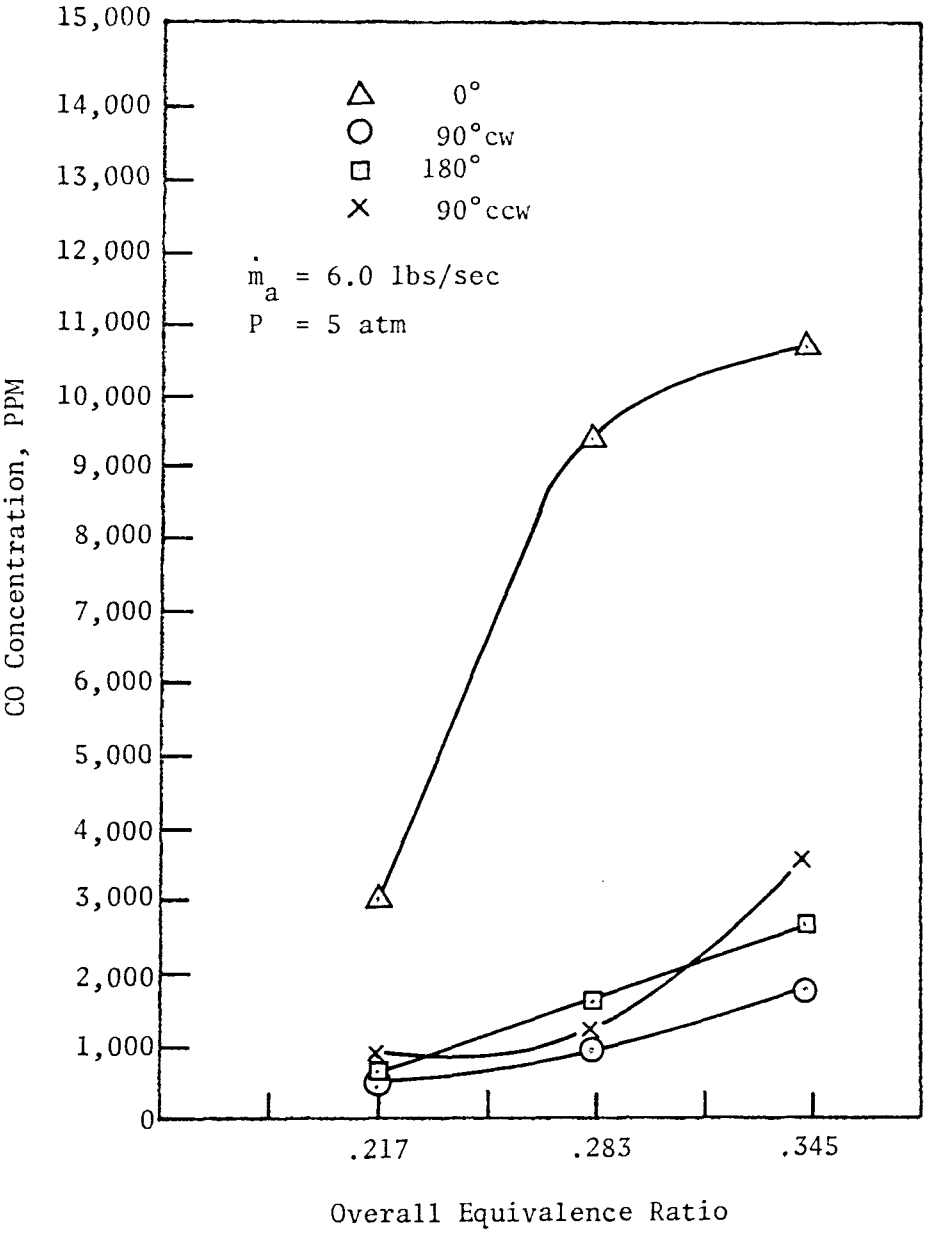

Figure 3-23. Radial CO concentrations at the combustor exit plane versus overall equivalence ratio (average)

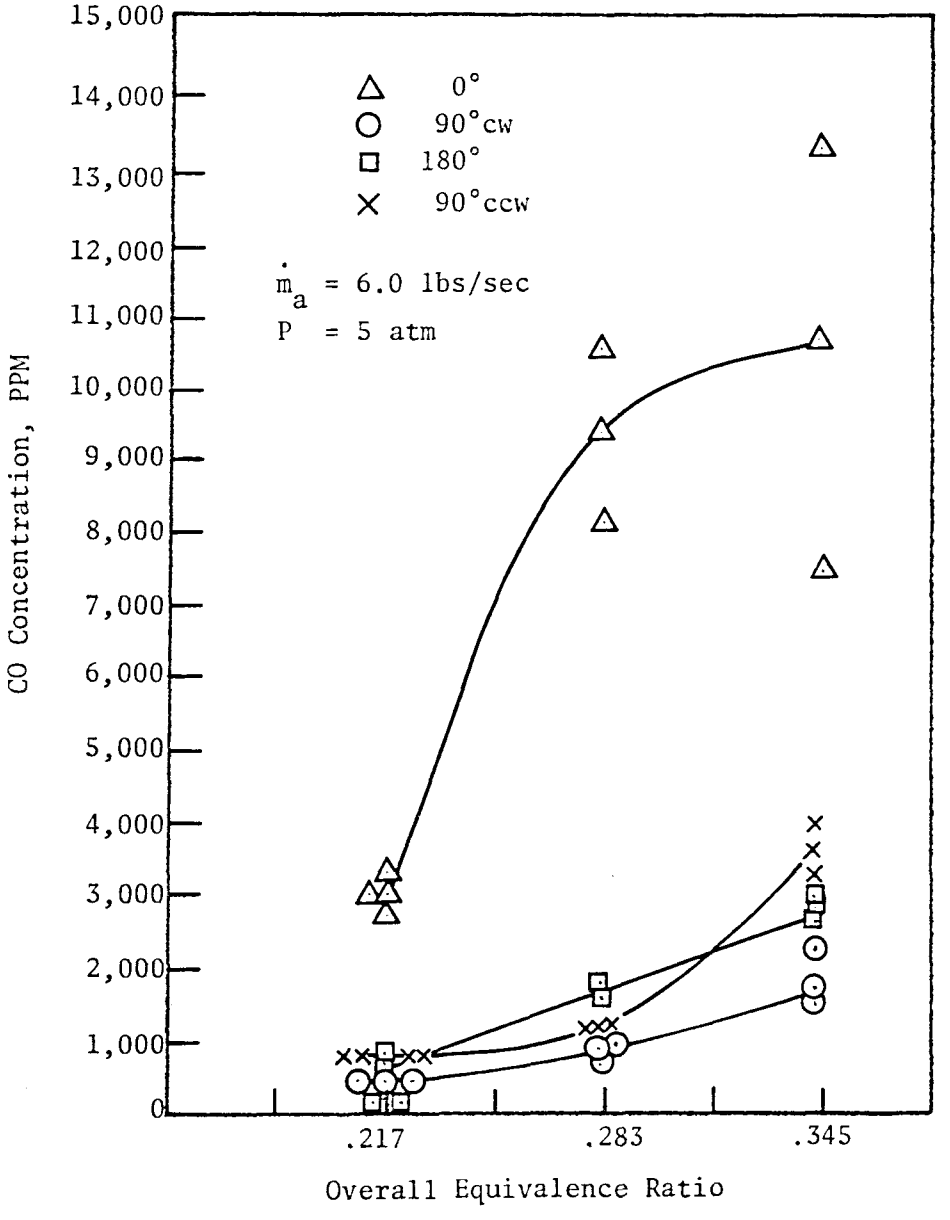

Figure 3-24. Radial CO concentrations at the combustor exit plane versus overall equivalence ratio

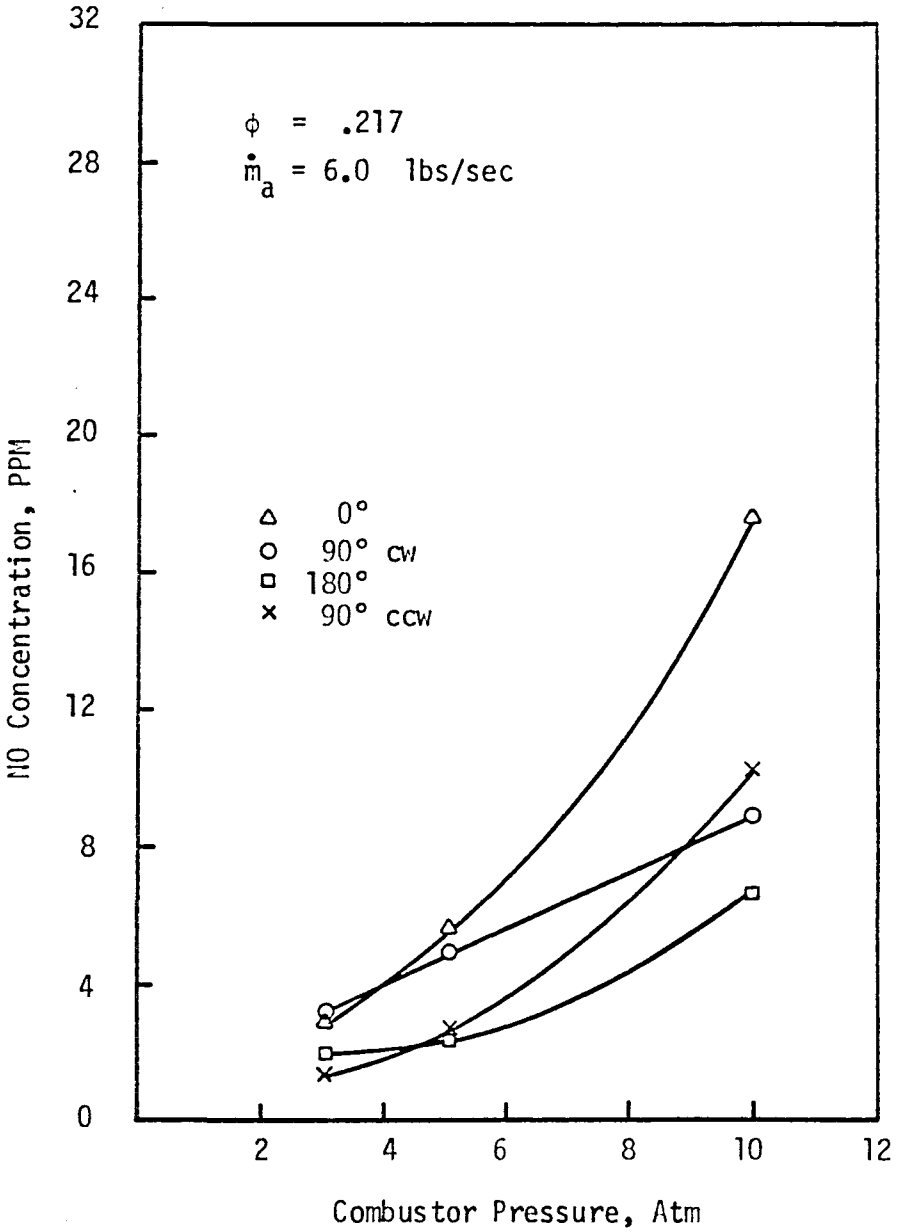

Figure 3-25. Radial NO concentrations at combustor exit plane versus pressure (average)

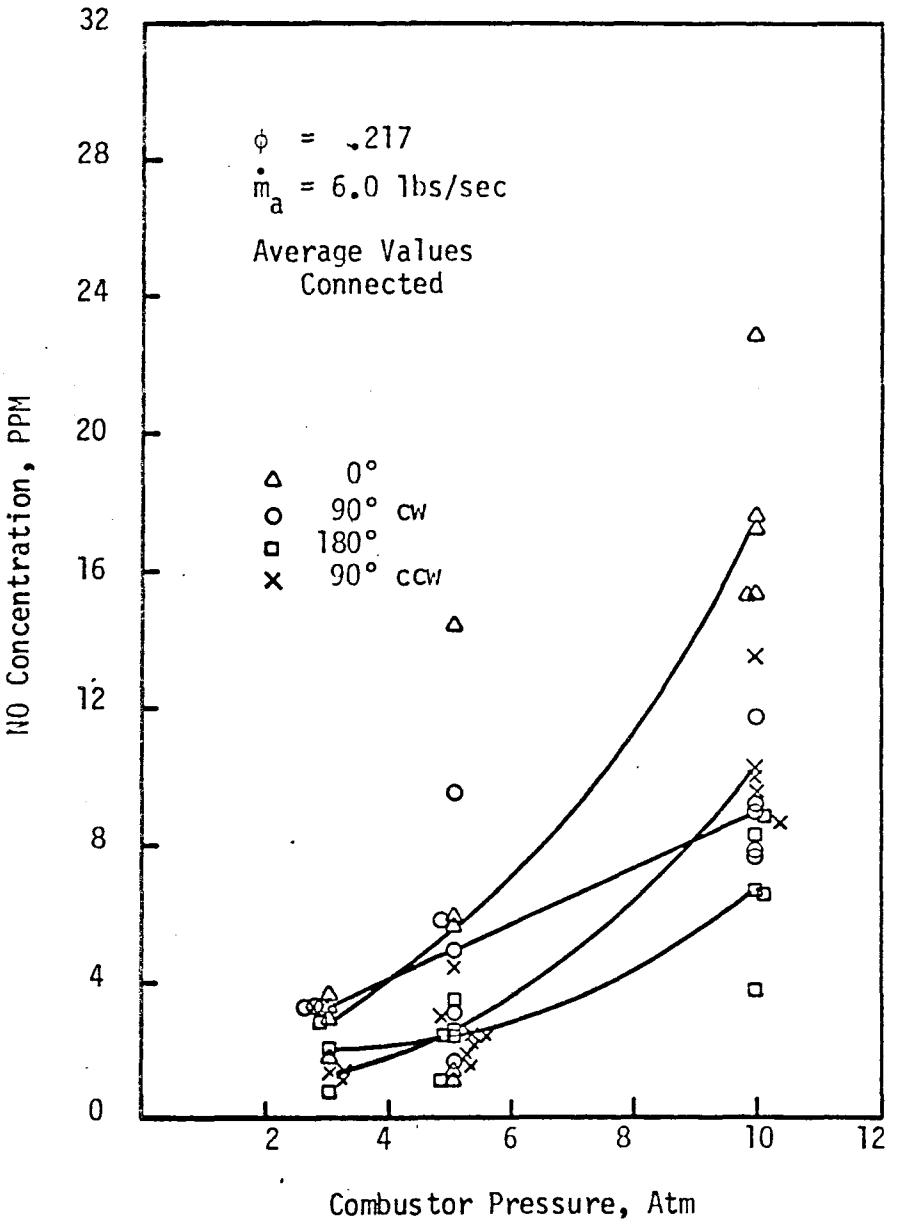

Figure 3-26. Radial NO concentrations at combustor exit plane versus pressure

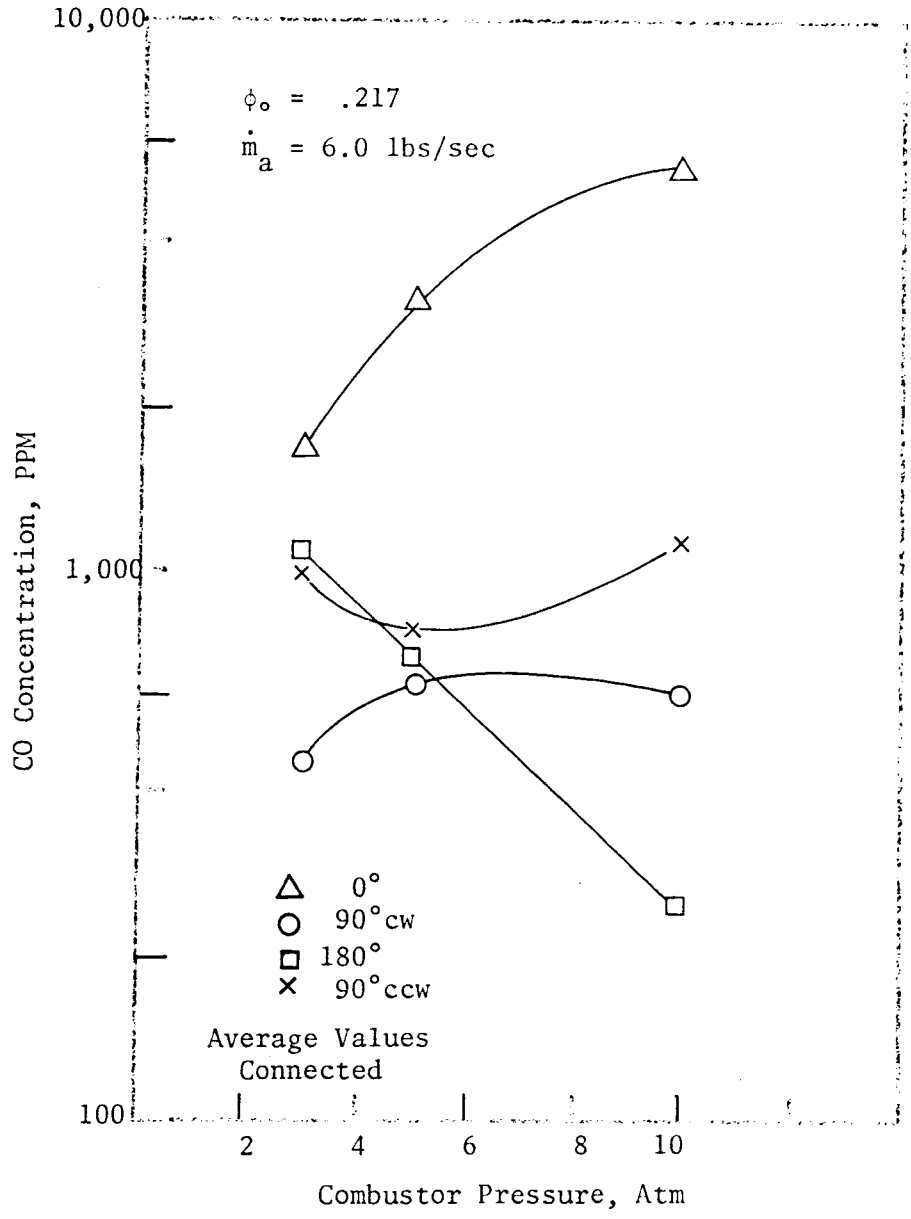

Figure 3-27. Radial CO concentrations at combustor exit plane versus pressure (average)

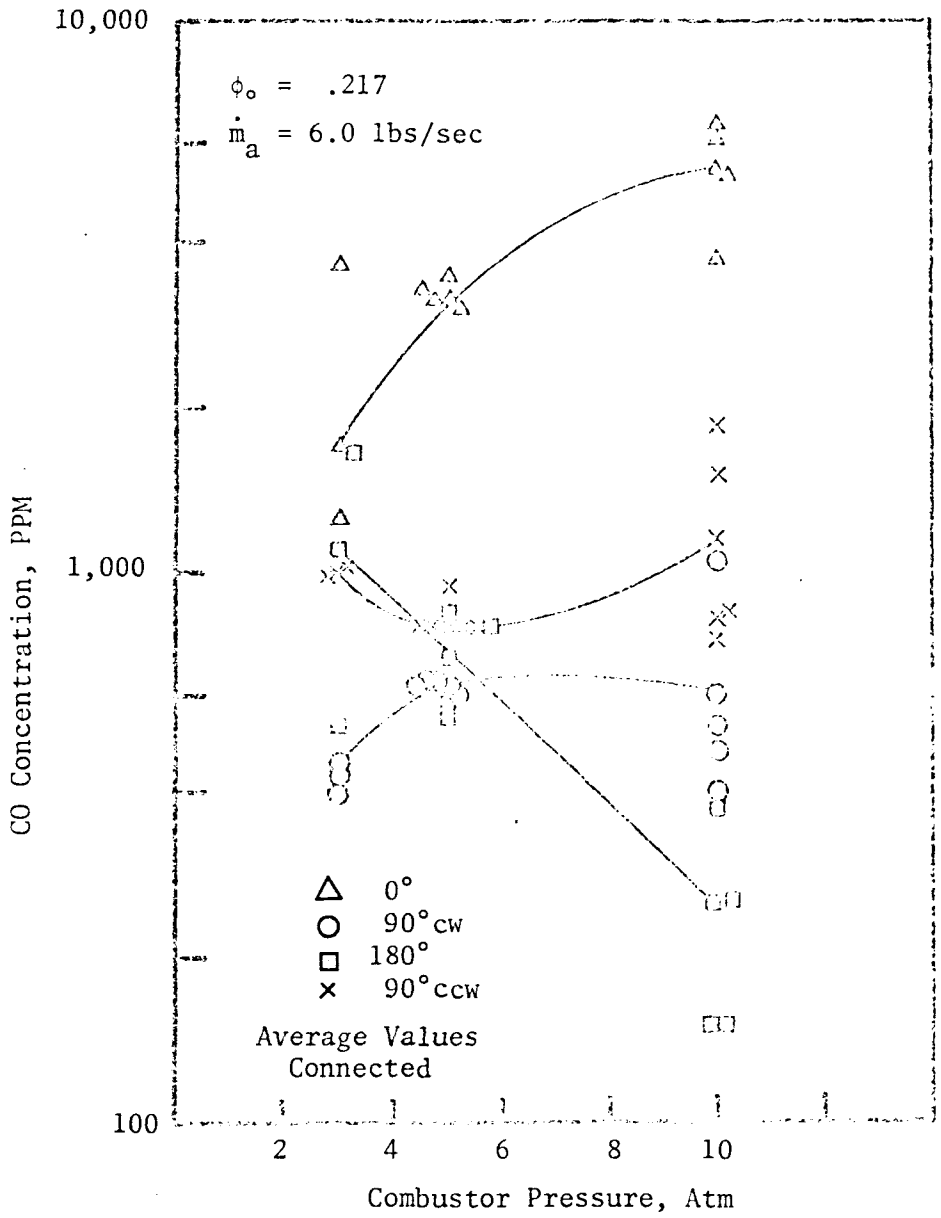

Figure 3-28. Radial CO concentrations at combustor exit plane versus pressure

should be only about 2.8 times that at 5 atm. Thus the observed increase cannot be explained on the basis of homogeneous kinetics.

In holding the fuel flow rate constant as the pressure was increased, it was generally found necessary to decrease the pressure drop across the injector. Consequently, larger fuel droplets capable of forming increased concentrations of NO were probably present at the higher pressures.

The CO exhaust plane data are shown in Fig. 3-27 and 3-28 and do not show a single trend with increasing pressure: the centerline concentration increases as the wall value decreases. These observations are attributed to a decrease in injector spray cone angle with increased pressure and are consistent with the combustion model shown in Fig. 3-14.

D. OTHER PARAMETERS

The heat release rate and combustion intensity are not parameters that can be varied independently of others such as combustor pressure, overall equivalence ratio, and air flow rate once the combustor geometry and fuel are defined. Consequently, since the experimental investigation discussed here employed a J-33 combustor burning liquid propane, the isolated effects of heat release rate and combustion intensity on pollutant emissions were not determined.

E. SUMMARY

In summary, the temperature and concentrations of CO and NO at various axial and radial positions within the J-33 combustor have been

presented and discussed. These profiles are similar to those reported by Sawyer et al. (1969) but definitely show the effects of the particular J-33 combustor configuration.

Having acquired some fundamental information concerning the internal combustor mechanisms responsible for the net CO and NO emissions (at the base operating point), the effects of combustor pressure, overall equivalence ratio, and air flow rate were isolated insofar as possible and measured at the combustor exit plane. General support was obtained from these data for the model of the combustion process in the J-33 combustor which had been postulated on the basis of the internal measurements.

IV. FUTURE EFFORTS

Emissions studies of the J-33 combustor using unheated inlet air were reported in Section III; however, as noted previously these results constituted only a preliminary effort due to this unrealistic combustor inlet temperature. Gas turbines under consideration as alternatives to the internal combustion engine in automobiles are of the regenerative type, and the trend in aircraft engines is to higher compression ratios. Thus it is of interest to add air inlet temperature to those cycle design parameters which can be varied in the experimental facility.

To this end the double combustor facility shown in Fig. 4-1 has been constructed. The first J-33 combustor is used as an air heater for a second J-33 mounted downstream. Although the heated air will contain pollutants, at levels of contamination similar to those reported in the previous section, since the primary purpose of the facility is to indicate trends in emissions as functions of cycle and combustor design parameters (as opposed to absolute or baseline values) the use of vitiated air is considered acceptable.

For assistance in evaluating the performance of the double combustor facility in meeting the objectives mentioned above, a few experiments have been conducted to date. Because these runs were of an exploratory nature and the data are not complete, the successful operation of the facility is of more interest than the actual data to be reported here.

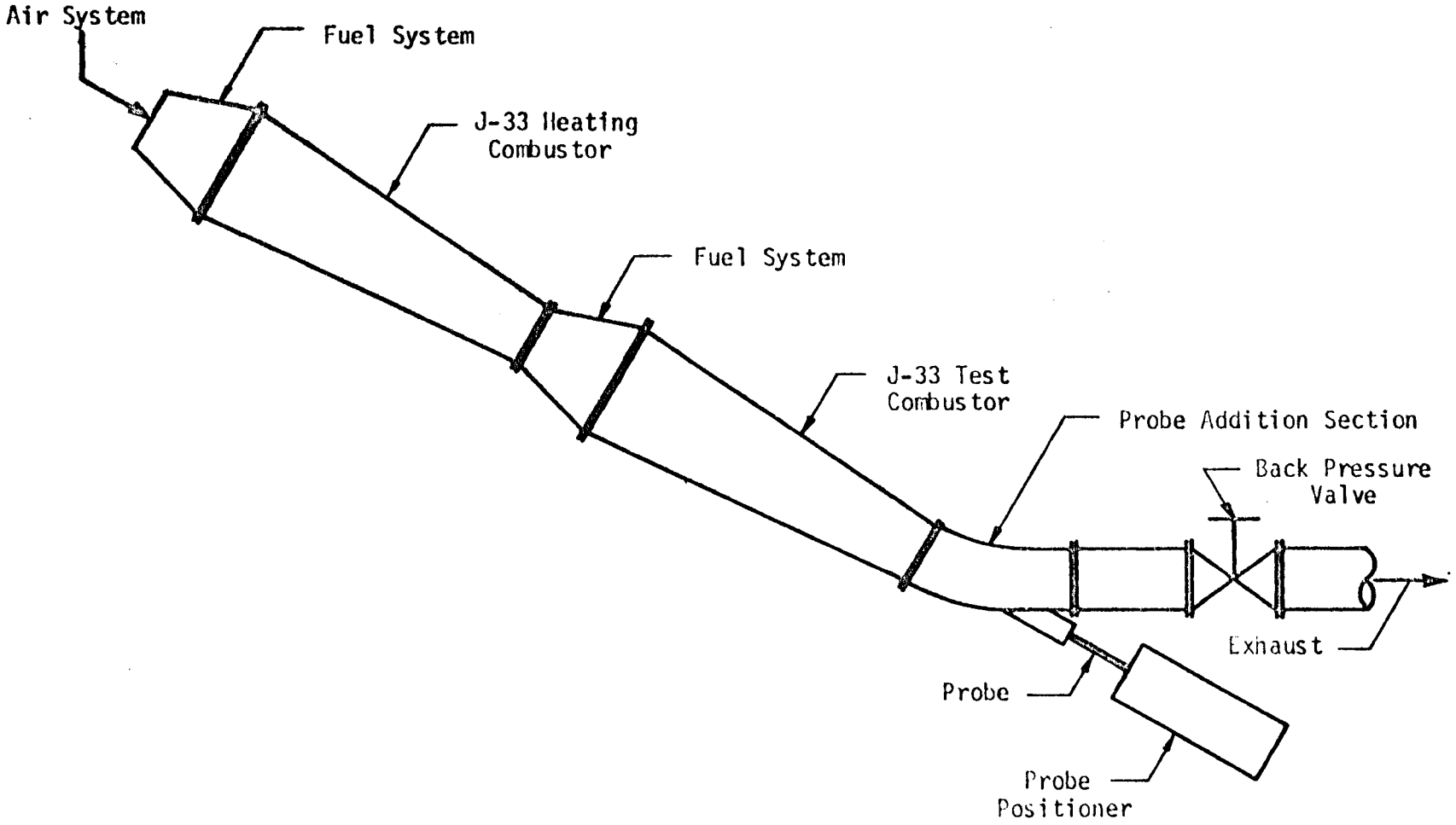

Figure 4-1. Complete combustion facility schematic

The probe addition section and back pressure valve were mounted at the exhaust flange of the second J-33 combustor, and the gas sampling probe was placed at the exit plane of the test combustor. Although the thermocouple portion of the probe was destroyed during one overly long and hot ignition transient, the gas sampling probe has withstood over one-half hour at this station to date. We are presently replacing the Pt/PtRh couple.

A gas sampling rake and chromel/alumel thermocouple rake for mounting in the diffuser section just upstream of the test combustor are under construction but were not available for the emissions measured to date; thus the data to be reported are composites for both combustors. In later studies the rakes will provide for null measurements to obtain the true emissions from the test combustor.

In Table 4-1 are presented those data obtained to date for the following run conditions for the test combustor: air flow rate 6 lb/sec, combustor pressure 3.4 atm abs, overall equivalence ratio 0.217, and inlet air temperature 630° K. Without the null measurement to be provided by the rakes, no attempt will be made to discuss these preliminary emissions data since the equivalence ratio and pressure for the first or heating combustor do not correspond to any of the operating points listed in Section III. To repeat, the purpose of this experiment was simply to gain experience with the complete facility and associated instrumentation (including the FID hydrocarbon analyzer).

After the gas sampling and temperature rakes are installed upstream of the J-33 test combustor, detailed gas sampling (including CO, NO and HC)

Table 4-1. Operating Point and Emissions Obtained from Two J-33 Combustors in Series*

Air Flow Rate	6.0 lb/sec
Combustor Pressure	3.4 atm abs
Overall Equivalence Ratios	
First or Heating Combustor	0.130
Second or Test Combustor	0.217
Inlet Temperature to Test Combustor±	630° K (680° F)

Pollutant	Radial Probe Position at Test Combustor Exhaust Plane			
	0°	90° cw	90° ccw	180°
NO, ppm	1.89	2.61	1.61	1.43
CO, ppm	2250	1800	4500	2020
HC, ppm CH_4	950	400	2600	1000

* Emissions are composites for both combustors.

± Calculated following Zucrow and Warner (1956).

and temperature measurements are to be made at various stations within the test combustor as functions of four overall cycle design parameters: inlet air temperature, combustor pressure, equivalence ratio, and air flow rate. Each parameter will be varied independently from a standard run condition.

The possibility of NO_2 formation in the combustor is a point of current discussion. Significant amounts of NO_2 have recently been found in the exhausts of commercial and military jet engines, particularly at idle (Anon., 1971, Hare et al., 1971 and Vaught et al., 1971). These data were obtained primarily by use of the $NO_2 \rightarrow NO$ converter in conjunction with a chemiluminescent NO analyzer. In view of the possibility of catalytic decomposition of NO by these converters (see Appendix A), the observation of NO_2 by Hare et al. (1971) is questionable since only the converter and a chemiluminescent detector were used in the study to obtain NO_x concentrations.

More confidence can be placed in the results of Airesearch (Anon., 1971) because they also used a NDUV analyzer at selected points to measure NO_2 directly. They noted that "a check of several test power settings using a NDUV analyzer ... confirmed the magnitude of NO_2 readings received on the chemiluminescent analyzer," but apparently no quantitative comparisons are presented in their report (Anon., 1971).

Detroit Diesel Allison (Vaught et al., 1971) compared NO as obtained on a NDIR analyzer with that from a chemiluminescent analyzer and generally found agreement within 10%. However, total NO_x from a converter-chemiluminescent analyzer was considerably less than that obtained with the

Saltzman method (27% less at low speed ground idle and 6% less at take-off for the T-56 engine). Note that if the converter is destroying NO, as well as converting NO_2 to NO, a lower NO_x would be obtained with the chemiluminescent analyzer.

The present investigation after completion of the J-33 study will turn to measurements at the exhaust plane and within an Allison T-56 combustor, particularly with respect to independent verification of the reported NO_2 levels (Vaught et al., 1971), as well as the identification of those zones within the combustor which are responsible for the production of NO_2. Instrumentation will consist of the converter-chemiluminescent analyzer for NO and NO_x, and it is hoped that these data can be substantiated via the NDUV method for NO_2. CO, HC, and temperature measurements will be made simultaneously with the NO_x surveys.

Although it will probably not be possible to simulate T-56 low speed ground idle in the facility due to flameholding requirements in the heating combustor, since substantial NO_2 was observed at all of the engine operating points (Vaught et al., 1971), it is felt that a reasonable simulation of the T-56-A-15 operation and investigation of NO_2 formation in the combustor can be accomplished.

Another study which is planned is to use a gaseous rather than liquid fuel; an example of the success of this technique for emissions reductions is the widespread use of natural gas in stationary combustion systems as a short range method of reducing pollution. For the aircraft or automotive turbine engine, however, natural gas is not a practical fuel, and thus prevaporizing burners represent one compromise design (see for example

Zwick et al., 1971, for a Rankine cycle application).

In spite of this concensus, there has been no demonstration of the importante of heterogeneous effects with regard to emissions presented in the open literature for a current combustor can (Mellor, 1971). The Berkeley group (Sawyer et al., 1969, Starkman et al., 1970, and Parikh et al., 1971) has shown that gaseous methane produces less HC, CO, and NO than liquid heptane, when burned in a model laboratory combustor. However, inlet conditions to the combustor were not realistic (room temperature air and pressure only slightly in excess of atmospheric), and not only the physical state, but also the chemical nature of the fuel was changed as well.

It is apparent that a controlled investigation of the effect of using gaseous rather than liquid fuel is needed. It is proposed here that the experiments carried out with the T-56 combustor be repeated using gaseous propane fuel. Internal and exhaust plane surveys of temperature, HC, CO, NO, NO_2, and NO_x will again be made.

In summary, the experimental setup using a single J-33 combustor or two combustors in series has proven to be operable. Preliminary data have been obtained, but interesting and important investigations are left to be carried out. Future efforts are to include the study of a high inlet temperature combustor, the investigation of NO_2 formation in combustors with emphasis on the T-56 can, and a determination of the effect on pollutant emissions when gaseous fuel rather than liquid fuel is used.

LIST OF REFERENCES

Anon., 1971, "Exhaust emissions test-Airesearch aircraft propulsion and auxiliary power gas turbine engines," Report GT-8747-R, Airesearch Manufacturing Co. of Ariz.

Chase, J. O. and Hurn, R. W., 1970, "Measuring gaseous emissions from an aircraft turbine engine," SAE Paper 700249.

Fontijn, A., Sabadell, A. J., and Ronco, R. J., 1969, "Feasibility study for the development of a multifunctional emission detector for air pollutants based on homogeneous chemiluminescent gas phase reactions," TR-217, AeroChem Research Laboratories.

Fontijn, A. Sabadell, A. J., and Ronco, R. J., 1970, "Homogeneous chemiluminescent measurement of nitric oxide with ozone," Anal. Chem. 42, 575.

Fontijn, A., 1971, AeroChem Research Laboratories, Personal communication to A. M. Mellor.

Hare, C. T., Dietzmann, H. E., and Springer, K. J., 1971, "Gaseous emissions from a limited sample of military and commercial aircraft turbine engines," Report AR-816, Southwest Research Inst.

Hodgeson, J. A., Bell, J. P., Rehme, K. A., Krost, K. J., and Stevens, R. K., 1971, "Application of a chemiluminescence detector for the measurement of total oxides of nitrogen and ammonia in the atmosphere," AIAA Paper 71-1067.

Mellor, A. M., 1971, "Current kinetic modeling techniques for continuous flow combustors," Emissions from Continuous Combustion Systems Symposium, General Motors Research Laboratories.

Nelson, A. W., 1972, "Collection and assessment of aircraft emissions baseline data - turbine engines," Report PWA-4339, Pratt and Whitney Aircraft, United Aircraft Corporation.

Owens, C. W. and Mellor, A. M., 1971, "An investigation of gas turbine combustors with high inlet air temperatures. Second Annual Report: Part II: Heat Transfer," TM-71-2, Jet Propulsion Center, Purdue University, USA TACOM Report No. 11328.

Owens, C. W., 1972, "Heat transfer in high temperature gas turbine combustion chambers," M.S.M.E. Thesis, Purdue University.

Parikh, P. G., Sawyer, R. F., and London, A. L., 1971, "Pollutants from methane fueled gas turbine combustion," College of Engineering Report No. TS-70-15, University of California, Berkeley.

Sawyer, R. F., Teixeira, D. P., and Starkman, E. S., 1969, "Air pollution characteristics of gas turbine engines," ASME Trans., J. Eng. Power, 91, 290.

Starkman, E. S., Mizutani, T., Sawyer, R. F., and Teixeira, D. P., 1970, "The role of chemistry in gas turbine emissions," ASME Paper 70-GT-81.

Tacina, R. R. and Grobman, J., 1969, "An analysis of total pressure loss and airflow distribution for annular gas turbine combustors," NASA TN D-5385.

Vaught, J. M., Parks, W. M., Johnsen, S. E. J., and Johnson, R. L., 1971, "Final technical report collection and assessment of aircraft emissions base-line data-turboprop engines (Allison T56-A-15)," Report EDR 7200, Detroit Diesel Allison Division, General Motors.

Zucrow, M. J. and Warner, C. F., 1956, "Constant pressure combustion charts for gas turbines and turbojet engines," Purdue University Engineering Experiment Station Bulletin No. 127.

Zwick, E. B., Mills, T. R., and Fio Rito, R., 1971, "Evaluation of a low NO_x burner," Report USG-1, Paxve, Inc.

APPENDIX A

EFFECT OF NO_2 CONVERTER ON NO

A NO_2 converter was added to the nitric oxide detector system so that the existing chemiluminescent NO detector could be used to measure the NO_2 concentration of the sample gas. In principle, the converter operates by heating the sample gas to a sufficient temperature (approximately 600° C) such that the NO_2 will dissociate to NO. The NO_2 converter-NO system is shown schematically in Figure 2-15. Parallel flow paths to the NO detector are provided for the sample: one goes directly to the detector and the second passes through the converter. By intermittently changing the flow path taken by the sample gas, the concentrations of NO and NO_x can alternately be recorded. The total NO_2 concentration is then the difference between the alternating concentration levels.

The converter was constructed according to specifications furnished by the Environmental Protection Agency, which called for six feet of one-eighth inch by .028 inch wall 316 type stainless steel tubing. The tubing was resistance heated by flowing an electric current directly through it. A thermocouple was attached to the tube so that the tube temperature could be continuously monitored.

No NO_2 concentration measurements were recorded, as preliminary testing showed that the NO concentration in a 215 ppm sample gas (balance N_2) was greatly reduced when the gas was flowed through the converter. It was observed that an increase in the converter temperature

from 23° C to 600° C was accompanied by a decrease in the NO concentration level recorded by the chemiluminescent detector. Similarly, the recorded concentration level rose with decreasing converter temperature. The recorded results for four individual runs are shown in Fig. A-1. The slopes of the curves of Fig. A-1 depend upon the rate of temperature increase, with run one having the highest rate. The lowest concentrations recorded are within an order of magnitude of the dark current of the detector.

In experiments using a commerical chemiluminescent detector with a similar converter, reported quite recently by Nelson (1972), similar irreproducible effects were observed with the "unconditioned" converter when either NO in N_2 or NO_2 in air was flowed through the system. Converter conditioning was accomplished by repeated exposures to NO_x with the converter at high temperature.

It is presently thought that the observed results can be attributed to a surface catalytic reaction along the walls of the stainless steel tubing (Fontijn, 1971). Such a reaction is consistent with the lack of reproducibility shown in Fig. A-1, the dependence on applied heating rate, and the failure of Hodgeson et al. (1971) to find a similar effect for samples containing less than 1 ppm NO.

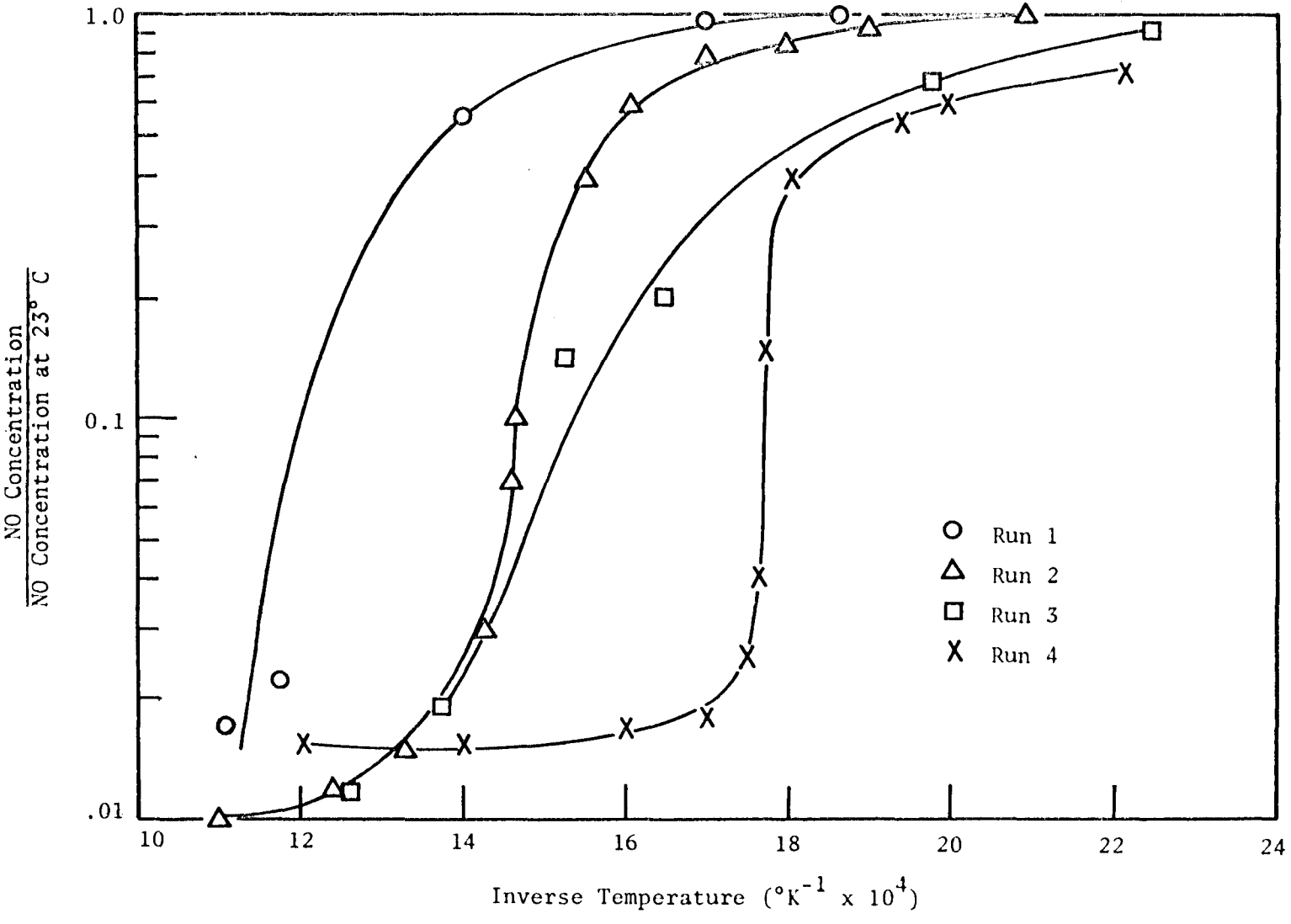

Figure A-1. Normalized concentration versus inverse temperature